TÉCNICO LISBOA

Effects of non-conventional sterilization methods on PVA-Zylon hydrogels for cartilage repair

Tomás Macedo Faria Matoso Pires

Thesis to obtain the Master of Science Degree in

Bioengineering and Nanossystems

Supervisor(s): Prof. Ana Paula Valagão Amadeu do Serro
Dr. Diana Cristina Morais da Silva Pereira

Examination Committee

Chairperson: Prof. Jorge Manuel Ferreira Morgado
Supervisor: Dr. Diana Cristina Morais da Silva Pereira
Member of the Committee: Prof. Célio Gabriel Figueiredo Pina
Dr. Raquel Sofia Cardoso Galante

November 2021

Dedicated to my family and friends.

Declaration

I declare that this document is an original work of my own authorship and that it fulfills all the requirements of the Code of Conduct and Good Practices of the Universidade de Lisboa.

Preface

The work presented in this thesis was performed at the Biomaterials Laboratory in Centro de Química Estrutural (CQE) and Materials and Nanotechnologies Laboratory of Instituto Superior Técnico (Lisboa, Portugal) as well as Instituto Universitário Egas Moniz (Almada, Portugal), during the period of March-October 2021, under the supervision of Prof. Ana Paula Serro and Dr. Diana Silva Pereira.

Acknowledgments

First and foremost I would like to express my gratitude to my advisors Professor Ana Paula Serro and Diana Silva Pereira for all their mentorship, encouragement, availability and trust which helped me develop as an individual and researcher during this period and without whom this work wouldn't be possible. Thank you Professor Ana Paula for tirelessly coordinating this work, always making sure I had all the necessary materials, equipment and guidance to perform my studies. To Diana Silva Pereira, thank you for all the unending help in all factors related to this thesis, from the crucial help in almost all of my experiments and supporting me in interpreting my results. I truly appreciate all your help and for making me feel at home in this group.

I would like to express my deep gratitude to Andreia Sofia Oliveira for patiently explaining me step-by-step how to produce the hydrogels and help me correctly interpret my results. Thank you for all the good talks, motivation and support which allowed to get through the initial stages of this research and finish my work. I express my deep appreciation for Professor Madalena Oom for her tireless help in performing the cell experiments and teaching me so much, always pushing me to become a better researcher. I would also like to gratefully acknowledge Professor Célio Pina for his contagious excitement and all his help in the mechanical and tribological tests.

My utmost thanks to Professors Benilde Saramago, José Mata, Rogério Colaço and all other members of the Biomaterials Research Group (BIOMAT), Nanostructured Materials and Nanotechnologies Laboratory (NanoMatLab) and Centro de investigação Interdisciplinar Egas Moniz (CiiEM), for allowing me to perform my experiments in their facilities and providing the financial support for the elaboration of this work, through the research project CartHeal – Cartilages for hip prosthesis with controlled drug release ability PTDC/CTM-CTM/29593/2017 and the unit projects of CQE.

A big mention to all my other colleagues at the BioMat/NanoMat Lab which created an awesome working environment where I always felt welcome and appreciated. To Ana Catarina Branco, Carolina Costa, Diana Nobre, Leonor Garcia, Maria João Godinho, Mariana Donato and Nadia Toffoletto, thank you for always being available to help and for keeping me in good company during the long hours in the lab.

To all my friends who closely accompanied me throughout these years, in and out of IST whose listing would be too extensive and thus I won´t name or I would run out of pages. You all know who you are and know that I wouldn´t be who I am today without each and every one of you. Thank you all for being there through the good and bad times. All these years of studying wouldn´t have been possible without them.

Last but not least I would like to thank my wonderful family who always provided me with all the love and support I needed. They are the main reason I could achieve everything I have done so far and I hope to make them proud.

Resumo

A degradação de cartilagem articular é uma patologia recorrente que afecta milhões de pessoas. Devido à falta de vascularização, este tecido apresenta uma baixa capacidade de regeneração e as atuais estratégias terapêuticas apresentam diversas limitações. Hidrogéis têm gerado interesse como possíveis substitutos de cartilagem, devido à sua biocompatibilidade e altos conteúdos em água. Álcool polivinílico (PVA) é considerado um dos hidrogéis mais promissores, no entanto, as suas propriedades mecânicas dificultam a sua aplicação. Para melhorá-las, o reforço do PVA é necessário. Em contexto clinico, os biomateriais têm de ser sujeitos a um processo eficaz de esterilização. No entanto, os hidrogéis de PVA podem ser sensiveis às altas temperaturas sentidas durante métodos de esterilização comuns como autoclave. Assim, há uma necessidade de desenvolver métodos alternativos de esterilização.

Neste trabalho, um novo hidrogél de PVA, reforçado com nanofibras de Zylon, pelo método "cast-drying", foi sujeito a três métodos de esterilização não convencionais: irradiação com microondas, alta pressão hidrostática (HHP) e descarga de plasma de Argon. Todos os métodos provaram ser capazes de esterilizar o material, mas criaram alterações nas suas propriedades. A irradiação com microondas aumentou a quantidade de ligações duplas nos hidrogeis e melhorou as propriedades mecânicas e tribológicas. HHP aumentou ligações singulares, o que melhorou a maioria das propriedades, excepto a resistência à compressão em cargas altas. O tratamento com plasma resultou na quebra de ligações, diminuindo as capacidades tribológicas e de carga do hidrogel. No entanto, a resistência à tração e cisalhamento mehoraram. Nenhum dos métodos induziu citotoxicidade. Os hidrogéis de PVA-Zylon após irradiação com microondas provaram ser os materiais mais promisores para substituição de cartilagem.

Palavras-chave: Cartilagem, esterilização de hidrogéis, PVA , microondas, alta pressão hidrostática, plasma

Abstract

Articular cartilage degradation is a recurrent pathology that affects millions of people worldwide. Being an avascular tissue it shows limited healing capacity, and current therapeutic strategies show several limitations. Hydrogels have gained great attention as possible cartilage substitutes, due to their biocompatibility and high water contents. Poly-vinyl alcohol (PVA) is considered one of the most promising hydrogels, however its mechanical properties hinder their application. Reinforcement of the PVA is required to tailor the hydrogels' mechanical properties. To be used in a clinical setting, biomaterials must undergo an effective sterilization. Common sterilization methods such as autoclaving can degrade heat sensitive PVA hydrogels, which justify the need to develop alternative sterilization procedures.

In this work, a novel PVA hydrogel, reinforced with Zylon nanofibers, obtained by cast-drying, underwent three non-conventional sterilization methods (i.e., microwave irradiation, high hydrostatic pressure (HHP) and Argon plasma glow discharge). All methods proved capable of sterilizing the material, but led to changes in its properties. Microwave irradiation increased the amount of double bonds, and improved the tested mechanical and tribological properties. HHP increased single bonding, which improved the tested properties, except the compressive stiffness at high loads. Plasma treatment resulted in breakage of bonds, thus decreasing the PVA-Zylon's tribological and load bearing capabilities, but improved both the tensile and shear resistance. None of the sterilization methods induced cytotoxicity. PVA-Zylon hydrogels after microwave irradiation proved to be the most promising materials for cartilage substitution.

Keywords: Cartilage, hydrogel sterilization, PVA, microwave, high hydrostatic pressure, plasma.

Contents

List of Tables

List of Figures

Nomenclature

Ω	Applied electric field strength
ϕ	Diameter
φ''	Dielectric loss factor
φ_0	Permittivity of free space
δ	Phase angle
ϵ	Strain
ψ	Shear strain
σ	Stress
τ	Shear stress
ACI	Autologous chondrocyte implantation
AS	As-spun
ATR	Attenuated total reflectance
BSA	Bovine serum albumin
BSE	Backscattered electron
CA	Contact angle
CAM	Chorioallantoic membrane
CASO	Soybean Casein digest Broth
CoF	Coefficient of friction
DD	Distilled and deionized
DMEM	Dulbecco's Modified Eagle's Medium
DMSO	Dimethyl sulfoxide

E Young Modulus

E_c Compressive Young modulus

E_t Tensile Young modulus

E_Σ Tangent modulus

ECM Extracellular matrix

EtO Ethylene oxide

EWC Equilibrium water content

f Frequency

F_N Normal force

F_T Frictional force

FS Frequency sweep

FTIR Fourier transform infrared spec-troscopy

G' Storage modulus

G" Loss modulus

G^* Complex shear modulus

GAG Glycosaminoglycan

HA Hyaluronic acid

HET-CAM Hen's egg test – Hen's egg test – chorioallantoic membrane

HHP High Hydrostatic Pressure

IS Irritation score

LF Loss factor

LMAEM Laboratory of Applied Microbiology of Egas Moniz

LVE Linear viscoelastic regime

MF Microfracture

MIR Mid-infrared

MSA Methanesulfonic acid

MTT 3-(4,5-Dimethylthiazol-2-Yl)-2,5-Diphenyltetrazolium Bromide

MW Molecular weight

OA Osteoarthrithis

OAT Ostheochondral autograft transfer

PBO Poly(p-phenylene-2,6-benzobisoxazol)

PBS Phosphate buffer solution

PG Proteoglycan

PGR4 Proteoglycan 4

Ph.Eur European Pharmacopoeia

PVA Polyvinyl alcohol

Q Volumetric heating rate

SAL Sterility assurance level

SAPL Surface active phospholipids

SC Swelling capacity

SE Secondary electrons

SEM Scanning electron microscope

SF Synovial fluid

SSF Simulated synovial fluid

T_C first appearance of coagulation

T_H first appearance of hemorrhage

T_L first appearance of lysis

TFA Trifluoroacetic acid

TIO Thioglycollate Liquid Medium

W_d Dry weight

W_w Wet weight

WC Water content

Chapter 1

Introduction

1.1 Topic Overview and Objectives

Articular cartilage is a highly hydrated connective tissue that covers the ends of bone in diarthrodial joints. It shows an extremely efficient aqueous lubrication, due to its biphasic composite structure, consisting on a porous elastic solid matrix containing interstitial fluid, and simultaneously exhibits high load-bearing and low-friction capabilities. In the event of physical injury or disease, the ability of cartilage to repair and regenerate is limited, due to its aneural and avascular nature. As such, the progression of the cartilage degradation is recurrent, and may lead to cases where patients are unable to carry out simple daily tasks. This entails a significant reduction of the patients' quality of life and it is turning into a prevalent occurrence in hospitals worldwide.

To date there is no cure for cartilages' degradation, and no satisfactory approach that can duplicate the normal tissue in a reduced post-operative period, that is capable of sustaining load at an early implementation state, while being cost-effective. Hence, there is an increase need for potential cartilage substitutes to treat the most severe lesions.

The unique biphasic and heterogeneous structure of articular cartilage proves to be a challenging task to replicate. Hydrogels have become a promising and attractive material, owing to their high water contents, porous structure and viscoelastic mechanical properties that resembles cartilage tissue. Among the different polymers that have been studied to produce cartilage substitution materials, polyvinyl alcohol (PVA) has deserved special attention. PVA hydrogels show excellent biocompatibility and non-toxicity, however, their mechanical and lubrication behavior are still inferior to those of natural cartilage. One strategy to reinforce PVA hydrogels relies in the addition of nano/micro fibers to the polymer network, mimicking the collagen fibers present in the extracellular matrix (ECM) of natural cartilage.

In order to be used in a clinical setting, implantable biomaterials sterilization is mandatory. Steam heat is one of the most used methods of sterilization due to its simplicity and easy access. However, PVA hydrogels are generally sensitive to heat, degrading or suffering significant changes. Besides, there are microorganisms that are resistant to high temperatures such as those used in steam heat sterilization (e.g. *Bacillus sp.* spores). Also, exposition to heat may be a drawback when considering the

incorporation of thermosensitive active agents (e.g. some drugs, growth factors). All these factors justify the need of developing alternative sterilization methods.

In this line, this work aims to study the effect of three non-conventional sterilization methods (microwave irradiation, high hydrostatic pressure (HHP) and glow-discharge argon plasma) on a novel Zylon^{TM} nanofiber-reinforced PVA hydrogel as cartilage substitution material. The efficacy of sterilization in the chosen conditions was accessed and the synthesized hydrogels were characterized in terms of their structural and mechanical properties, wettability, swelling capacity and rheological behavior, to evaluate possible effects due to the sterilization procedures. Finally, biocompatibility of the hydrogels was ascertained via irritability (HET-CAM test) and cytotoxicity assays.

1.2 Articular Cartilage

Diarthrodial or synovial joints are structural features that allow locomotion and other movements to occur between articulating bones. They are present in several locations in the human anatomy, namely ankle, elbow, hip, knee, shoulder, and in the fingers and wrists. One crucial component that constitute this complex system is the thin layer of hyaline, or articular cartilage, which covers the articulating ends of the adjacent bones. In major human joints (i.e., hips and knees), the articular cartilage thickness ranges between 1 and 4 mm in thickness and its main functions are the transmission of loads to the underlying subchondral bone, absorption of impact forces and promotion of a smooth, low-friction movement [1].

Cartilage mainly consists of a dense extracellular matrix (ECM) composed of a biphasic network of collagen fibers, glycosaminoglycans (GAGs), proteoglycans (PG), glycoproteins, water and electrolytes. This ECM is populated by a low volume ($\approx$2%) of cells (chondrocytes) [2] and is characterized by a limited capacity for healing due to its lack of blood and lymphatic vessels. The absence of a direct supply of nutrients and oxygen makes the cartilage solely dependent on an anaerobic metabolism to subsist. In the event of physical injury or disease, the ability of the tissue to repair and regenerate is limited, difficult and sometimes inefficient. Thus, a thorough understanding of the composition, structure and properties of articular cartilage, is crucial in order to hopefully develop biomaterials that can efficiently substitute it.

1.2.1 Composition

The ECM of cartilage accounts for its biomechanical properties, combining compressive stiffness, resilience and shear resistance. From a materials perspective, two phases can be recognized within articular cartilage [3]: 1) a solid phase, composed of a network of collagen fibers, mainly type II, filled by GAGs, PGs and some small amount of glycoproteins and 2) a liquid phase of water and electrolytes (e.g. Ca^{2+}, K^{+},Na^{+}, Cl^{-}), where all the solid components are immersed. Water accounts for $\approx$65%-80% of the wet weight of the articular cartilage (i.e., depending on structural layer, person's age, underlying pathologies and others) and provides a transport environment for oxygen and nutrients, needed for chondrocyte´s activity and survival. The diffusion and mass transport across the ECM occurs during compression-relaxation movements of the tissue [4]. In mature cartilage, collagen type II fibers take

approximately half of the dry weight of the matrix , however, collagens types VI, IX, X and XI can also be found [5]. Type II collagen presents a high amount of bound carbohydrate groups, which allow more interactions with water than some other types. Types IX and XI, along with type II, form interweave to form a mesh, providing tensile strength and physical entrapping of other macromolecules. PGs are the third most prevalent macromolecule present in articular cartilage, accounting for 10-15 $\%$ of its dry weight and are crucial to sustain the balance of fluids and electrolytes within the tissue [6]. They are composed of one or more GAG chains covalently attached to a protein core [3]. These GAGs, in turn, are composed of repetitive disaccharide units, containing sulphated hexoamines, chondroitin sulphate and keratin sulphate. Figure 1.1 shows the various structural features of articular cartilage at different scales.

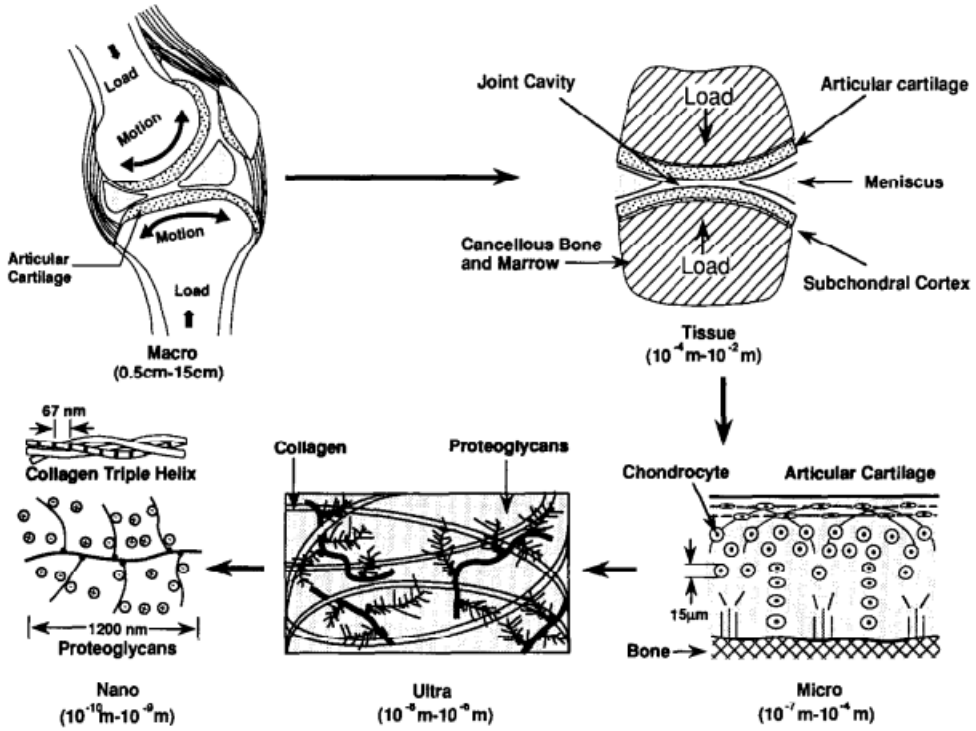

Figure 1.1: Structural features of articular cartilage at different length scales [7]

Depending on the organization of its components, cartilage ECM can be divided into different regions [8]: 1) The pericellular region, composed mainly of PGs and characterised by the presence of collagen type VI, which creates a 2 μm wide protective capsule for cells, and acts as a transducer of biochemical and biomechanical signals; 2) The territorial region, defined by a high content of PGs rich in chondroitin sulphate and thicker collagen fibers than in the pericellular region; and 3) The inter-territorial region, which is rich in thick collagen fibers and PGs that contain keratin-sulphate.

The ECM of healthy cartilage tissue is populated by a low volume (i.e., occupied volume ≈2%) of a mature, highly specialized cells, which are responsible for its production and repair, by replacing degraded matrix molecules, thus maintaining the correct size and mechanical properties of the tissue [9]. Due to their common derivation from mesenchymal stem cells, articular chondrocytes are classified

as a single cell type, but show significant differences in morphology, density and organisation across the depth of the cartilage. This heterogeneity is related to differences in the orientation of collagen fibers, proteoglycan distribution and strain during loading [3].

1.2.2 Structure

Articular cartilage shows an elaborate compartmental structure, histologically arranged in four distinct and parallel parts in accordance to the orientation of the collagen fibers, starting at the surface of the articulation and ending at the connection to the subchondral bone (see Figure 1.2). The separation between each histological zone is gradual, as each zone merges in the subsequent zone as the collagen fibers change their arrangement.

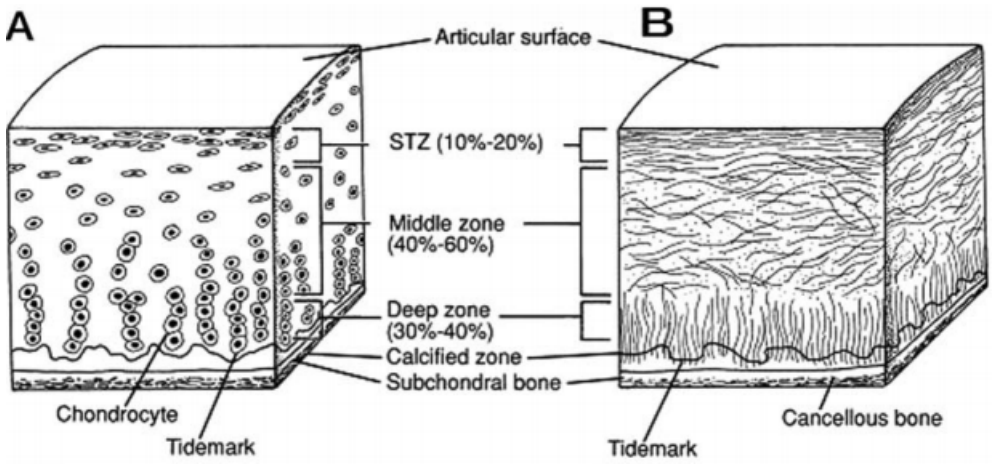

Figure 1.2: Diagrammatic representation of the zones of articular cartilage and subchondral bone [1]

The superficial layer is composed of collagen fibers aligned parallel to the surface of the joint, populated by high-density flat chondrocytes (alongated across their axis). The presence of the lubricating protein proteoglycan 4 (PGR4), also known as lubricin, is typical of this zone and contributes to the low friction that is necessary in diarthrodial joints. The fibers horizontal conformation provides the superficial zone with the highest tensile properties, ensuring high resistance against mechanical tensile forces caused by the sliding between opposite ends of the articulation joint. Also, it prevents the entrance and exit of molecules with diameters higher than 6 nm, allowing for the maintenance of PGs aggregates inside the ECM. The superficial zone shows the highest water content ($\approx$80%), and the lowest concentration of PGs of all the cartilage layers [3].

Beneath the superficial zone lies the middle zone, populated by spherical chondrocytes with an ECM composed of a disorganized collagen network made up of thicker fibers. This zone provides a functional bridge between the superficial and deep zones. The deep zone is characterized by large sized chondrocytes surrounded by a pericellular matrix containing collagen type VI, that form a composed unit known as a chondron [3]. Parallel to stacks of these chondrons run vertical oriented thick collagen fibers. In this zone, the PG content is at its highest, while the water content is at its lowest ($\approx$65%). These perpendicularly oriented fibers have the maximum diameter within the structure of articular cartilage,

and provide the greatest resistance to compressive forces.

The interface between cartilage and subchondral bone is known as calcified cartilage and has a peculiar composition in GAGs and glycoproteins. It gets its name from the presence of a thin calcification front, visible as a thin line (tidemark) following haematoxylin staining. In this tidemark, non-mineralised cartilage matrix starts to contain hydroxyapatite and in its vicinity, enhanced metabolic activity (consistent with mineralization) has been found, such as alkaline phosphatase expression, the ability to bind tetracycline *in vivo* and collagen type X deposition [10]. As this is the interface between the soft cartilage and the much stiffer bone, significant shear stresses can be produced in this area. The chondrocytes here are smaller, showing almost no endoplasmatic reticulum and in some places, seem to be completely surrounded by a calcified ECM. Additionally, the calcified zone stabilizes and secures the articular cartilage to the subchondral bone through collagen fibers strongly anchored to the bone, by forming arcade shapes designated as the Benninghoff's arcades [11].

In summary, articular cartilage shows a complex architecture which allow it to resist different types of forces. Close to the surface its ECM is denser and smoother while in deeper zones becomes more porous, the innermost part providing tissue stabilization through the anchoring of the collagen fibrils to the subchondral bone.

1.2.3 Properties

Lubrication

As articular cartilage covers the surface of bones in the articulating joints of the body, it is constantly subjected to cyclic loads. Major human joints such as knees and hips are remarkable biotribological systems, able to withstand large local pressures while exhibiting extremely low coefficients of friction (CoF) and almost no damage. These properties are made possible due to a synergistic interaction between cartilage tissue and the synovial fluid (SF), which acts as a biological lubricant, providing low-friction and low-wear properties to the contacting surfaces of the articular cartilage. SF shows a shear-thinning behavior, thus at high shear rates and sliding velocities its viscosity decreases [12]. Additionally, SF functions as a biochemical pool, through which nutrients and regulatory cytokines are transported to the connected tissues. The low friction environment is created due to the shared contribution of PGR4 (i.e., lubricin), hyaluronic acid (HA) and surface active phospholipids (SAPL). The bottle-brush-like PGs known as aggrecans also play a role in the lubrication of joints [6]. The main source of lubricating molecules in the SF are synoviocytes, cells present in the synovial membrane, although chondrocytes in the superficial layer of cartilage also contribute to their production [13]. Table 1.1 shows the range in concentrations of the lubricating molecules present in the SF.

Articular cartilage can operate in different lubrication modes, depending on the type of musculoskeletal movement. Those lubrication regimes can be correlated with how CoF depends on the sliding speed, applied normal force and viscosity of the fluid between the sliding surfaces (Stribeck curves). In general, three distinct lubrication regimes can be defined: a) boundary lubrication; b) mixed lubrication and c) elasto/visco-hydrodynamics lubrication (Figure 1.3). The boundary lubrication regime is characterized

Table 1.1: Concentration of lubricating molecules in synovial fluid, [13]

Molecule	Concentration in SF (mg/ml)
PGR4	0.05-0.35
Hyaluronic Acid	1-4
SAPL	0.1

by a monolayer or absence of a fluid film between the contacting surfaces, and usually occurs in heavy loads and low shear rate conditions. Dissipation of the friction forces typically occurs by molecular rearrangements and deformations [6]. The mixed lubrication regime, as the name implies, works in a mixed regime between the boundary lubrication and the hydrodynamic lubrication, i.e., the opposing surfaces can be in direct contact or completely separated by a thick fluid film. Elasto/visco-hydrodynamics lubrication, also known as fluid film lubrication, occurs at low applied forces or high sliding speeds, and is characterized by separation distances larger than the surface roughness and thicker lubricating layers [14]. In this regime, the applied loads are dissipated by hydrostatic, hydrodynamic and elastohydrodynamic forces in the fluid leading to lower friction coefficients [15].

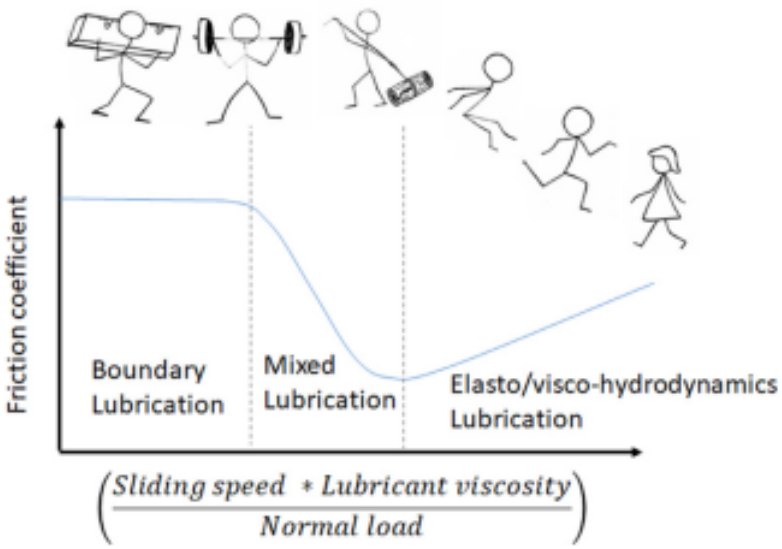

Figure 1.3: Schematic representation of the Stribeck curve for lubrication regimes correlated with typical human movements [15]

In order to better understand the complex lubrication mechanism of synovial joints, different theories have been proposed [16]. The early weeping theory suggests that cartilage on cartilage contact is prevented by local fluid exudation and interstitial fluid flow, resulting from the compression of asperities on opposing cartilage surfaces upon contact [17]. The boosted or ultrafiltration theory, on the other hand, proposes that loading creates a pressurization of SF towards the inside of the cartilage structure, promoting a sieving effect on cartilage pores. This leads to an enrichment of lubricating macromolecules at the synovial interface, preventing direct cartilage-cartilage contact [18].

The symbiotic association of the lubricant molecules that compose the SF favours the movement

between the cartilage surfaces, reducing shear stress. As such the fluid shows a stress shielding effect that reduces the damage articular cartilage endures [19]. Additionally, at higher applied loads, liquid is often expelled from the ECM of cartilage due to fluid pressure. As we will see in the next section, this process plays a crucial role in the overall capacity of the articular cartilage to bear large applied loads [20].

Load Bearing

Articular cartilage cushions the impact and maintains the separation of underlying bone surfaces under static and dynamic loads. This ability is a conjugation of the biphasic and viscoelastic nature of this tissue. Its elastic component grants it enough stiffness to support static load of the joints while the viscous component provides damping of dynamic forces during movement [21].

The heterogenous structure of hyaline cartilage means it shows anisotropic and nonlinear properties in compression and tension. In order to quantify and interpret the mechanical properties of this tissue, complex biomechanical models have been developed. One such model that explains the viscoelastic behaviour of articular cartilage against loads is the biphasic poroelastic theory developed by Mow et al. [22]. In this theory, articular cartilage is modeled as a composite material, consisting of a porous and elastic solid phase (i.e., PGs, collagen, cells and lipids) and a fluid phase (i.e, interstitial fluid) that moves through the matrix. Within the loaded tissue, three major internal forces occur: 1) stress within the deformed collagen-PG matrix; 2) pressure in the fluid phase and 3) frictional drag between fluid and solid phases. Thus, the mechanical response of articular cartilage is caused by two separate mechanisms, flow dependant and flow independant [21].

In the flow-dependent mechanism, as cartilage is compressed, the interstitial fluid pressure sharply increases and the ECM starts to consolidate. Liquid will start to be expelled from the ECM and the cartilages' volume will decrease, which will counteract the compressive forces. As the rate of displacement slows down, so does the fluid flow, until the tissue reaches a state of equilibrium and the load is resisted entirely by the solid matrix. When the compressive load is removed, the osmotic pressure drops and the fluid flows back from the inner joint space into the cartilage tissue [23]. This time-dependant response to loading is highlighted in Figure 1.4.

The flow-independent component relates to the intrinsic viscoelasticity of the solid collagen-PG matrix. As this matrix is compressed, the negatively charged sites on aggregated PG molecules are pushed together, until the repulsive forces are high enough to counteract the compressive load [21]. Research supports the idea that the interstitial fluid pressurization mechanism supports most of the load transmitted across the articular layers, even in the case of unconfined compression, especially in the more superficial layers of cartilage [24]. Nevertheless, the capacity of articular cartilage to bear the applied load is therefore a combination of load transfer and fluid pressurization. As such, cartilage is able to resist to compressive, tensile and shear loads [20]. Additionally, ligaments, tendons, muscles and bones, directly involved in the synovial joint allow the reduction of the devastating impact of abnormal movements, as well as permitting load transfer [1].

Measuring and characterizing the time-dependant or transient responses of articular cartilage is a

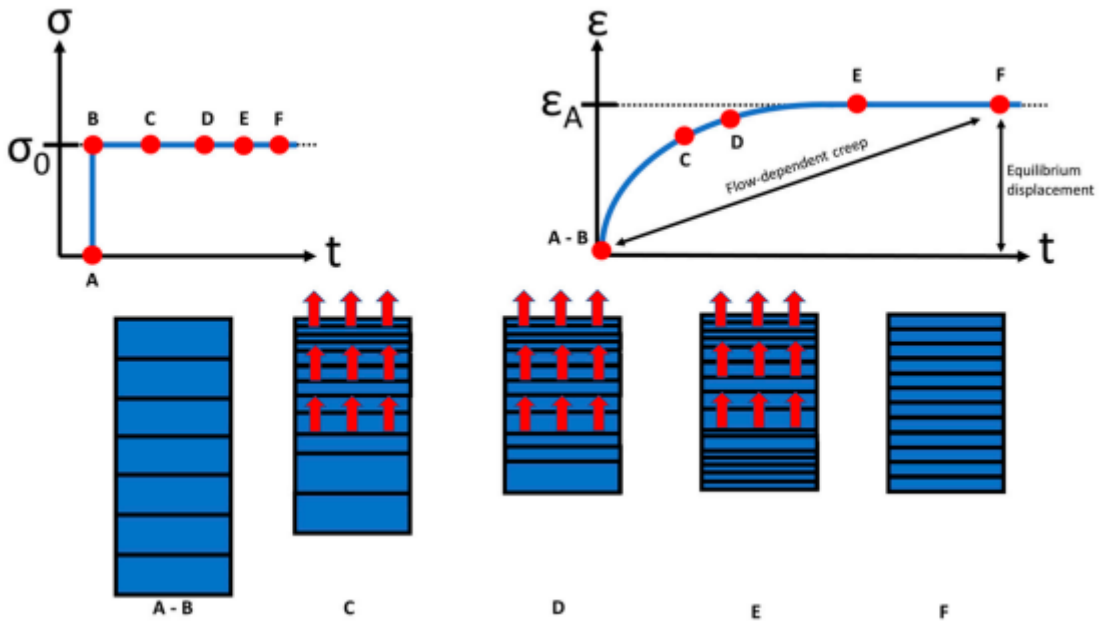

Figure 1.4: Fluid flow due to creep response ϵ of cartilage tissue under a constant load σ_0, from [21]

complex endeavour, especially in an *in vivo* environment. A large dispersion is found on the measured mechanical properties between different studies. Differences in test type, conditions and data analysis, as well as variations in tissue, i.e. origin (animal vs human), location, type and donor age, all significantly alter the results. Nonetheless, a range of the biomechanical values for articular cartilage is reported in Table 1.2.

Table 1.2: Biomechanical properties of natural articular cartilage

Property	**Value**	**Source**
Young Modulus (Compressive)	0.24–0.85 Mpa	[25]
Young Modulus (Tensile)	5–25 MPa	[25]
Complex Shear Modulus	0.2–2.5 MPa	[25]
Tensile strength	0.8-25 MPa	[25]
Poisson ratio	0.06–0.3	[25]
Shore A Hardness	87.5	[26]
Hydraulic Permeability	10^{-16}-10^{-15}	[25]
Water Content	65-80%	[3]
CoF	0.001-0.03	[6]

1.2.4 Pathologies

The synovial joint can be affected by several genetic conditions, mutations, tumors, and external physical injuries that lead to severe damage to the articular cartilage. Being aneural, some cartilage diseases may remain symptom free until irreparable damage occurs and be too late to proceed to early-stage

treatments. Moreover, due to the avascular and alymphatic nature of articular cartilage, it also shows a low capacity for regeneration, which impairs treatment. Early stage diseases are characterized by a rise in the water content of the ECM, cleavage of the collagen network, activation of the chondrocytes matrix synthesis and loss of mechanical stress resistance [26].

Two main types of chondral injuries can be identified [27]: traumatic lesions, usually caused by high intensity sports activity, and degenerative arthritis, also known as osteoarthritis (OA). OA is a degenerative disease that alters the mechanical and rheological behavior of the SF, causing musculoskeletal disorders, pain and limiting mobility. The hip and knee joints are the most commonly affected, due to the large loads sustained, but other joints can also be severely affected. OA is thought to result from a set of events, starting with damage to the cartilage tissue, which results in a disruption of the lubricating mechanism. This disruption, in turn, causes progressive damage to the cartilage and subchondral bone. The onset of OA may lead to significant changes in the concentration of important regulatory cytokines in the SF such as TGF-β, IGF1, TNF-α, IL-1 and IL-6 [13], affecting the secretion of lubricating molecules by cells. The lower concentration of PGR4, HA and SAPL in the SF, leads to a reduction of its friction lowering capabilities and the subsequent erosion of articular cartilage surfaces. The damage to the cartilage tissue can also result in the loss of chondrocytes, compromising even further the maintenance and synthesis of the ECM. Moreover, as the mechanical response of cartilage is different, the chondrocytes being mechanosensitive can inevitably show inadequate mechano-responses to the ECM needs [9]. Conventional OA treatment aims to reduce severe pain and restore mobility to the joints with common non-surgical treatments including the use of non-steroidal anti-inflammatory drugs (NSAIDs) and intra-articular injection of hyaluronic acid to restore the rheological properties of the SF [15].

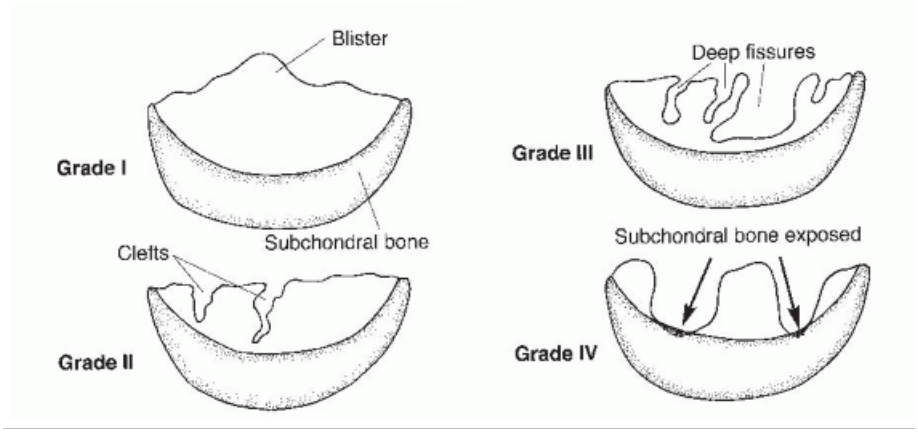

Figure 1.5: The Outerbridge classification for articular cartilage lesions, taken from [28])

The severity and complexity of defects in this tissue are typically graded based on the depth of the injury (see Figure 1.5) [28, 29]. Grade I defects are very mild and are characterized by a softening of the tissue; Grade II includes fissures or craters, with depths less than half of the full thickness; Grade III are deep defects, present throughout most of the thickness of the cartilage tissue; Grade IV, the most severe, refers to lesions in the full thickness of the tissue, where the underlying bone is left exposed. If the bone is also affected, these injuries are designated as osteochondral injuries. Severe injuries become more

prevalent in older patients. A review of 31,516 knee arthroscopies from Curl *et al.*[30] reported articular cartilage lesions in 63% of patients. Of these, 19% were found to have Grade IV lesions but only 4% of those patients with severe defects were younger than 40 years of age. Similarly, another study, from Hjelle *et al.* [31], reviewing 1000 knee arthroscopies, reported cartilage lesions in 61% of patients of which only 5.3% were younger than 40 years of age.

Overall, articular cartilage lesions have become increasingly more widespread due to the increase in life expectancy and obesity in the population worldwide. As this load bearing tissue lacks the healing response found in other natural body tissues, the need for improved techniques to repair function to patients is further exacerbate.

1.2.5 Treatment

Total joint arthroplasty is the common procedure to deal with the most dramatic situations of joint damage. However, whenever it is possible, more conservative approaches are followed. In recent years, several interesting strategies, focusing on biomechanics, biomaterials and tissue engineering, as well as improved surgical techniques, have emerged for cartilage tissue repair. Various surgical treatment options can be considered for symptomatic focal articular cartilage defects [32]. Arthroscopic marrow stimulation and microfracture (MF) techniques perforate the underlying bone, promoting blood clot formation and eliciting a migration of mesenchymal stem cells in the bone marrow to repair the defect. Another technique, known a autologous chondrocyte implantation (ACI), involves the reinjection of chondrocytes from the patient, usually harvested from a biopsy of a non-load bearing area of cartilage and expanded *ex vivo* [27]. In more severe, Grade IV lesions, where the subchondral bone is affected, osteochondral autograft transfer (OAT), or mosaicplasty, is usually employed. This technique involves the transfer of mature autologous cartilage tissue from non-load bearing regions, to the injured area [33].

However, these techniques show some disadvantages. In MF and ACI, the newly formed tissue lacks the structural organization of the collagen network that characterizes healthy cartilage ECM, especially in patients over 50 years of age, due to limitations of the stem cells' and autologous chondrocytes' potential to proliferate and differentiate [27]. In the case of OAT, it involves the transfer of healthy tissue from the same patient, increasing surgical risks and might not be adequate for larger defects, due to the limited amount of transplant material. Thus, there is still a need for improved strategies to impair the progress of cartilage defects to an eventual catastrophic failure, and allow to restore a proper joint functionality to the patients.

1.3 Strategies for Cartilage Substitution

An alternative treatment option to circumvent the current downsides of the available treatments, and avoid the need to resort to total joint arthroplasty, is the use of synthetic materials to substitute the articular cartilage [34]. The substitution can be either by filling the defect, or in the form of a hemiarthroplasty counterface or even through an interpositional device to alleviate pain and/or correct joint deformity [35].

These materials should be biocompatible and show mechanical properties resembling the native tissue. If the dissipation of energy is not sufficient to counterbalance friction forces, molecular bonds start to irreversibly break, forming wear debris. Major failure mechanisms of orthopedic implants are caused by the formation of wear debris, which cause a biological response and the activation of macrophages, releasing inflammatory agents that can lead to bone resorption and implant loosening [6, 7, 36].

The unique biphasic and heterogeneous structure of articular cartilage proves to be a challenging task to replicate. Hydrogels in particular, have become a promising and attractive material, owing to their high water contents, porous structure and viscoelastic mechanical properties, making their structure more similar to natural human tissues. Nevertheless, their mechanical properties usually hinder their applicability as cartilage substitutes, as these materials will be subjected to harsh continuous mechanical cycles. However, recent strategies have been studied to improve the mechanical properties of the hydrogels, by tailoring the materials towards biomimicry of the articular cartilage [37].

1.3.1 Hydrogels

Due to the structural similarity between hydrogels and cartilage and in particular to their swelling capacity, hydrogels have been regarded as quite promising materials for cartilage substitution, and have been target of many studies [38]. Hydrogels have a wide range of tunable parameters (including polymer chemistry, crosslinking density, degradation, mechanical properties, and release kinetics of biochemical factors). Hydrogels have evolved from simple crosslinked monopolymer structures, with simple chemical modifications, to complex engineered co-polymer materials that can mimic natural tissue properties and function. Some can even be made to respond to environmental stimulus (e.g., light, temperature, pressure, electric and/or magnetic fields, pH, solvent composition, and recognition of ions and specific molecules) and change their structural properties accordingly (i.e. "smart hydrogels") [39, 40]. The increasing knowledge and control over materials chemistry and biological response has enabled the creation of versatile biomaterials to be used for healthcare applications [41].

Hydrogels can be categorized in two main groups, depending on the type of bonds that constitute its network: 1) chemically crosslinked hydrogels, and 2) physically crosslinked hydrogels. Chemically crosslinked hydrogels are characterized by strong and stable covalent bonds, while physically crosslinked hydrogels show physical entanglements between the polymer chains, such as hydrogen bonding and electrostatic and hydrophobic interactions [42]. Hydrogels can also be classified depending on their source (natural, synthetic or hybrid), sensitivity to stimulus (physical, chemical, biochemical) and polymer network charge (nonionic, ionic, zwitterionic and amphoteric). These materials can even be classified according to their physical appearance (micro/nano particle, film, matrix, gel) and configuration of chains (amorphous and semicrystalline) [43].

The most distinguishing feature of hydrogels is the presence of hydrophilic functional groups attached to the polymeric backbone, which allows them to absorb and retain significant amounts of water. The presence of crosslinks between network chains prevents the material from dissolving, and grants it a solidified shape. This process happens in three steps [43]: 1) diffusion of water molecules; 2) relaxation

of polymeric chains through hydration and 3) expansion of the crosslinked polymer network. Hydrogels can absorb water up to a maximum level, known as equilibrium water content (EWC), that depends on the polymer-water interaction, as well as the density of crosslinking in the material [41].

To be used as cartilage replacement materials, hydrogels must present adequate mechanical and tribological properties, while maintaining high water contents and biocompatibility. In that line, several different hydrogel materials have been studied for cartilage substitution applications, from natural polymers such as collagen, chitosan and silk fibroin, to synthetic materials such as Poly(ethylene glycol) (PEG) Poly(glutamic acid) (PGA) and PVA [37].

PVA Hydrogels

One material that shows great promise, and has been extensively studied as a possible cartilage replacement is PVA, a synthetic hydrophilic polymer that shows excellent biocompatibility, tunable swelling and mechanical properties, and some level of biodegradability. PVA powder is typically produced by removing the acetate groups of polyvinyl acetate by partial or full hydrolysis (see Figure 1.6) [44]. The vast number of hydroxyl side groups in PVA allows it to form a semi-crystalline structure through intramolecular hydrogen bonding, forming hydrogels which can be used as a biomaterial [45].

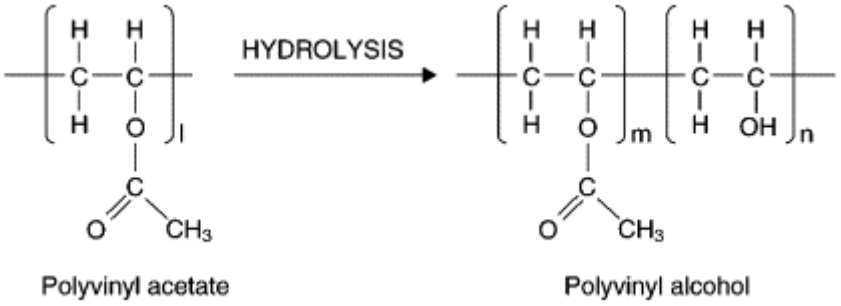

Figure 1.6: Chemical structure of PVA, adapted from [46]

PVA hydrogels can be crosslinked via both chemical, physical or irradiative methods. For the first, chemical agents such as borates, glyoxal and aldehydes are used, in conjunction with methanol, acetic acid or sulfuric acid, creating acetal bridges between the pendant hydroxyl (-OH) groups of the PVA chains [43]. The main drawback to this method is the possibility of leaving toxic residues, compromising the biocompatibility of the hydrogels. Irradiative techniques, using electron beam or gamma radiation can also be employed to further crosslink the hydrogel. This approach does not leave toxic residues and has also been shown to improve cellular adhesion [43, 47], however, they can be expensive and require specialized personnel and equipment. Meanwhile, physically crosslinked PVA gels can be formed through the cast-drying, freeze-thawing, freeze-drying and theta gelation methods [43, 48, 49, 50]. These physically crosslinked hydrogels usually present a high degree of swelling, elastic nature and higher mechanical strength when compared to chemically crosslinked PVA gels [43]. Cast-drying and freeze-thawing are the most common methods to create these hydrogels, of which cast-drying was found to create

structures that more closely resemble natural cartilage tissue, in terms of morphology, water content and mechanical and tribological properties [51].

Overall, the properties of PVA hydrogels can be modified and affected due to changes in the molecular weight, degree of hydrolysis and initial concentration of the polymer, the method and conditions used for crosslinking, as well as, the addition of other compounds into the matrix [51, 43]. The tunable characteristics of PVA hydrogels, combined with its excellent biocompatibility have led to their development for several biomedical applications, such as contact lenses, artificial pancreases, hemodialysis membranes, and implantable cartilage-substitute biomaterials [44]. For its use as a substitute of cartilage tissue, however, simple PVA hydrogels usually lack sufficient mechanical response to resist the high loads felt in diarthrodial joints [52]. Depending on their production method, PVA hydrogels can also show inadequate wear resistance which can lead to delamination and eventually, the formation of wear debris and inflammatory response, when subjected to repeated cyclic loading against harder cartilage surfaces [53].

In summary, hydrogels for cartilage replacement must ensure a set of properties to avoid malfunction. As PVA hydrogels can lack the load-bearing capability and wear resistance necessary, tailoring of this polymer is mandatory. Thus, different strategies have been used to improve the hydrogel's mechanical properties, such as thermal annealing [35, 54] or the introduction of nanofibers or nanoparticles into the hydrogel matrix [55, 56, 57, 58].

Reinforced hydrogels

While thermal annealing of PVA hydrogels has been shown to increase their mechanical resistance [35], the process usually leads to a reduction in porosity, lowering swelling and lubricity of the hydrogels [54]. As such, other strategies have been pursued, namely the introduction of other materials in the hydrogel's matrix, usually in the form of nano/micro fibers, mimicking the natural collagen fiber network found in cartilage ECM. Different nanofiber materials have been studied for the reinforcement capabilities on PVA hydrogels, such as boron nitride [55], cellulose [56, 57] and carbon nanotubes [58]. In this thesis, the studied material is a novel PVA hydrogel, which has been reinforced with Zylon^{TM} nanofibers, a rigid-rod polymer known to present the highest tensile modulus of all commercially available fibers.

Zylon fibers

Poly(p-phenylene-2,6-benzobisoxazole) (PBO) (trade name Zylon^{TM}) designates a range of synthetic thermoset liquid-crystalline polyoxazoles, invented and developed by SRI International in the 1980s and first commercialized in 1998 in Japan, by the Toyobo Company [59]. Zylon fibers are typically synthesized by polycondensation of AA-type monomers and BB-type monomers. The key monomer (BB-type) for PBO is 4,6-diaminoresorcinol (DAR), typically synthesized using resorcinol and di- or trichlorinated benzenes as starting materials. AA-type monomers can include terephtalic acid (TA) and terephthaloyl chloride (TC) [59].

Zylon (PBO) fibers show extremely high tensile strength, in the order of 5.8 GPa [60], which is 1.6

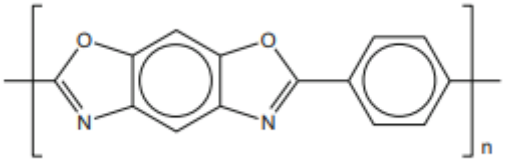

Figure 1.7: Chemical structure of PBO fibers [59]

times higher than that of another well known high strength fiber, Kevlar^{TM}. It's tensile Young's modulus, is approximately 180 or 270 GPa, depending on the type of zylon fiber, "as spun" (AS) or "high modulus" (HM) respectively. Zylon's compressive strength is significantly lower than its tensile strength, ranging from 0.469 to 0.561 GPa. Zylon also shows thermal stability up to 650ºC [61]. These fibers have also been found to suffer from photoaging, a common phenomenon which affects many polymeric materials. It is caused by exposure to sunlight, which can change some of their chemical, physical, and mechanical properties.

Commercial Zylon microfibers can be disintegrated into uniform nanofibers by a treatment with strong acids or NaOH [61], allowing them be dispersed in polymeric solutions. The length, diameter and size uniformity of the nanofibers can be controlled by adjusting the conditions of the acidic treatment (concentration, acid-polymer ratio and treatment time). In a downsizing process of Zylon fibers using NaOH by Ifuku *et al.* [62], FTIR analysis indicated that the treatment induced a partial alkaline hydrolysis in the oxazole ring of PBO, converting it into carboxyl, amino and phenolic hydroxyl groups. These charged functional groups originated repulsive electrostatic forces between fiber surfaces, allowing the disintegration and homogeneous dispersion of the microcrystalline fibers into nanofibers . The authors found that the Zylon nanofibers exhibited high cationic charges at low pH (+56.6 mV, pH=3.1), and high anionic charges at high pH (-32.1 mV, pH=9.1). Thus, the mechanism of downsizing Zylon fibers should be similar (albeit resulting in opposite charges and different functional groups) when using strong bases or acids [61].

1.4 Sterilization of Hydrogels

In order for any biomaterial to be used in clinical trials, it has to first obtain approval from regulatory organizations (e.g., ERS–Entidade Reguladora da Saúde, Portugal and ECDC-European Centre for Disease Control, European Union). Sterilization is a crucial and mandatory step for biomaterials intended for articular cartilage replacement, and as any biomaterial for direct contact with biological fluids/tissues should follow international norms (e.g., EN 556-1:2001/articular cartilage:2006 –Sterilization of medical devices). First, to obtain this approval the material is required to withstand an efficient sterilization, in order to minimize the incidence of medical device-related infections.

Briefly, sterilization corresponds to any chemical or physical process that allows the elimination/removal of all living microorganisms, including virus. Absolute sterilization cannot be proven. As such, the safety

of a sterilization method is given by a statistical probability known as sterility assurance level (SAL). SAL expresses the probability of a certain medical product being non-sterile after being submitted to a validated sterilization process. This probability should be as low as possible but can never reach zero. For example, the SAL for materials that have contact with blood is a minimal of 10^{-6}, i.e., the probability of the material not being sterile is one in a million [63]. We can obtain a sterile product by either aseptic processing or terminal sterilization. In the first case, all the materials involved in product manufacturing (e.g. raw materials, drugs, containers and closures) are sterilized separately, and then brought together to construct the final product, in optimized conditions by handling in a clean room, so as to maintain the product's sterility. This method is prone to failure, and used mainly for materials incapable of sustaining the harsh sterilization process currently available [64]. In terminal sterilization, the final product is sterilized in its final container, in one single step, in other words it eliminates the existing inherited microbial load (i.e., bioburden) of the material.

Despite the beneficial properties of hydrogels for many biomedical applications, they are known to be sensitive to conventional sterilization methods [65]. Terminal sterilization methods can induce negative or positive effects on several of the material's properties (e.g. aspect, size, color, chemical structure, mechanical integrity, and biocompatibility). The presence of water in hydrogels makes their sterilization even more complex, as the water molecules may potentiate the harmful effects of the procedure such as breaking of chemical bonds. Due to the complexity of the involved factors, it is virtually impossible to predict the precise outcome of a specific sterilization method on a biomaterial. Thus, each system requires a case-by-case testing in order to select which method is more suitable to sterilize a given material, without altering its main properties [66].

1.4.1 Commonly Used Methods

Several sterilization methods are currently available, and can be differentiated according to the sterilization agents involved (Figure 1.8). The most commonly used method for sterilization in laboratories is steam heat and pressure by autoclaving. This technique uses moist heat, in the form of saturated pressurized steam and is recommended to be performed for 15 min at 121-124ºC, with a pressure of 10^5 Pa [67]. These conditions effectively destroy all microbes, spores and viruses on the material, by irreversibly denaturating and coagulating their structural proteins and enzymes. This method is highly trustworthy, non-toxic, inexpensive and user friendly, and has been used for more than a century to sterilize all sorts of biomaterials and medical equipment. However, the high temperatures (>120ºC) felt during this process can lead to a degradation of some heat-sensitive hydrogels [68].

Another commonly used method for sterilization is exposing the biomaterials to ionizing radiation, namely radioisotope decay (gamma irradiation) and energized electrons (via an electron accelerator). Sealed radiation sources produce highly penetrating radiation, that collide with atoms, causing a loss of the bound electrons, a process known as ionization. Gamma irradiation is usually produced by using a radioactive source of cobalt 60 (^{60}Co). The reference sterilization is a dose of 25 kGy, however other doses can be applied depending on the biomaterial's bioburden and its resistance to radiation [67]. This

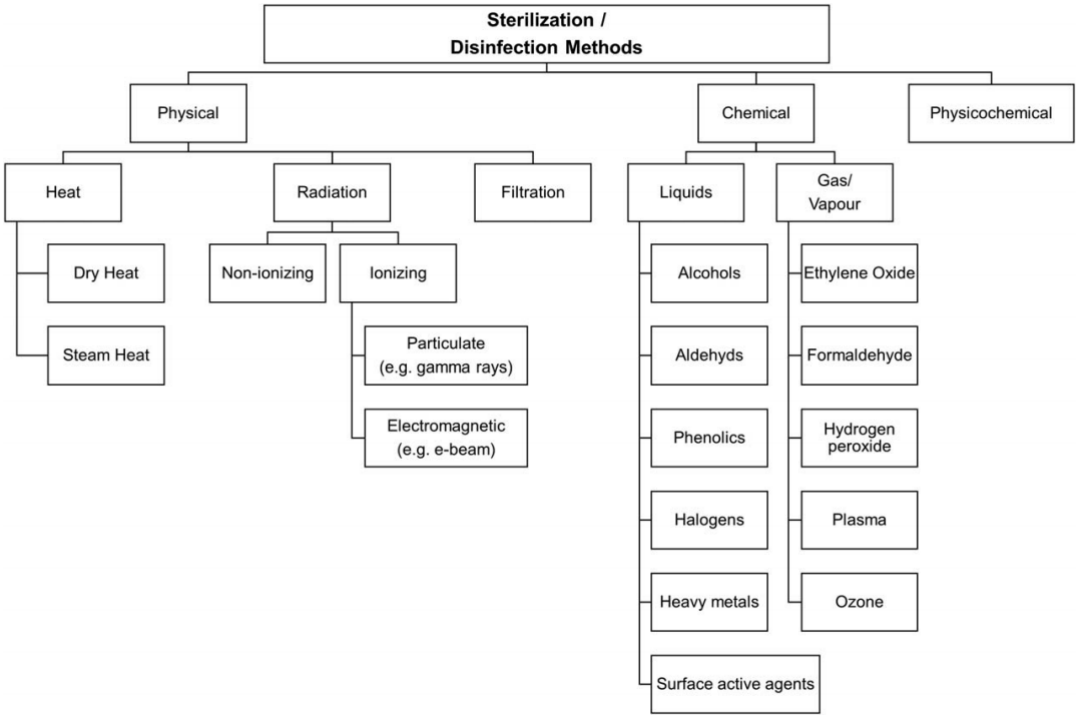

Figure 1.8: Commonly used methods for disinfection and sterilization of medical devices, taken from [67]

method leads to damage in the DNA chains or vital functions of microorganisms, resulting in their inactivation. The procedure is highly penetrating, enabling the biomaterials to be efficiently sterilized inside their final packaging, as the highly energetic radiation is able to cross through the molecules of the packaging material. However, the highly energetic nature of the radiation will, in most cases, inevitably affect the structure of polymeric materials, leading to changes in their physio-chemical properties. Concerning PVA hydrogels, for example, this technique has been found to induce further crosslinking of the hydrogels [43]. Overall, this method shows high penetration, good assurance of product sterility, no chemical residue, the ability to operate at low temperatures, and the immediate availability of the product after sterilization. Nevertheless, gamma irradiation is a complex method, it is expensive, requires well trained staff and highly specialized equipment, and can result in undesirable changes in the irradiated products [69].

For materials that are sensitive to heat or radiation, gas sterilization with highly reactive substances can serve as an alternative method to ensure a sterilized product. Ethylene oxide (EtO), ozone, hydrogen peroxide (H_2O_2) and formaldehyde are some of the commonly used substances for gas sterilization. The efficiency of the process depends on the gas concentration, humidity, exposure time, temperature and the nature of the bioburden [70]. The exact sterilizing mechanism depends on the used substance, and can involve oxidation or alkylation of chemical groups that damage proteins and nucleic acids. It is important to ensure that residues from the procedure are eliminated after exposure, as this method can cause some deposition of volatile residues on the materials surface, negatively affecting their biocompatibility. The low temperatures and compatibility to most products make this method attractive for

heat or radiation sensitive devices, however, some of the used reagents, like EtO, raise some safety concerns, as it is a flammable, toxic and carcinogenic substance. Moreover the toxic residues require lengthy aeration time to be removed, which make this a time-consuming process [71, 72].

Biomaterials can also be sterilized/disinfected by performing liquid chemical washes, using alcohols, aldehyds, phenolic, halogens and heavy metals, each causing specific consequences that cause cellular death. Alcohols in aqueous solutions at 70% (e.g., ethyl, isopropyl or methyl alcohol) are more effective at killing microbes than when in pure concentration [67]. They cause the dehydration of cells, disrupting the cellular membranes and causing proteins to coagulate. Phenols disrupt the cellular membrane, precipitate proteins and inactivate enzymes. Both alcohols and phenols are bactericidal, fungicidal, and mycobactericidal but are ineffective against spores and most viruses [73]. Concerning PVA hydrogels, Sasaki *et al.* showed an increase in the materials' rigidity and frictional behavior after chemical treatment with ethanol [74]. Aldehydes, on the other hand, are alkylating agents which damage nucleic acids, and so are capable of killing all microorganisms, even spores. Contrary to volatile alcohols, phenols and aldehydes are usually toxic, corrosive, and/or irritating and require a rinsing step to remove chemical residues. Additionally, aldehydes require longer exposition to be effective. Therefore, the use of liquid chemicals is only recommended in specific devices that are proven to be incompatible with other conventional methods [67].

1.4.2 Non-Conventional Sterilization Methods

The limitations of the aforementioned sterilization methods have created a need to develop alternative techniques to sterilize biomaterials. The ideal sterilization technique should provide: 1) short sterilization times (ideally less than that of steam heat and pressure, ≈ 20 min); 2) low processing temperatures (ideally at room temperature); 3) capability of being used for a wide range of materials and objects (keeping the materials' functionality and properties) and 4) be safe, easily applied and cost-effective [75].

Less common processes have been used to sterilize biomaterials, such as mechanical filtration (microbes are removed using a 0.22 µm pore size membrane), ultrasonic sterilization (ultrasonic vibrations cause destruction of the microbes structure), UV irradiation and supercritical carbon dioxide exposure. [76]. Besides these, microwave irradiation, high hydrostatic pressure (HHP), and reactive plasma exposure have also garnered attention for the potential sterilization of biomaterials. These three methods will be the focus of this study, and their effect on the synthesized PVA-Zylon hydrogel will be assessed in a thorough manner.

Microwave Irradiation

A non-conventional method that has been studied for its capability of sterilizing biomaterials is microwave irradiation. It has been shown to be efficient at sterilizing hydrogel contact lenses contaminated with common bacterial and fungal pathogenics (*Staphylococcus aureus, Streptococcus pneumoniae, Pseudomonas aeruginosa, Proteus vulgaris, Bacillus cereus, Escherichia coli, Serratia marcescens,*

Aspergillus fumigatus , and Candida albicans), as well as virus (rhinovirus, parainfluenza virus type 3, adenovirus type 1, and herpes simplex virus type 1) [77]. Researchers determined the minimum time for killing bacteria and fungi ranged from 45 seconds for *S. pneumoniae* to 8 minutes for *S. aureus*, using a standard 2,450-MHz microwave oven at 700 W. After 1 min of exposure, less than 5% of virus activity persisted, and by four minutes, all four viruses, mentioned above, were completely inactivated. This method has also been deemed capable of sterilizing soft denture liners contaminated with *C.albicans* at 5 min of exposure when the samples were immersed in water [78]. Further studies also showed the efficacy of this method, Neppelenbroek *et al.* sterilized contaminated hard chairside reline resins (*C. albicans, S. aureus, B. subtilis, P. aeruginosa*) after 6 min exposure at 650W [79], and Dunsmuir *et al.* studied contaminated femoral head allografts (*S aureus, B subtilis*), which were inactivated at 800 W in only 2 minutes of exposure [80].

Microwaves are electromagnetic waves ranging from 300-300 000 MHz frequency and a wavelength of 1-1000 nm. Exposure to microwave radiation can lead to a sharp increase in temperature within dipolar substances, particularly water. In an alternating current electric field, the field polarity varies with the rate of frequency and the molecules attempt to align themselves with the changing field (i.e. dipole rotation). This causes an internal molecular friction which results in a rapid generation of heat. The back and forth movement of the ionic molecules trying to align themselves with the oscillating electric field also causes ionic polarization [81]. Thus, these two mechanisms (dipole rotation and ionic polarization) allow microwave irradiation to achieve high temperatures with a greater efficiency and speed when compared to other common heating systems.

In summary, the microwave sterilizing method is thought to be essentially moist heat. Typical practice involves immersing the materials in an aqueous solution, within a thermoplastic or glass vessel and then submitted to microwave irradiation, using a domestic microwave oven [77, 82]. One study measured the temperature of the liquid inside irradiated storage cases, by inserting Thermax B heat strips into the solution [82]. The researchers found that a 800W microwave oven operating at full power was capable of heating a 10 ml saline solution to $\geq 100^{o}$C in just 10 to 12 seconds. One important aspect to consider is that individual ovens may manifest different patterns of radiation distribution, depending on the age and cleanliness of the equipment, which may lead to differences in the efficacy of sterilization [83]

The volumetric heating rate (Q) of microwaves at a particular location is dependant on the strength of the applied electric field strength (Ω), as well as the type of material being heated, by the following equation:

$$Q = 2\pi f \varphi_0 \varphi^{''} \Omega^2 \tag{1.1}$$

where f is the frequency of the microwaves, φ_0 is the permittivity of free space (physical constant) and $\varphi^{''}$ is the dielectric loss factor, a material property which represents its ability to absorb the wave. Moisture content significantly affects the dielectric properties of the product and thus, the penetration depth of the microwaves. High-moisture foods have been observed to show a uneven heating rate due to low microwave penetration depth, while low moisture foods have more uniform heating rates [84].

This relation explains the higher exposure times necessary to sterilize highly hydrated materials such as hydrogel lenses [77].

One study has also reported a removal of up to 97% of pathogenic bacteria from bovine pericardial biomaterial, using nonthermal microwave radiation (18 GHz, 16 W) [85]. This indicates that, not only the temperature effects, but also the microwave radiation itself can have sterilizing capabilities. Studies on the destruction kinetics of microorganisms by microwave heating started in the 1940s with a work by Fleming [86]. More recently, conflicting research has argued between the capacity of microwaves to kill microorganisms without heat [87, 88]. A clear knowledge gap exists in this field, and thus, there is a need of further research into this topic.

The main advantages of this method over conventional moist heat sterilization such as autoclaving are its lower costs (of both equipment and energy requirements), greater accessibility, is user-friendly and shows lower processing times, reducing possible thermal degradation of the material. It also has no need of toxic chemical components, which precludes toxic or hypersensitivity complications. Microwaves are also known to be able to pass through polymeric materials allowing materials to be sterilized in their final packaging. However, the high temperatures achieved during exposure as well as the effect of the microwave radiation itself may have unwanted effects on the structure and composition of the sterilized materials, especially in thermal sensitive polymers.

High Hydrostatic Pressure

Another alternative method to sterilize biomaterials is high hydrostatic pressure (HHP). This method is widely used in the food processing industry, as it does not rely on chemicals, heat or irradiation to destroy pathogens. Instead, it relies on the compression of surrounding water to transmit high pressures (usually in the range of 100-1000 MPa) throughout the product uniformly and rapidly. The range of temperatures of this process can be adjusted between 0ºC and 100ºC , with exposures time ranging from a few seconds to over 20 min [84].

According to the Le Chatelier principle, under equilibrium conditions, pressure encourages any phenomenon that is associated with a decrease in volume and inhibits those associated with volume increase. Hydrostatic pressure causes an alteration of interatomic distances, affecting the interactions for which bonding energy is dependant on distance. This is the case for electrostatic interactions, as well as hydrogen bonding and van der Waals forces. In contrast, covalent bonds are unlikely to be affected by pressure as their bonding distance can only be minimally compressed . The efficiency of HHP depends on the duration and level of the applied pressure, temperature and on the chemical environment of the product [89]. The alteration of interatomic distances due to high pressures can cause consequences such as: (a) changes in physical properties (melting point, solubility, density, viscosity, etc); (b) effects in equilibrium processes (dissociation of weak acids, acid-base equilibrium, ionization); and (c) alterations in rates of processes [90].

HHP induces the inactivation of microorganisms by a combination of changes in their morphology, cell membrane or biochemical equilibrium. The cell membrane especially is considered to be the main target of this method, leading to leakage of intracellular constituents through the permealized membrane

and subsequent cellular death. The fluidity of the cellular membrane has been found to play an important role in the susceptibility of microorganisms to HHP, where microorganisms with higher membrane fluidity are more resistant against the effects of pressure. Generally, vegetative cells are inactivated at pressure levels of around 400-600 MPa, while more resistant bacterial spores are able to resist pressures higher than 1000 MPa [84]. However hydrostatic pressures of 100-300 MPa can induce spore germination by causing the influx of water and eflux of Ca^{2+} from the spore, turning them into more sensitive vegetative cells [91]. Spore inactivation can also be achieved through the use of higher pressures with elevated temperatures [92].

Pressure is considered to act isotropically on systems, which means that pressure effects are instantaneously and homogeneously distributed within the sterilized material, independent of its size and geometry. This principle explains why nonporous materials with high water contents are not macroscopically damaged by HHP treatment. Nonetheless, the difference between the compressibility of air and water under pressure, can affect the structure and shape of porous materials that contain air pockets, unless the material is perfectly elastic and from which air cannot escape [90]. Hydrogels, despite being porous materials, are characterized by being highly hydrated, which means their pores are completely filled with water if immersed, making them ideal candidates for HHP. For example, Topete *et al.* used HHP as a possible alternative to conventional sterilization methods on unloaded and drug loaded intraocular lens hydrogel materials. Optimization of the processing conditions with highly contaminated samples led to the establishment of the following values: 600 MPa, 70ºC during 10 min. These parameter values were found to be optimal for the maintenance of the materials' desired properties, while retaining drug functionality and release kinetics [93].

Despite the popularity of HHP for food preservation and the great promise it holds for biomedical sterilization, it does show some drawbacks, especially in the costs to purchase and install the specialized equipment and build safety-coded environment with special protection walls [94].

Plasma

Low-temperature glow discharge plasma treatment has also been investigated for its potential to sterilize polymeric materials. Gas plasma is considered to be the fourth state of matter and can be thought of as a gas composed of only ions and free electrons. In a sterilization procedure, gas plasma is created through the application of strong electromagnetic fields (known as cold plasmas). Here, the temperature of heavy particles (atoms, molecules and ions) is usually at ten times lower than that of electrons. Thus, electrons are the particles responsible for ionizing the atoms of the discharge gas, requiring lower energy costs, by enabling the use of glass and metal discharge vessels without heavy cooling equipments. In short, plasma sterilization consists in exposing the materials to free radicals created during the electric discharge in a gas [75].

Different factors influence the efficacy of the plasma sterilization procedure, such as: 1) type of gas; 2) electric field strength; 3) pressure; 4) gas flow rate and 5) exposure times. A wide range of discharge gases has been used with positive results, such as Ar, O_2, N_2, H_2, N_2O, H_2O, H_2O_2, CO_2, SO_2, SF_6, halogens, aldehydes, organic acids, and others [75]. More reactive gases usually show

higher degrees of sterilization, but also create more toxic residues. Research indicates that the main inactivation mechanism of plasma is related to the adsorption of reactive electrons, ions and radicals, which causes etching on the cell's surface, eroding cellular material (e.g. crust lipoprotein and inner fat amylase of the cell membrane) and causing a leakage of inner contents, killing the cells [75, 95].

One study reported efficient inactivation of *P. aeruginosa* within 60 seconds of exposure to argon plasma (30W power, Ar flux 20 cm^3/min) [95]. Plasma sterilization was capable of inactivating *E.Coli*, using a 2.45 GHz, microwave-induced argon plasma system at atmospheric pressure and gas flow rate of $\approx$ 100 l/min at 8 kgf/cm^2, after only 1 second of exposure. With 10 seconds of exposure, the inactivation of pyrogens ocurred [96]. The sterilization efficiency of this method was also demonstrated for PLGA scaffolds, after 4 min exposure to argon plasma using 100W power [97].

While plasma sterilization has been shown to be efficient using low processing times and low temperatures, the effect of the highly energetic particles could produce some unwanted effects on the biomaterials, specifically etching of their surface [98].

Table 1.3: Advantages and drawbacks of the used sterilization techniques

Sterilization Method	*Microwave*	*HHP*	*Plasma*
Low processing time	+	+	+
Low temperatures	-	+	+
Lack of toxic residues	+	+	+
Specialized equipment	+	-	-

Chapter 2

Materials and Methods

2.1 Materials

For the production of the hydrogel material, PVA powder (99% hydrolized, MW=146,000-186,000) was obtained from Sigma-Aldrich. Zylon^{TM} (PBO) fibers (type: AS) were obtained from Toyobo Co. Ltd., Japan. Trifluoroacetic acid (TFA) (CF_3COOH), was purchased from CARLO ERBA Reagents and 99% extra pure methanesulfonic acid (MSA) (CH_4O_3S, MW=96.10) was purchased from Acros Organics. Distilled and deionized (DD) water (18 MΩ cm, pH 7.7) was obtained with a Millipore water purifying system. The weighing of materials was performed in a semi-micro analytical balance OHAUS (Model Discovery DV215CD).

For sterility assessment, Thioglycollate Liquid Medium (TIO) and Soybean Casein digest Broth (CASO) were obtained from PanReac (Spain) and Sigma-Aldrich (USA) respectively.

Simulated synovial fluid (SSF) used in the tribological testing was formulated with hyaluronic acid sodium salt (HA), with an average molecular weight of 1–2 million Da (3 mg/mL) and lyophilized bovine serum albumin (BSA), Fraction V, pH 7 (4 mg/mL), dissolved in phosphate buffer solution (PBS). The HA and BSA used in the preparation of simulated synovial fluid were individually supplied by Carbosynth (Compton, Berkshire, UK) and Serva Electrophoresis GmbH (Heidelberg, Germany) while PBS (pH 7.4) was obtained from Sigma-Aldrich (USA). SSF was stored in a refrigerator at 4ºC between each use.

Cartilage pins used in the tribology assays were harvested from porcine cartilage, obtained from a local butcher's shop. After removing all soft tissue from the femoral condyles, the cartilage surfaces were exposed and full-depth osteochondral plugs (ϕ = 6 mm) were harvested using 6 mm hole punchers on randomly selected sites. The cartilage surface was carefully cut with a scalpel, to prevent sharp edges in the sides thus avoiding possible tearing of the hydrogel's surface. It is reported that freezing and thawing, as well as preloading of samples, show no effect on the wear of cartilage [99]. Thus, after preparation, the specimens were washed in DD water and stored at -20 ºC in PBS solution (pH = 7.4, buffer strength = 150 mM), as done in other publications [100, 101]. The pins were glued to a titanium pin using cyanoacrylate glue in order to be mounted on the tribometer. Extra care was taken so that the cartilage surfaces were properly levelled.

For biological tests, Dulbecco's Modified Eagle's Medium (DMEM) and dimethyl sulfoxide (DMSO) were provided by Sigma-Aldrich (USA). Sodium hydroxide (purity $\geq$ 99%, NaOH) was obtained from Merck (USA). Sodium chloride (purity $\geq$ 99%, NaCl) was purchased from PanReac (Spain).

2.2 Production of PVA-Zylon Hydrogel

6% w/v PVA powder was mixed with 100% TFA. In the meantime, 1% w/v Zylon fibers were mixed with a 80%TFA, and 20% MSA solution. Both solutions were left with a magnetic stirrer until complete dissolution of the solutes. After visually confirming the dissolution of both materials, the vials are placed in a warm bath (45ºC) for 30 minutes, to decrease the viscosity of the solutions and facilitate mixing. Then the solutions were mixed vigorously, placed in closed borosylicate petri dishes, and left to rest for 1 hour. After this time, airflow was permitted to enter the dish by elevating the lid, and left for a further 2 hours. Following, the lid was completely removed, and the gel was left for 24 hours at room temperature.

After complete gelation, the hydrogel was placed in DD water, with constant water changes during the course of several days to induce the release of the acidic solvents. The washing process continued until the pH of the water was neutral. The samples are then placed in a dry oven at 45ºC for at least 48 hours, to finalize the crosslinking process.

2.3 Sterilization

2.3.1 Microwave

Microwave sterilization was performed using a common household 2450 MHz microwave oven (Kunft KMW-1698), with the highest possible setting (high), at 700 W for 3 and 5 minutes. The samples were placed in special sealed bags (poly-amide and polyethylene, 90 m, 10×10 cm2, Penta Iberica), with $\approx$3 mL of DD water to avoid dehydration, and aid in the sterilizing effect of the microwave radiation. The bags were triple heat sealed to avoid possible holes or leaks. The sterilized samples were kept inside the bags until further use.

2.3.2 High Hydrostatic Pressure

HHP sterilization was carried out in a specialized high pressure equipment (Hiperbaric 55, Burgos, Spain), at the University of Aveiro. Preparation of the samples was similar to that of the microwave sterilization process. In summary, the samples were placed in special sealed bags, and immersed in DD water to maintain their hydrated state. The samples were sterilized at 70ºC and 600 MPa for 10 minutes. The optimization of the HHP conditions were previously carried out for several other types of hydrogels [93].

2.3.3 Plasma

Plasma sterilization was performed using a compact Harrick PDC-32G Plasma Cleaner/Sterilizer (115 V). The equipment was connected to a gas-compatible oil-based vacuum pump (LVO 100, Leybold), in order to pump nonreactive Argon (Ar) gas into the chamber. Pure Ar gas was supplied from a compressed gas bottle at 20 MPa pressure (ALPHAGAZ^{TM} Ar, from Air Liquide). Dry hydrogel samples were placed into the quartz glass chamber, which was then vacuum closed, and connected to the Ar gas bottle. The hydrogels were exposed for 5 minutes at maximum settings (18 W). Visual confirmation of the presence of ionized gas in the chamber was possible due to the characteristic appearance of a purple glow. To avoid contamination, all surfaces in the immediate vicinity of the equipment were disinfected with 70% ethanol and a bunsen burner was strategically placed to ensure an aseptic environment. The chamber was then opened and the samples were carefully placed into previously sterilized falcon tubes containing DD water, using sterilized tweezers.

Figure 2.1 shows the sterilization equipment used in this thesis.

(a) (b) (c)

Figure 2.1: Sterilization equipment for (a) microwave, (b) HHP, and (c) plasma methods.

2.3.4 Sterility Assessment

To determine the success of the sterilization procedures, the European Pharmacopoeia (Ph.Eur) describes two sterility tests: direct inoculation of the culture medium and membrane filtration [102]. Membrane filtration (pore size of $0.45\,\mu$m) is the preferred method for pharmaceutical products, while the direct inoculation is usually chosen for biomaterials. The latter is also preferred when there are solubility issues or inability to filter antibiotic suspensions. In the scope of this work, the direct inoculation method was used to assess the capacity of the microwave, HHP and plasma sterilization procedures.

The sterilization tests were performed at the Laboratory of Applied Microbiology of Egas Moniz (LMAEM), following the Ph.Eur. 10th edition [102]. Aseptic conditions were ensured by carrying out the assay in a laminar flow cabinet. TIO medium, for potential bacterial growth and CASO-Broth, for fungal growth were prepared in Schott flasks, and sterilized according to fabricant instructions in an autoclave at 121ºC, 10^5 Pa for 20 minutes.

The sterilized hydrogels with a diameter of 8 mm were aseptically removed from their sterilized packaging, and placed directly into the flasks containing 100 mL of growth medium. Two positive controls for bacterial contamination were created through inoculation of *Pseudomonas aeruginosa* (ATCC 15442)

and *Staphylococcus aureus* (ATCC 6538) in the flasks containing TIO medium. A positive control for fungal contamination was created in a similar way, with inoculation of *Candida albicans* (ATCC 10231) in a flask containing CASO medium. As negative controls two flasks, each containing only one of sterilized mediums.

All prepared flasks were incubated for 14 days, at 35ºC for TIO medium, and at 25ºC for Caso. Validation of sterility was performed through comparison of the samples' incubated flasks with both the positive and negative controls, in which the positive control must demonstrate the growth of microorganisms, and the negative controls just show a clear culture medium. For each method of sterilization, three replicates of hydrogel material were tested for each medium.

2.4 Material Characterization

The most relevant material's properties for cartilage replacement were addressed. In all cases, they were determined before and after sterilization, in order to understand if the sterilization procedures caused changes in the material.

2.4.1 Microstructure Analysis

As the sterilization processes used in this work can induce chemical alterations on the PVA-Zylon hydrogels structure, the materials' chemical structure was studied through Fourier transform infrared spectroscopy (FTIR) with attenuated total reflectance (ATR). A Spectrum Two from PerkinElmer (Waltham, MA, USA) FTIR equipment equipped with a lithium tantalite (LiTaO3) mid-infrared (MIR) detector (signal/noise ratio 9300:1) and a UATR Two accessory was used. Additionally, a diamond ATR crystal was utilized to control the applied force ensuring a good contact between the crystal and the samples, thus reducing variations on the spectra intensity. The dry (after 2 days at 45ºC) sterilized and non-sterilized PVA-Zylon hydrogels were studied. Spectra were carried out in different parts of the samples to verify possible discrepancies on the chemical structure of the hydrogels. All obtained spectra were normalized ("Normalize" function, normalize method [0,1]) by using the OriginPro 8.5 software, collected at 4 cm^{-1} resolution and 8 scans of data accumulation were carried out.

A dry 14 mm disk of each hydrogel condition (non sterilized and sterilized) was used for this analysis. Plasma sterilized samples were also cut, separating the surface from the bulk, to see if there were differences across the hydrogel's depth.

2.4.2 Swelling

The studied hydrogels when placed in water or in a biological solution demonstrated to be capable of absorbing large quantities of these fluids without losing their structural integrity. The swelling capacity of a hydrogel depends not only on the number of hydrophilic groups present in the polymeric matrix, but also on the density of the cross-links and the existence of pores. Temperature is also a determining

factor in the amount of liquid absorbed. To characterize the hydrogels' capacity to absorb and retain water molecules in its network swelling measurements were performed.

Hydrogel disks with 6 mm diameter were dried for 2 days at 45ºC before being weighted (dry weight, W_d). Afterwards, the hydrogels were placed in 5 mL of DD water, incubated at 37ºC and periodically weighted (wet weight, W_w) until a constant value was achieved. The samples were carefully blotted with absorbent paper before each measurement to remove any remaining water droplets from their surface. The swelling capacity (SC) was calculated along the tested time range (120 hours) and the water content (WC) was calculated at equilibrium, using the following equation:

$$SC(\%) = \frac{W_w - W_d}{W_d} * 100 \tag{2.1}$$

$$WC(\%) = \frac{W_w - W_d}{W_w} * 100 \tag{2.2}$$

2.4.3 Tension and Compression

Articular cartilage demonstrates mechanical properties characteristic of its function that allow it to support compressive and tensile loads. Compressive tests were performed using a TA.XT Express Texture Analyzer (Stable Micro Systems). Uniaxial compression was performed with a load cell of 49 N in unconfined mode. Hydrated 8mm diameter samples, with a thickness of ≈4mm were immersed in DD water at room temperature, and compressed at a strain rate of 0.1 mm·s^{-1}, up to a 40% strain of the material. The compressive probe was moved down until the software registered a force of 1 g (≈0.01 N), to ensure full contact of the metallic probe and hydrogel samples. Repeated loading and unloading of viscoelastic material usually leads to a difference in the obtained hysteresis curves. Thus, each hydrogel sample underwent several cycles of loading-unloading, until the hysteresis curves were deemed reproducible (5 cycles). At least 2 different samples were tested for each sterilization method and non sterile material (n≥2).

Tensile resistance tests were performed in the same equipment with a force of 49 N at a speed of 0.5 mm/s in hydrated dumbbell-shaped specimens of hydrogel (5 mm width, 2.5 mm gauge width, 8 mm gauge length, total length 18 mm), cut with a mold. The samples were clamped into place and moved to a registered force of 0 g until equilibrium was reached, taking care to not allow the hydrogels to dry. For each material condition, a minimum of 4 different specimens were tested (n≥4).

Compressive and tensile Young's Modulus were measured at the linear portion of the stress-strain curves, at 1% strain, using the standard Young's modulus equation:

$$E = \frac{\sigma}{\epsilon} \tag{2.3}$$

The tangent compressive and tensile modulus (E_Σ) were calculated in the strain range of 5-35%, in 5% increments by the finite difference method [103], according to the obtained stress-strain curves, expressed with the following equation:

$$E_{\Sigma} = \frac{\sigma_{\epsilon+\Delta\epsilon} - \sigma_{\epsilon-\Delta\epsilon}}{2\Delta\epsilon} \tag{2.4}$$

where E_{Σ} is the tangent modulus of the hydrogel at the strain ratio value of ϵ. The difference in strain value $\Delta\epsilon$ was 1%.

2.4.4 Rheology

Rheology allows for an appropriate characterization of the hydrogel's mechanical properties, through a dynamic analysis of the structural recovery of the materials after the application of a deformation. This type of test allows for the material to be kept at the Hookean elastic region for the entire duration of the experiment, unlike other mechanical tests (e.g. compressive and tensile tests) [104].

As natural cartilage the hydrogels are viscoelastic materials, and this behavior is dependent on the shear stress (τ) and the shear strain (ψ) and is described by the complex shear modulus (G*) (equation 2.5). Thus, hydrogels simultaneously show an elastic and viscous behavior. The elastic component is represented by the storage modulus (G'), associated with the maximum energy stored during deformation to return to the original state with the removal of the applied stress (equation 2.6). The viscous portion shows the dissipation of energy that occurs during deformation, and is given by the loss modulus (G") (equation 2.7) [105].

$$G^* = G' + iG'' = \frac{\tau}{\psi} \tag{2.5}$$

$$G' = \frac{\tau}{\psi} * \cos\delta \tag{2.6}$$

$$G'' = \frac{\tau}{\psi} * \sin\delta \tag{2.7}$$

where δ is the phase angle. The tangent to δ is known as loss factor (LF), or damping factor, and describes the contribution of G' and G" to the viscoelastic behaviour (equation 2.8). A $\delta = 0^o$ or LF=0 describes an ideally elastic behavior while for an ideally viscous behavior $\delta = 90^o$ and LF approaches infinity [106, 107].

$$LF = tan\delta = \frac{G''}{G'} \tag{2.8}$$

Rheological measurements were performed in rotation oscillation, using a Modular Compact Rheometer (MCR92, Anton Paar), at 37ºC with a 25 mm diameter parallel measuring plate (PP25). Hydrated hydrogel samples were cut into 25 mm diameter disks, with a height between 2 and 3 mm, and mounted on the equipment (Figure 2.2). Approximately 5 mL of DD water was added to the dish where the hydrogel was placed, to ensure the samples remained hydrated throughout the tests. Each sample's thickness was measured before the test, to ensure the material was not overly compressed, which could lead to compromised results. Before testing, the specimens were held at the measurement gap for 15

min to eliminate thermal and shear artefacts. A minimum of two different specimens from each material condition were tested (n≥2).

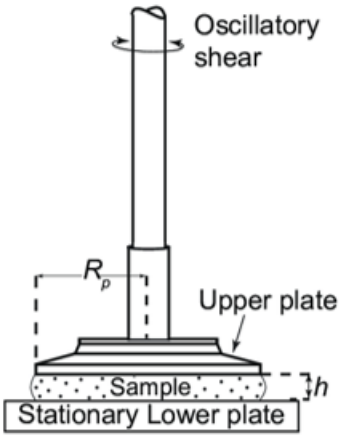

Figure 2.2: Schematic representation of the rheological measurement setup for the parallel plate arrangement, R_p is the radius of the geometry, and h represents the gap [108]

First, an amplitude sweep test was carried out at a fixed frequency of 1 Hz, to determine the range of strains at which the material maintains its elastic nature (linear viscoelastic regime, LVE), i.e., G'>G". Inside this region, the material structure is in equilibrium and the relation between applied stress and measured quantities is linear, and solely a function of time, frequency or temperature [109]. All subsequent tests were performed at a fixed shear strain within the LVE (0.1%). The PVA-Zylon hydrogels were also submitted to an isothermal time test, for 1 hour, with a constant frequency (1 Hz), to determine if changes occurred to the viscoelasticity of the material during prolonged stress. Finally, a frequency sweep (FS) measurement, between 0.1 to 100 Hz was performed. This frequency range represents typical physiological activities from slow walking (<1 Hz) to jumping and high impact sports (100 Hz) [110, 111].

The steady shear rate viscosity of the SSF used in the tribology tests was also measured, for a shear rate range of 0-100 s^1, at both room temperature and normal human body temperature (37ºC). This measurement was performed using a cone-plate geometry (CP50).

2.4.5 Hardness

Mechanical hardness is a measure of the resistance capacity of a material to an imposed deformation under compressive and shear loading. Hardness can be measured in different scales such as Shore, Brinell and Rockwell. The Shore scale is the most commonly used in the rubber and polymer industries. A hardened steel indenter with 1.3 mm diameter is used to apply a defined load, recording the penetration depth and expressing it in a scale from 0 (very soft) to 100 (very hard) [112].

A Shore A Durometer was used to measure the hardness value of the hydrogel materials. Cylindrical samples (h=4mm; ϕ=8mm) for each condition were tested for the Shore A hardness value. The used equipment and schematic of operation are presented in Figure 2.3.

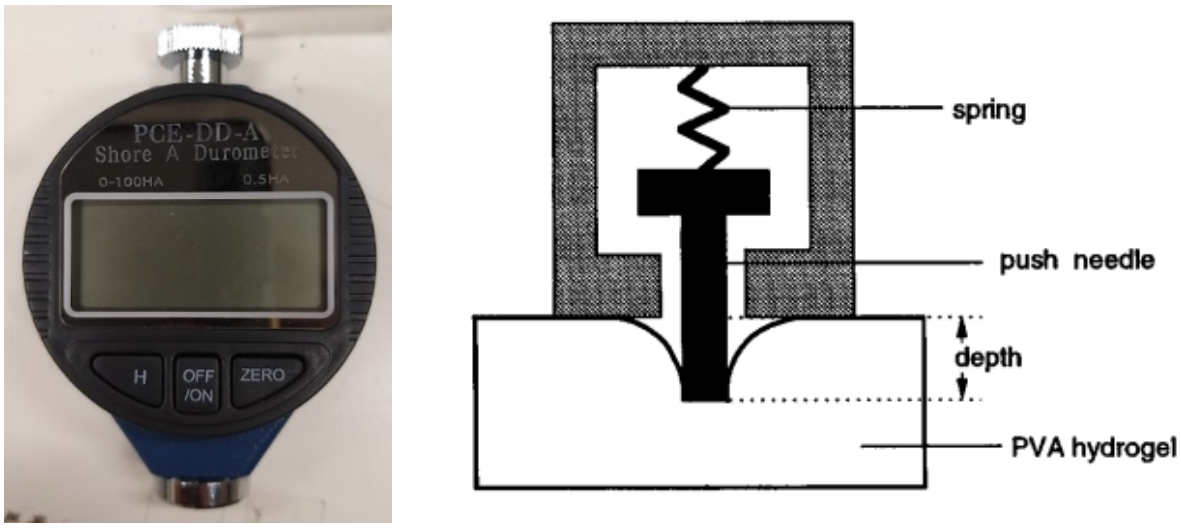

(a) (b)

Figure 2.3: Shore A Durometer used for hardness measurements (a) and schematic of the apparatus, from [53]

2.4.6 Wettability

Wettability measurements are used to quantify the capacity of a liquid to spread across a material's surface, by measuring the contact angle (CA) between the solid/liquid and liquid/vapour interfaces at the three-phase boundary. It is a defining factor that influences the tendency for biomolecules to adhere to the surface of materials, but also can affect lubrication and friction. The CA can be measured using several techniques, but the most commonly used is the sessile drop method. However, in the case of cartilage substitutes, the captive bubble technique is more suitable as it allows the measurement of the CA of the materials in their hydrated state. For this method, an air bubble is deposited below the surface of the material, mounted upside-down and completely immersed in a liquid. Figure 2.4 depicts a schematization of the sessile drop and captive bubble methods.

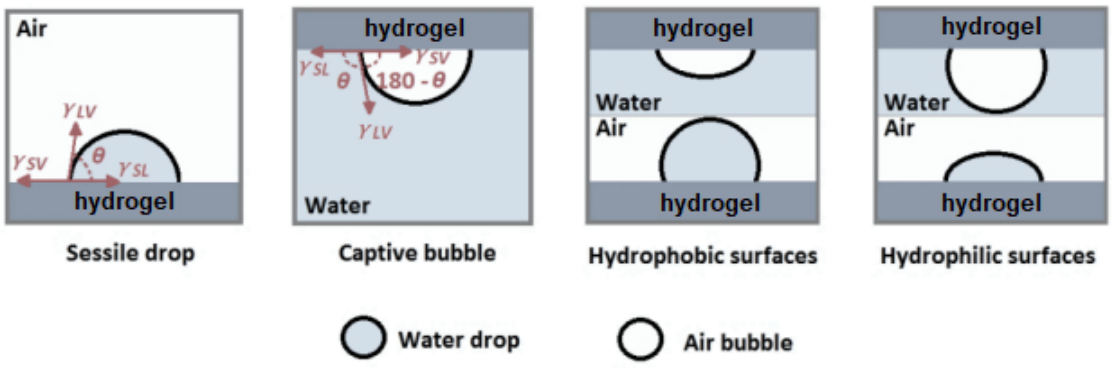

Figure 2.4: Schematic representation of the sessile drop and captive bubble methods, adapted from [113]

The water CA of the PVA-Zylon hydrogel was measured at room temperature using the captive bubble method. Hydrated hydrogel samples were fixed to a metallic support and placed upside-down inside a quartz glass liquid cell, filled with DD water. Using an inverted needle from a micrometric syringe, an air bubble was created at the surface of the material. The pictures of the air bubbles produced were taken with a video camera (JAI CV-A50) connected to an optical microscope (WildM3Z) and to a frame grabber Data Translation DT3155 (Figure 2.5).

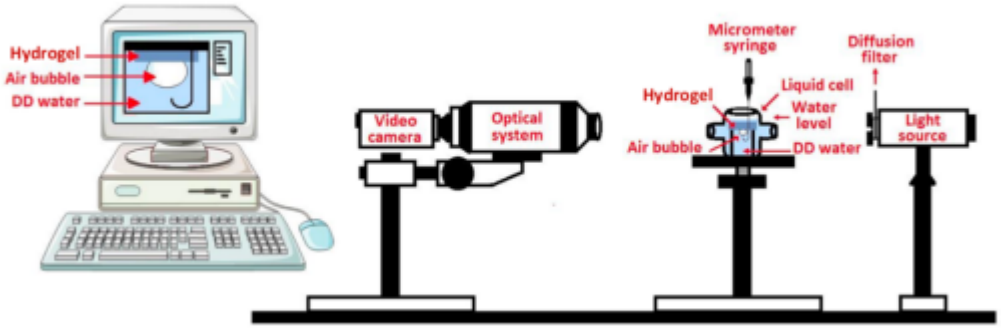

Figure 2.5: Schematic representation of the apparatus used for captive bubble analysis, [114]

Images were acquired at pre-defined times during 30 s. The value of the CA was obtained by image analysis of the last picture of each bubble, using the ADSA-P software (Axisymmetric Drop Shape Analysis Profile, Toronto University) which fits a theoretical profile based on the Laplace capillarity equation to the experimental bubble profile. Images of 10 bubbles were captured in 3 different samples of the material before and after each sterilization procedure, for a total of 30 bubbles (n=30).

2.4.7 Tribology

The sole purpose of articular cartilage resides on its capacity for load-bearing, providing diarthrodial joints the ability to move with very low friction coefficients (e.g., ≈0.002) [115]. When two surfaces are in direct contact, subjected to an applied load (i.e., normal force, F_N), and movement with a predetermined velocity is imposed, in general, the movement of sliding surfaces suffers a dissipative phenomenon known as frictional force, which is anti-parallel to the sliding direction (F_T). The following equation shows the relationship between the frictional force and the normal force, defined as coefficient of friction (CoF) [116]:

$$CoF = \frac{F_T}{F_N} \tag{2.9}$$

In order to find the CoF of the hydrogel material against cartilage, the hydrated hydrogel samples were tested in a pin-on-disk tribometer (TRB3, Anton Paar), in reciprocal oscillating mode at room temperature, for 2500 cycles, full amplitude of 4.0 mm and a sliding velocity of 8.0 mm/s (resulting in a frequency of 0.64 Hz). The data was collected as a function of time using the InstrumX 9.0.12 software, with an acquisition frequency of 10 Hz. The total duration of the assays was 1 hour and 5 minutes. As

the counter body, 6 mm cylindrical porcine cartilage pins were used (the methods of preparation and handling can be found in section 2.1). Figure 2.6 shows a schematic representation of the tribological setup.

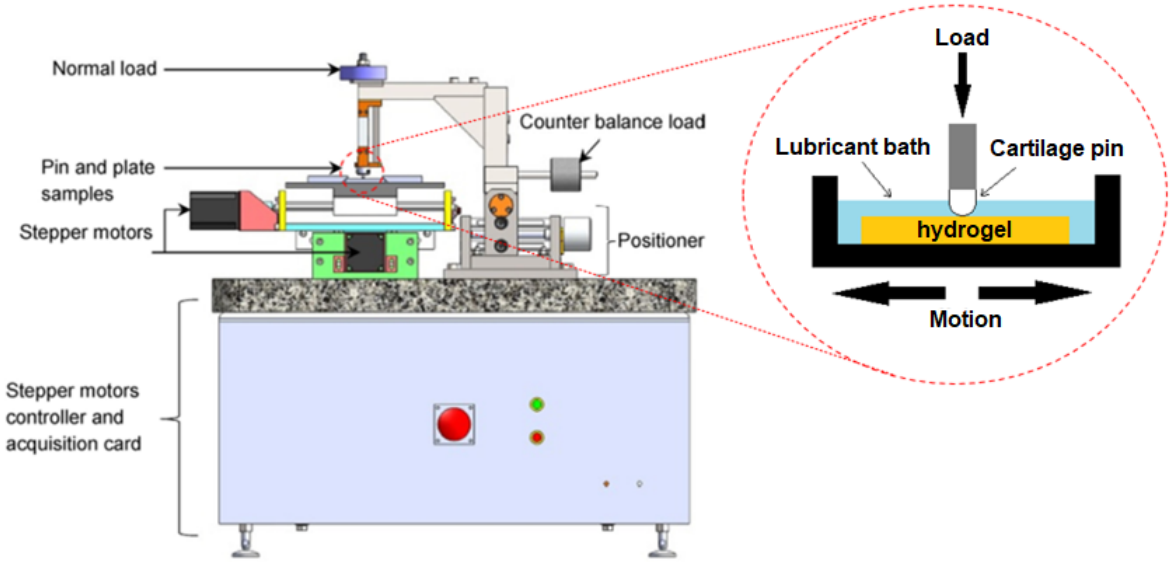

Figure 2.6: Schematic representation of the tribological testing setup, adapted from [117]

The non-sterilized material was tested at a load of 10, 20 and 30 N, corresponding to a Hertzian contact pressure of 0.354, 0.707 and 1.061 MPa, respectively. The samples were completely immersed in DD water and in SSF, using a liquid cell. The sterilized materials were tested only at a 30 N load and immersed in SSF, to simulate natural lubrication at high loads (boundary lubrication regime) [118]. Samples and cartilage pins were immersed for 1 hour in SSF prior to testing. At least three replicates were performed for each condition.

Linear tribology setups, such as the one used in this study, suffer from inertia effects when the sliding pin changes direction, which can lead to compromised CoF values. The InstrumX 9.0.12 software allows a treatment of the data using the "recyprocating analysis" mode, which gives an average, minimum and maximum CoF values, taking into account both motion directions and removing the effect of the inertial forces during the change of direction. Therefore, this analysis was considered the most adequate and will be reported in the results section.

2.4.8 Surface Morphology

The hydrogel's morphology greatly affects the CoF. Characterization of the PVA-Zylon hydrogel's morphology, after the tribological testing (30 N load), was done in a Hitachi S-2400 scanning electron microscope (SEM). SEM uses an electron beam to obtain tridimensional images in a wide range of magnifications (10 to 10000x). As the electrons interact with the material, different types of interactions can occur, that can be classified into elastic and inelastic. The elastic interactions give rise to the emission of

backscattered electron (BSE) from the deeper layers of the material, and with an energy similar to that of the incident electron beam. While for the inelastic interactions, energy transfer from electrons to the material occurs, which can lead to the appearance of X-rays, Auger electrons or secondary electrons (SE) (Figure 2.7). Secondary electrons are the result of the collision between the electrons of the incident electron beam and the electrons located in the atoms in the outermost layers of the material. Their energy is usually below 50 eV, and can be used to form images of the materials with high resolution [119].

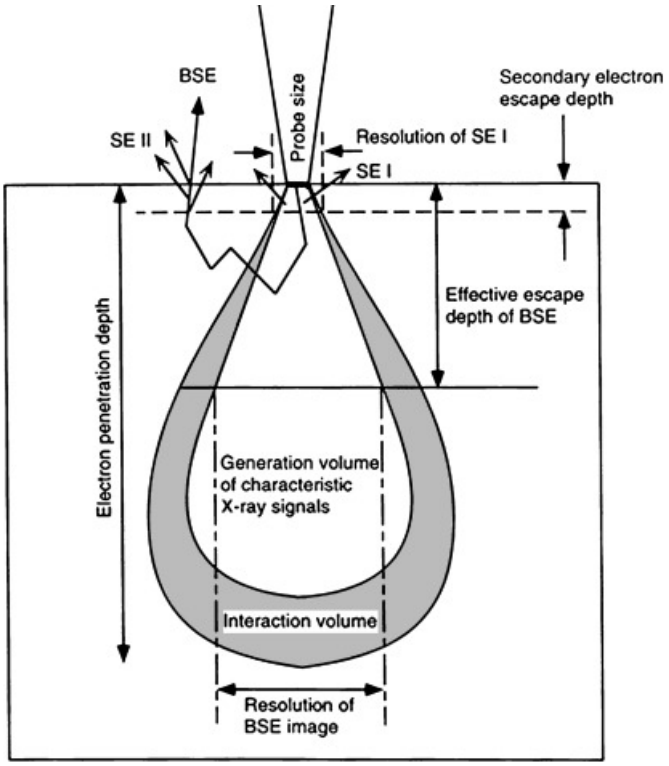

Figure 2.7: Schematic representation of the interaction volume of the electron beam on a sample [120].

The hydrogel samples were carefully cut around the areas where wear marking, caused by the tribological tests, was evident. Afterwards the samples were dried at 45 ºC for 48 hours, and coated with Au/Pd (100 nm) for conductivity purposes using a sputter coater and evaporator (Polaron Quorum Technologies, Laughton, East Sussex, UK). Each sample was observed inside and outside the wear marks, at magnifications ranging from 150x to 5000x.

2.4.9 Biocompatibility

The biocompatibility of a biomaterial is a crucial parameter in order to minimize harm to surrounding tissues. Extensive research has been done on the biocompatibility of PVA hydrogels, showing very good results [54, 44] even in *in vivo* studies [121]. However, most PVA hydrogels are produced without the use of highly acidic solvents. Moreover, while some studies state that PBO fibers show no toxic effects [122], extensive research on this topic is still lacking. Thus, it is important for the PVA-Zylon

hydrogels to undergo biocompatibility tests, to ascertain if the material or any of the unconventional sterilization methods could induce unwanted biological effects.

Irritability (HET-CAM test)

To evaluate if the materials could induce an irritation reaction on tissues, the Hen's egg test – chorioallantoic membrane (HET-CAM) test was carried out. The HET-CAM test uses fertilized chicken eggs (with 9 days of incubation), where the CAM is present. Normally, the designated test sample is directly placed on top of the CAM, and any acute effects related to irritability (i.e., hemorrhage, vascular lysis, and coagulation) are registered. No nerve tissue is developed until 11 days of the egg's incubation, and so, it is not classified as an animal experiment, as no feeling of pain occurs on the chicken embryo. The PVA-Zylon hydrogels were tested before and after sterilization to assess whether the sterilization procedures could induce some chemical processes through which the material became irritable. The irritation score (IS) is used to quantitatively analyze the irritation potential of the tested sample, using equation 2.10 [123]:

$$IS = (\frac{301 - T_H}{300} * 5) + (\frac{301 - T_L}{300} * 7) + (\frac{301 - T_C}{300 * 9}) \tag{2.10}$$

Where T_H, T_L and T_C represent the time (seconds) when the first appearance of hemorrhage, lysis and coagulation occurs, respectively. IS classification is given by Table 2.1.

Table 2.1: IS classification [124].

HET-CAM Score Range	IS
0-0.9	No irritation
1-4.9	Slight irritation
5-8.9	Moderate irritation
9-21	Severe irritation

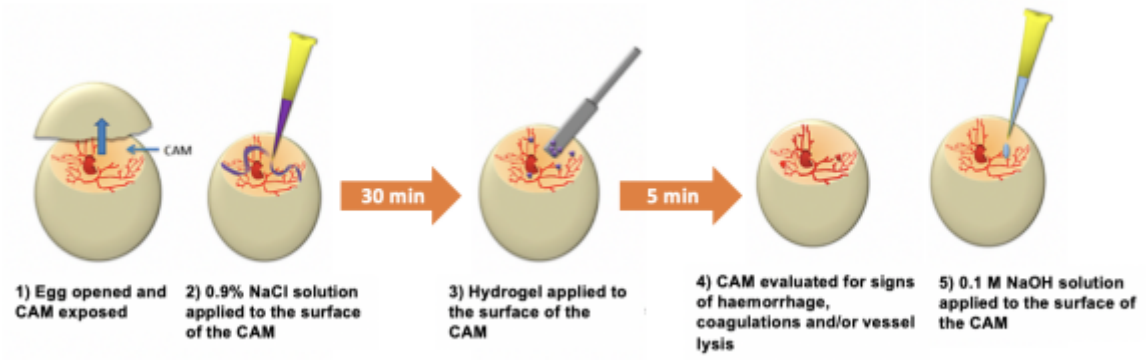

Figure 2.8: Schematic representation of the HET-CAM test, from [114]

Fertilized hen's eggs were incubated at 37 $\pm$ 0.5ºC, with 60 ± 2% relative humidity in a egg incubator

(Intelligent Incubator 56S) for 8 days. On the 9th day, a small opening was cut on the egg shell surface, using a rotary saw (Dremel 3000, Breda), and a scalpel. The inner membrane was moistened with a 0.9% NaCl solution, and the eggs were further incubated for 30 minutes. The inner membrane was then carefully removed, while ensuring no damage occurred to the underlying blood vessels, thus exposing the chorioallantoic membrane (CAM) (Figure 2.8). Triplicate samples for each sterilization type as well as non sterilized hydrogels were placed directly on the CAM, and left for 5 minutes while visually inspecting for signs of lysis, hemorrhage or coagulation, to calculate the IS. 300 µl of NaOH (0.1 M) and 0.9% NaCl solutions were used as positive and negative controls, respectively.

Cytotoxicity

To test whether any of the sterilization procedures would induce the release of toxic components that could cause harm to chondrocyte cells, cytotoxicity assays were conducted at Instituto Universitário Egas Moniz, Almada, using the extract test method, in accordance with ISO 10993-5 (ISO 10993–part 5: Tests for in vitro cytotoxicity). One week prior to the essays, human chondrocyte cells were cultured in Dulbecco's Modified Eagle's Medium (450 mL DMEM/F12 ham (1:1)+glutamine (Gibco11320-033)+50 mL FBS to a final concentration of 10% + 5 mL pen/Strep).

After visual inspection in an inverted optical microscope (Carl Zeiss Axiovert 25 Inverted Microscope), to ensure the presence of cells, the media was removed and the cell layer was carefully washed with 12 mL of pre-heated (36ºC) sterile PBS. The PBS was removed, and 3 mL of trypsine (0.25% (w/v) Trypsin - 0.53 mM EDTA) was added to the vial and left for 10 minutes, to induce separation of the cells from the bottom of the vial. 9 mL of DMEM media was then added to inhibit the trypsine and the cells were gently agitated with a sterilized plastic brush, in order to further ensure proper separation of the cells. The mixture was pipetted to a small flask and centrifuged for 5 min at 400 rpm, after which the supernatant at the top was quickly removed while ensuring the cells were deposited at the bottom. A volume of 2 mL of DMEM medium was added to the flask and carefully mixed to ensure proper cellular dispersion. 20 µL of this cell suspension was mixed in a 1:1 ratio with a 0.4% trypan blue solution in PBS and placed in a hemacytometer. Visual inspection in the microscope under a 10x objective enabled to ascertain cell viability and concentration. After counting the cells, more media was added to the cell suspension, to ensure that at least $0.5x10^5$ cells could be placed in each well. 400 µL of cell suspension was added to each well, in quadruplicate for each sterilization type. A positive (DMEM + 10% DMSO) and negative (DMEM only) control were also tested.

Hydrogel samples from each sterilization type were placed in a flask with DMEM media in a 3 cm^2/mL concentration, to obtain extracts containing leachouts of the hydrogels. The extracts and cells were left for 24 hours at 37ºC in a humified 5% CO_2 incubator. Afterwards, the wells were inspected in the microscope to ensure proper viability of the chondrocytes, and the media was removed and replaced with the same amount of sample extract. After 48 hours the cultures were again evaluated under the inverted microscope and photographed to qualitatively assess cell viability, morphology and eventual cell detachment.

Following visual inspection, MTT (3-(4,5-Dimethylthiazol-2-Yl)-2,5-Diphenyltetrazolium Bromide) as-

say was performed to quantify cell viability. The liquid media was carefully removed and substituted with 300 µL of 10% MTT solvent solution on simple DMEM medium (serum-free). Three empty wells were also filled with the same amount of solution for an absorbance control. The cells were left for 3 hours to react, and then 450 µL of pure MTT solvent (4 mM HCL, 0.1% IGEPAL in isopropanol) was added to each well. The plates were wrapped in foil, agitated in a orbital-shaker for 15 minutes and up-down pipetting was performed to fully dissolve the MTT formazan crystals that were formed. Finally the absorbance of the samples was read at 595 nm, using a microplate reader (Microplate reader AMP Platos R 496 AMEDA, AMP diagnostics), and the relative quantification of cell viability was normalized to the negative control.

Cell Adhesion tests

Cell adhesion tests were also carried out for the sterilized PVA-Zylon hydrogels. Two small samples from each sterilization method were placed in a 12 well plate after carefully drying their surface with a sterilized paper towel. The remainder of a cellular suspension from one of the cytotoxicity tests, with a cell concentration of 0,47*10^5 cell/mL, was again centrifuged and the supernatant thrown out. A volume of 20 µL of this concentrated cell suspension was carefully placed at the top of each sample, and left for 1 hour at the incubator (at 37ºC, 5% CO2) to ensure proper cell adhesion. Afterwards, the samples were immersed in approximately 1.5 ml of DMEM medium and further incubated. After 22 days the samples were visually inspected in the microscope for signs of cellular adhesion and photographed.

Chapter 3

Results

3.1 Production of PVA-Zylon Hydrogels

The synthesis of the PVA-Zylon hydrogels was arduous and complex. It presented several variables that can lead to considerable differences in the properties of the obtained material. Figure 3.1 shows some of the initial difficulties in the production of these materials. Figure 3.1(a) exemplifies how the gradual increase of the airflow is crucial for the proper gelation of the PVA-Zylon hydrogel. If too much air was allowed to contact with the hydrogel as it underwent the crosslinking process, the surface would gelate prematurely, and the hydrogel became covered in small lumps. Incomplete dissolution of PVA powder or Zylon fibers also leads to a compromised structure, leaving behind small pockets of polymer (Figure 3.1(b)). Finally, improper handling of the freshly prepared hydrogel prior to gelation often led to permanent physical damage (Figure 3.1(c)).

(a) (b) (c)

Figure 3.1: PVA-Zylon hydrogels with (a) lumps, (b) undissolved components and (C) physical damage

After some trial and error, it was possible to produce adequate PVA-Zylon hydrogels (Figure 3.2), presenting a visually homogeneous matrix.

Figure 3.2: Properly crosslinked PVA-Zylon hydrogels

3.2 Sterility Tests

The efficacy of the three sterilization procedures used in this thesis was determined through the direct inoculation method. The results are present in Figure 3.3.

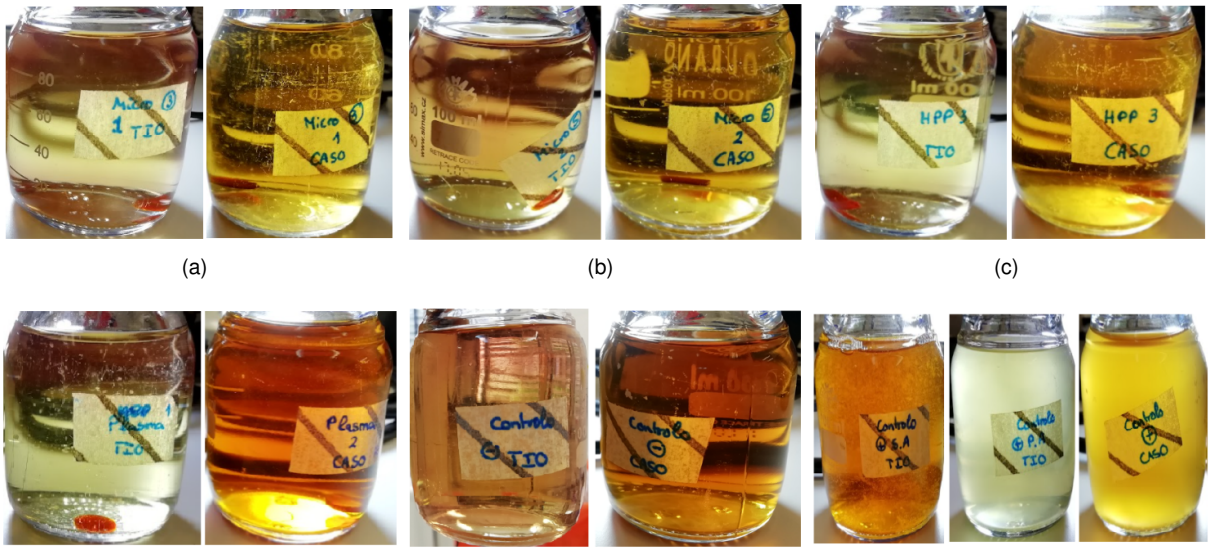

Figure 3.3: CASO and TIO culture medium after 14 days of incubation of the PVA-Zylon hydrogel samples after (a) microwave 3 min b) microwave 5 min , (c) HHP, and (d) plasma sterilization methods. The (e) sterile CASO and TIO mediums (negative control), and the (f) TIO incubated with *Staphylococcus aureus* and *Pseudomonas aeruginosa* and CASO incubated with *Candida albicans* (positive controls) are also shown.

Observation of the incubated culture medium flasks demonstrated that all chosen sterilization methods effectively ensured the sterilization of the samples, as after 14 days of incubation, no microorganisms grew in the mediums, contrary to what occurred in the positive controls. No difference was observed between the microwave sterilization with 3 and 5 minutes of exposure, so all further testing on microwave sterilized samples was performed with an exposure time of 3 minutes.

3.3 Microstructural Analysis

FTIR analysis was performed on the non-sterilized and sterilized hydrogels to attain information if the sterilization processes induce changes in the chemical structure in the hydrogels. As plasma sterilization method is known for a more superficial effect, FTIR analysis of the plasma subjected hydrogels was differentiated into two parts (i.e., bulk and surface).

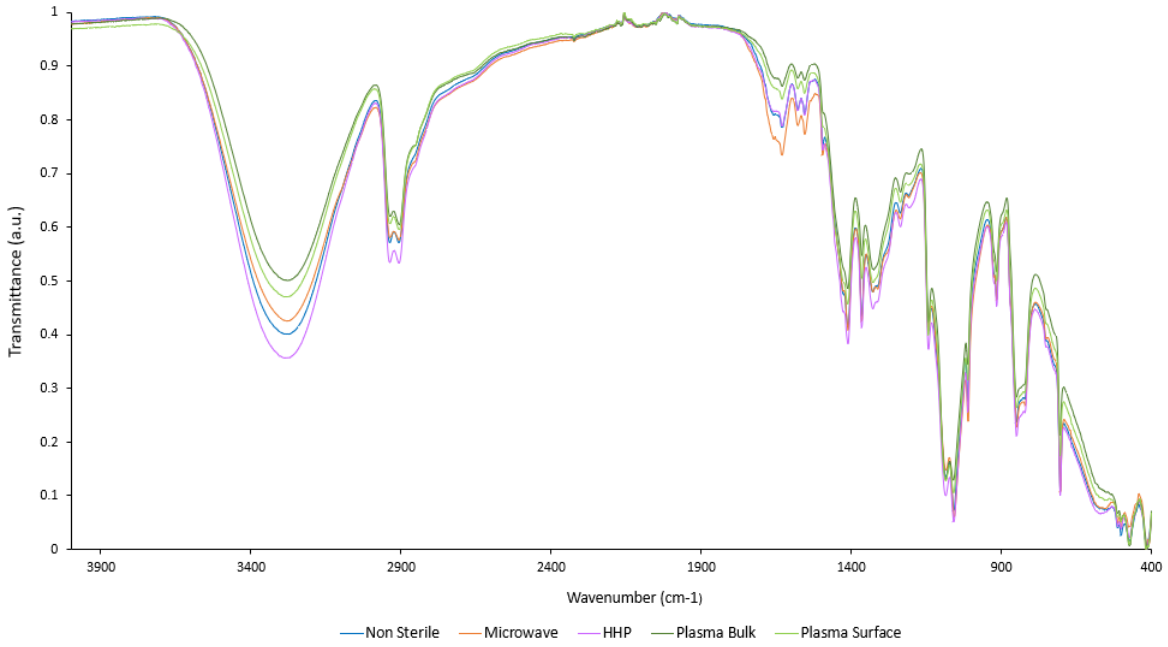

Figure 3.4: FTIR-ATR spectra of the non-sterilized and sterilized PVA-Zylon hydrogels, in the region of 4000–400 cm^{-1}.

Figure 3.4 shows the comparison between the FTIR spectrums of non-sterilized and sterilized samples. The hydrogels show a characteristic PVA spectrum, with no new peaks arising from the sterilization procedures. This means that no new chemical species appear on the hydrogels as a cause of the sterilization. However, the intensity of the peaks does change between the different methods, indicating variations in the amount (per unit volume) of functional groups associated with the molecular bonds.

At higher wavenumbers, the FTIR spectra show peaks usually related to hydrogen bonding (Figure 3.5). All samples show a characteristic broad peak across 3200-3400 cm^{-1}, which can be attributed to the stretching vibration of an alcoholic hydroxyl group (-OH) of PVA [125, 126] or a combination of O-H (from PVA) and N-H (from Zylon) stretching [127]. The peaks around 2850-2950 cm^{-1} pertain to alkyl (C–H) stretching, and have been found in both PVA [125, 126] and Zylon [127]. These peaks were most intense on the HHP sterilized samples while microwave samples showed a very slightly lower intensity compared to the non-sterilized. The plasma samples (both the bulk and the surface) presented the lowest intensity in these peaks.

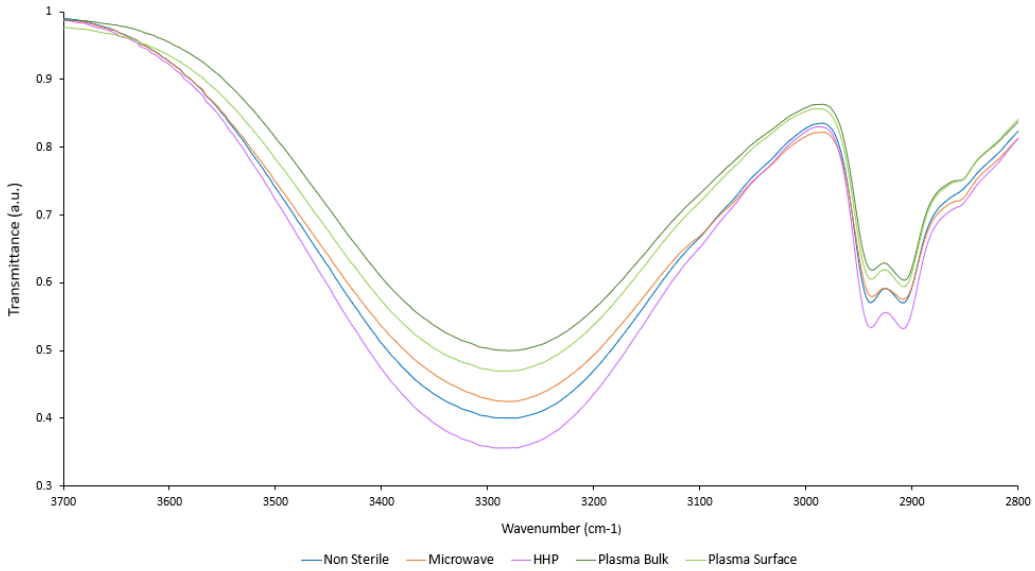

Figure 3.5: FTIR-ATR spectra of the non-sterilized and sterilized PVA-Zylon hydrogels, in the region of 4000–2800 cm^{-1}.

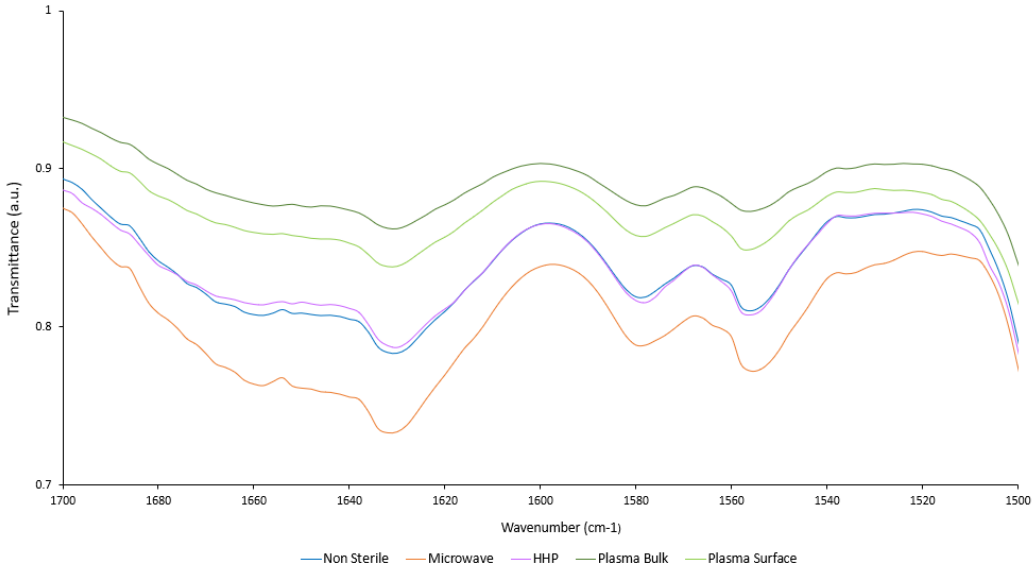

Figure 3.6: FTIR-ATR spectra of the non-sterilized and sterilized PVA-Zylon hydrogels, in the region of 1700–1500 cm^{-1}.

In the area between 1500-1700 cm^{-1} peaks are typically attributed to stronger covalent bonds (Figure 3.6), usually assigned to carbonyl (C=O) and C=N stretching in Zylon [127, 128] or C=O stretch in PVA [125, 126]. While the plasma samples retain the same behaviour seen previously, with the lowest peak intensity, the results of HHP and microwave were opposite. Here, the HHP spectrum is almost equal to the non-sterilized, while microwave shows an increase in peak intensity.

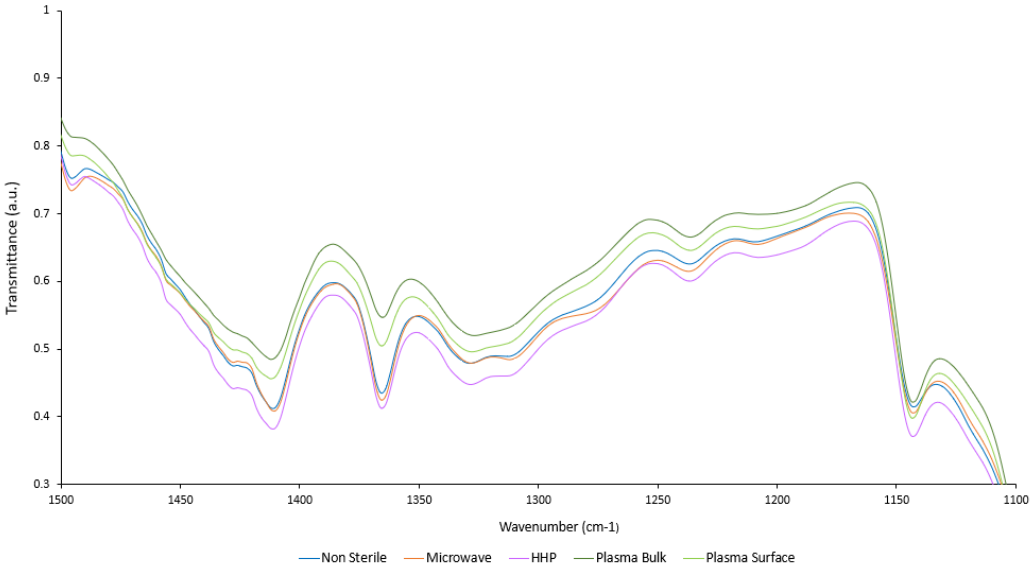

Figure 3.7: FTIR-ATR spectra of the non-sterilized and sterilized PVA-Zylon hydrogels, in the region of 1500–1100 cm^{-1}.

The same behaviour as in Figure 3.5 then occurs in the region between 1500 and 1100 cm^{-1} (Figure 3.7). The peaks in this region have been attributed to OH in-plane blending and C-H wagging in PVA [125], and to C-C and C-N-C stretching in the benzoxazole and imide rings of Zylon [127, 128, 129]. HHP once again exhibits a higher intensity of the peaks while the microwave samples remained closer to the non-sterilized samples' spectrum.

To better assess the differences in chemical structure derived from the sterilization methods, specific FTIR peaks were also analyzed. Table 3.1 shows specific FTIR peaks also found in other publications and the order of intensity found in our spectra.

Table 3.1: FTIR peaks for PVA and Zylon (PBO). N-non sterile; M-microwave; H-HHP; P-plasma; PS-plasma surface; PB-plasma bulk

Wavenumber (cm^{-1})	Association	Intensity	Source
1495	C=C stretch	M>H>N>P	[127]
1430	CH_2 bending	H>M=N>P	[130]
1141	C–C and C–O–C stretching	H>PS>M>N>PB	[131]
1132	CH_2 bending	H>M=N>P	[132]
1088	C-O stretch	H>P$\geq$N>M	[133]
1016	C-O-C asymmetrical stretching	M>H>N>P	[128]
916	CH_2 rocking	H>M=N>P	[132]
850	C-C band	H>M>N>P	[130]
705	C-H plane flexural vibration	N=M=H>P	[127]

3.4 Swelling

To characterize the effects of sterilization on the water absorption capabilities of the hydrogels, the SC and WC were determined in DD water at physiological temperature (37ºC). All samples were dried at 45ºC for 48 hours prior to testing.

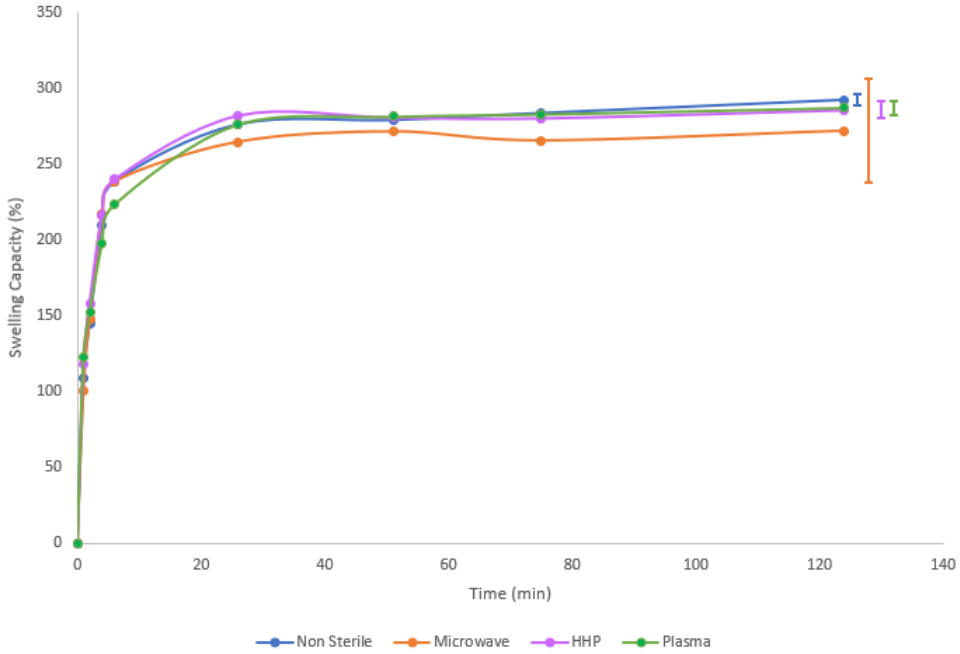

Figure 3.8: SC of the non-sterilized and sterilized PVA-Zylon hydrogels. The error bars represent the ± mean standard deviations (n=3).

The results of the swelling behaviour of the hydrogels are presented in Figure 3.8. A sharp rise in SC can be observed in the first 5 hours and, after 25 hours of hydration, the hydrogels seem to reach equilibrium. HHP and plasma sterilization seem to have no significant effect on this property. Meanwhile the microwave samples presented a high heterogeneity evidenced by the error bars. The dispersion of the results doesn´t allow for an appropriate conclusion on the effects of microwave irradiation on the SC of the hydrogels. Table 3.2 depicts the WC at equilibrium of all samples. The non-sterile samples showed the highest WC, and both plasma and HHP sterilization were similar. Microwave irradiation, also shows similar WC, but continued showing a much higher heterogeneity, even after increasing the number of tested samples (n=7).

Table 3.2: WC of the non-sterilized and sterilized PVA-Zylon hydrogels. The error represents the ± standard deviation (n=7).

Material	WC (%)
Non Sterile	74.5 $\pm$ 0.3
Microwave	73.1 $\pm$ 4.0
HHP	74.1 $\pm$ 0.4
Plasma	74.2 $\pm$ 0.5

3.5 Mechanical Properties

3.5.1 Compression

To measure the resistance of the PVA-Zylon hydrogels to compressive loads, an unconfined compression test was performed, at a strain rate of 0.1 mm·s^{-1}, up to a 40% strain. The material shows a typical viscoelastic behaviour. As the load is applied, the hydrogels suffer re-orientation of their polymeric chains and fluid begins to flow out of the network. This causes the initial portions of the curve (until ≈5% strain) to have a lower slope, as the fluid is responsible for counteracting the compressive load. Afterwards, the solid portion of the hydrogel starts to have a greater contribution to its compressive stiffness. A typical stress-strain curve for each of the sterilized and non-sterilized hydrogels is shown in Figure 3.9.

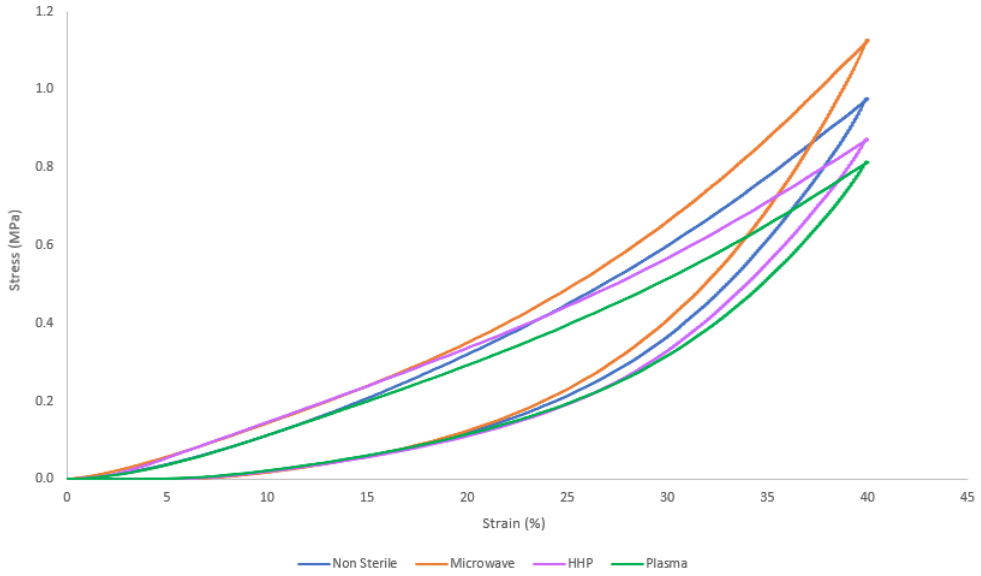

Figure 3.9: Typical compressive stress-strain curves of non-sterilized and sterilized PVA-Zylon hydrogels.

The compressive elastic, or Young modulus (E_c), calculated from the initial linear portion of the stress strain curves (1% strain) is shown in Table 3.3. Both HHP and plasma sterilization have no significant effect on the (E_c) of the hydrogels. The microwave irradiated samples on the other hand, show more than double increase of E_c than that obtained for the non-sterilized samples.

Table 3.3: Average compressive Young' Modulus of non-sterilized and sterilized PVA-Zylon hydrogels. The error bars represent the ± mean standard deviations (n=2).

Material	Young' Modulus (MPa)
Non Sterilized	0.25 ± 0.08
Microwave	0.55 ± 0.10
HHP	0.25 ± 0.06
Plasma	0.26 ± 0.05

More information can be obtained by measuring the evolution of the compressive modulus with increasing strains. Figure 3.10 depicts the compressive tangent modulus between 5-35% strain. Each of the sterilization methods differently affect the material. Microwave irradiation was found to increase the compressive stiffness of the hydrogels, across the whole tested strain range, from a minimum increase of 5.29%, up to a maximum of 32.41%. However, these increases were smaller than those observed at very low strains.

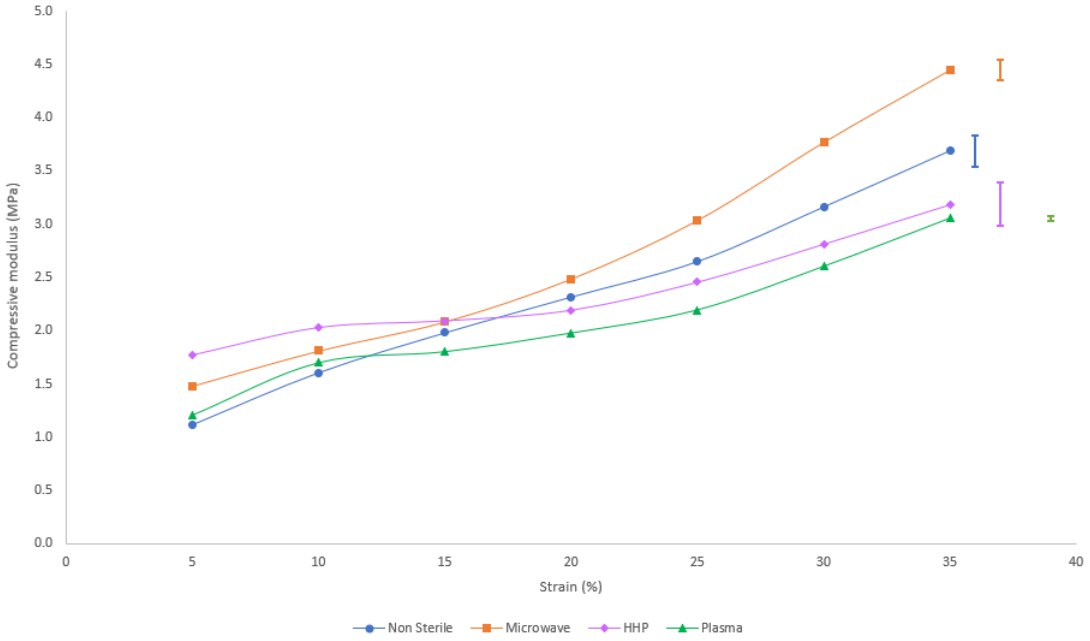

Figure 3.10: Comparison of compressive tangent modulus of sterilized and unsterilized samples obtained at different strains (5–35%). The error bars represent the ± standard deviations (n=2).

The other two procedures show a slightly different behaviour to those of the non sterilized and microwave samples, with a less linear increase. At lower strains, up to ≈15%, the HHP samples present the highest compressive modulus, with increases of up to 58% compared to the non-sterilized samples. However, at higher strains, HHP actually shows a lower compressive resistance than the non sterilized samples, with modulus up to 13.57% lower. Lastly, the plasma treatment resulted in a similar behaviour to the one observed in the HHP samples. While at lower strains, the plasma samples do show a slightly higher modulus than the non-sterilized, this increase is significantly lower when compared to the other methods (maximum 7.86%). As the strain increases, the plasma samples show the lowest compressive stiffness of all the tested materials, lowering the modulus by up to 17.67% compared to the non-sterilized samples.

3.5.2 Tension

The tensile properties of the non-sterilized and sterilized hydrogels were also tested. The typical stress-strain curve for each method is displayed in Figure 3.11. The average tensile Young's Modulus (E_t) measured from different hydrogel samples as well as the stress and strain at break are presented in

Table 3.4.

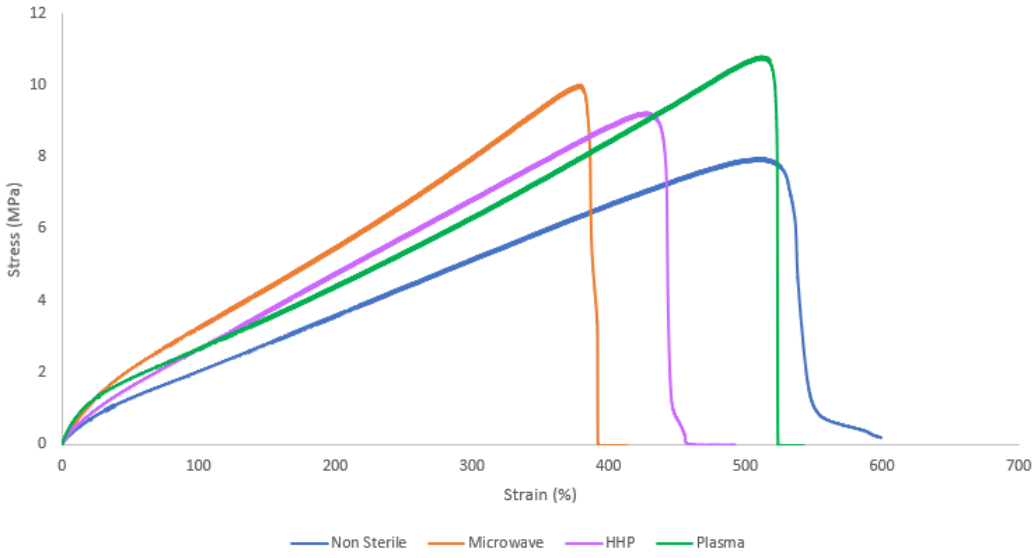

Figure 3.11: Typical tensile stress-strain curve of non-sterilized and sterilized PVA-Zylon hydrogels.

Table 3.4: Average tensile Young' Modulus, stress and strain at break of unsterilized and sterilized hydrogels. The error represents the ± standard deviations (n=4).

Material	Young' Modulus	Stress at break (MPa)	Strain at break (%)
Non Sterilized	5.74 ± 0.92	7.81 ± 0.84	516 ± 12
Microwave	10.22 ± 1.05	9.5 ± 0.68	374 ± 5
HHP	7.95 ± 0.49	8.35 ± 1.01	419 ± 4
Plasma	8.74 ± 1.81	11.14 ± 1.37	490 ± 23

All sterilization methods appear to have a significant effect on the tensile resistance of the hydrogels. Microwave, HHP and plasma sterilization increased the E_t to 177%, 138% and 152% of the original value, respectively. While all methods also increased the average stress at break, the maximum strain actually diminished in microwave and HHP sterilized samples, a behaviour which indicates an increase in stiffness of the polymer.

The variation of the tensile tangent modulus from 1-35% strain is shown in Figure 3.12. All sterilization methods had positive effects on the tensile resistance of the PVA-Zylon hydrogels, with an increase in tensile modulus across the tested strains. Microwave irradiation especially, shows very significant increases, ranging between 46 and 78%.

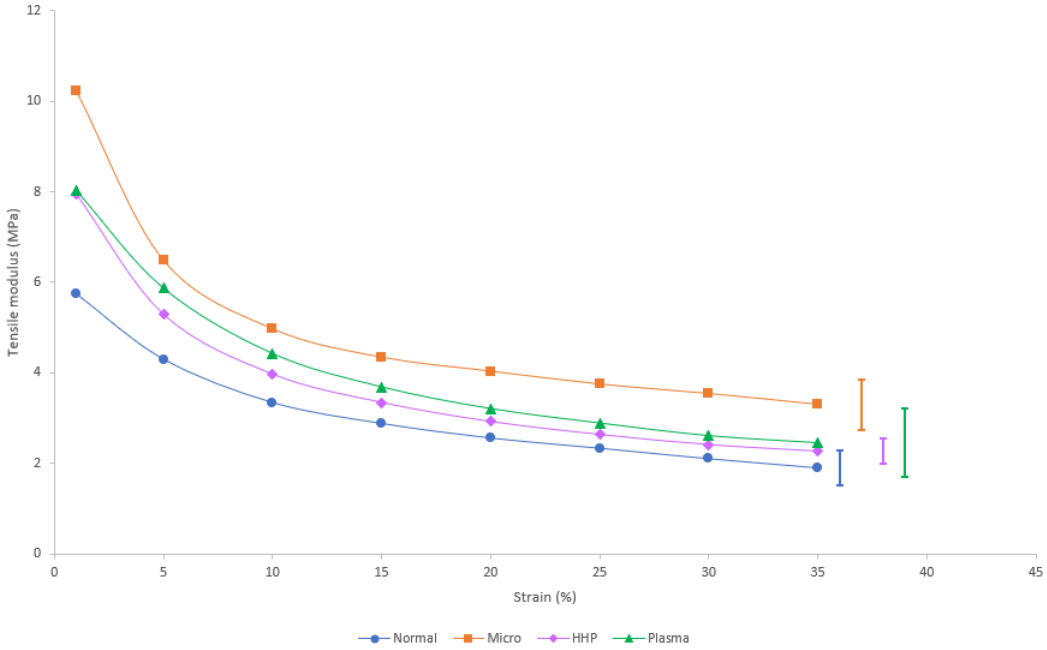

Figure 3.12: Comparison of tensile tangent modulus with increasing strain, on sterilized and unsterilized samples. The error bars represent the ± mean standard deviations (n=4).

3.5.3 Rheology

The linear viscoelastic regime (LVE) of the PVA-Zylon hydrogels was determined with an amplitude sweep test at a fixed frequency of 1 Hz (Figure 3.13). The storage (G') and loss (G") moduli remained almost constant throughout the strain range of 0.01-0.1%. With strains greater than 0.1% G' starts to decrease and G" increases. Thus a shear strain of 0.1% was the proposed optimal working strain for this material and was used for all subsequent testing.

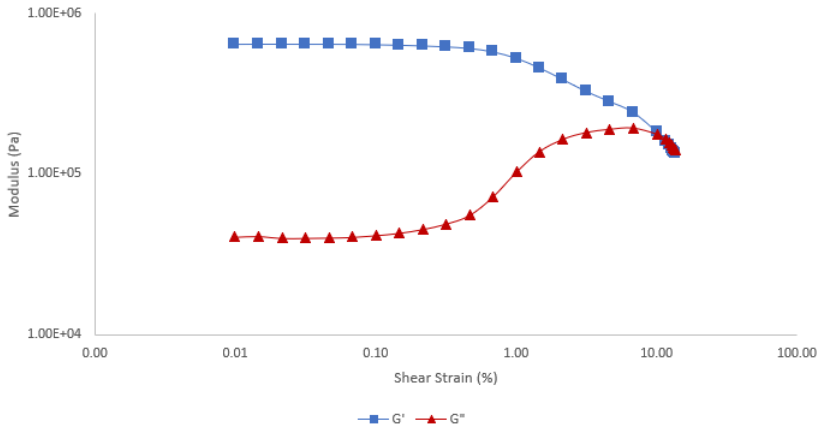

Figure 3.13: Amplitude sweep curve of PVA-Zylon hydrogels, at 37ºC and with a fixed frequency (1 Hz).

Figure 3.14 shows the angular frequency sweep curves obtained within the LVE (fixed 0.1% of strain). For all hydrogels G' is almost 1 order of magnitude larger than G" across the tested frequency range, indicative that the PVA-Zylon hydrogels show a rigid network, with elastic rather than viscous response

to stress. Overall, the effect of the angular frequency on G' and G" does not seem to be very significant. G' very slightly increased with frequency, in both microwave and HHP samples. This effect was seen especially after reaching a frequency of ≈70 Hz, where a decrease in G" can also be observed. Meanwhile, in the non-sterilized and plasma samples G' starts decreasing (very slightly) for frequencies >70 Hz. Comparing the hydrogels, the non-sterilized samples showed the lowest G' and G", while microwave subjected hydrogels demonstrated the highest values (G'≈5.5 x 10^5 Pa; G"≈5.0 x 10^4 Pa).

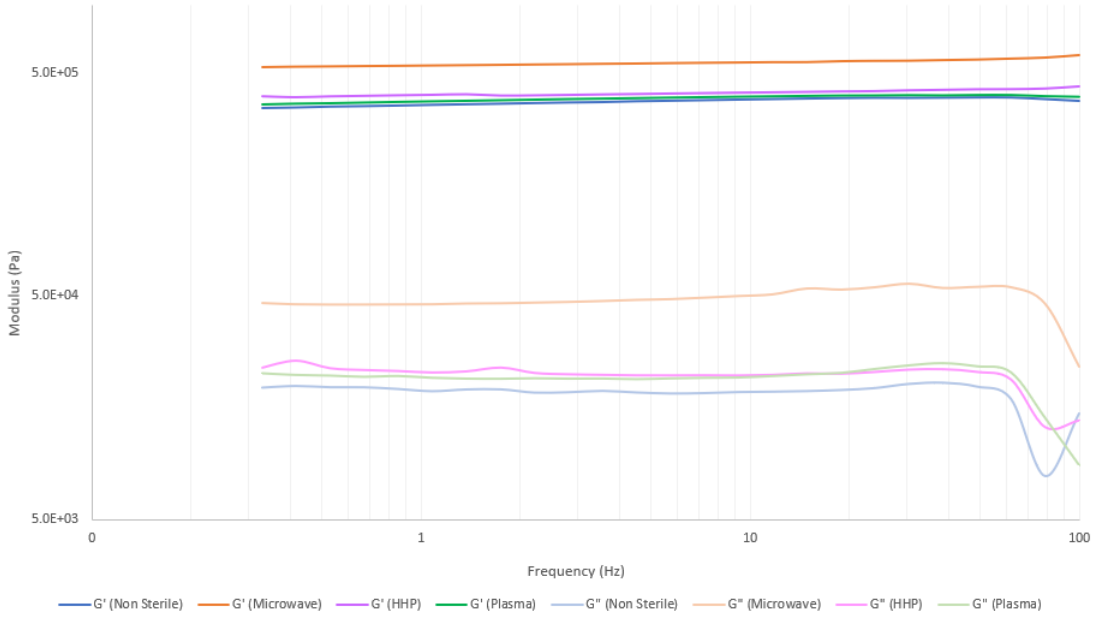

Figure 3.14: Frequency sweep curve (0.1–100 Hz) of the non-sterilized and sterilized PVA-Zylon hydrogels, within the LVE (0.1% strain).

Measurements of G' and G" at a fixed strain (0.1%) and frequency (1 Hz) were carried out as a function of time (1 hour) (Figure 3.15). As previously seen, G'>G" for all hydrogels, indicative of a predominant elastic behavior. Additionally, the hydrogels exhibit a minor decrease of G' over time, which could be caused by evaporation losses. The calculated phase angle (δ) of the hydrogels, obtained from the results of this test are shown in Table 3.5. As expected, the hydrogels show a predominantly elastic behaviour, with a δ close to 0º. The plasma treated samples show a δ almost equal to the non sterilized hydrogel, while HHP samples showed the lowest δ, indicating a lower amount of dissipated energy. Microwave irradiation slightly increased the δ, suggesting a higher viscous dissipation of energy.

Table 3.5: Phase angle of non-sterilized and sterilized PVA-Zylon hydrogels, obtained from the isothermal time test.

Material	Phase Angle (δ)
Non Sterilized	3.79º
Microwave	6.51º
HHP	2.47º
Plasma	3,82º

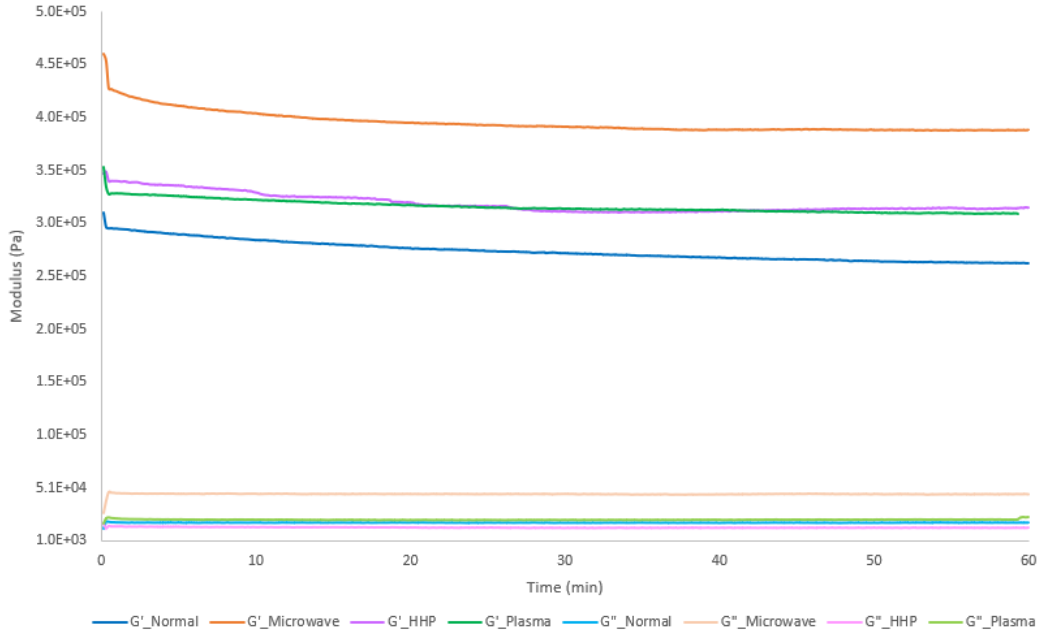

Figure 3.15: Storage (G') and loss modulus (G") as function of time (1 hour), at 0.1% strain and frequency of 1 Hz, for non-sterilized and sterilized PVA-Zylon hydrogels.

3.5.4 Hardness

The results of Shore A hardness measurements on the unsterilized and sterilized hydrogels are represented in Figure 3.16. Microwave irradiation and HHP increased the hardness of the material by 19.72% and 4.44%, respectively. Meanwhile, the plasma treatment reduced the hardness by 6.11%.

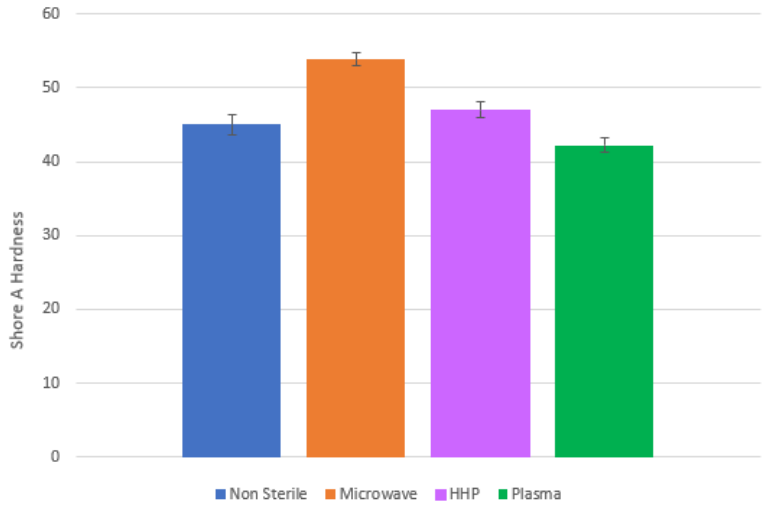

Figure 3.16: Shore A hardness values for the non-sterilized and sterilized PVA-Zylon hydrogels. The error bars represent the ± standard deviations (n=3).

3.6 Surface Properties

3.6.1 Wettability

Effects of the sterilization procedures on the surface wettability of the hydrogel were evaluated by measuring the CA with the captive bubble method. An example of the air bubbles formed on the bottom surface of the hydrogels is shown in Figure 3.17.

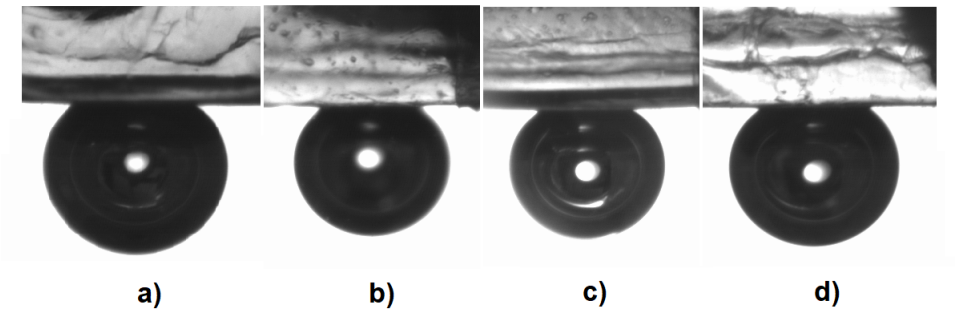

Figure 3.17: Comparison of air bubbles for wettability measurements on PVA-Zylon hydrogels (a-non sterile; b-microwave; c-HHP; d-plasma)

The measured CA of the sterilized and non-sterilized hydrogels are shown in Figure 3.18. No significant changes were observed in the wettability of the hydrogel after undergoing microwave, HHP or plasma sterilization. The largest variation was 3.13%, between the non-sterilized hydrogel and one that underwent microwave irradiation. All hydrogels show a hydrophilic behaviour, with a CA between 38.9º and 40.1º.

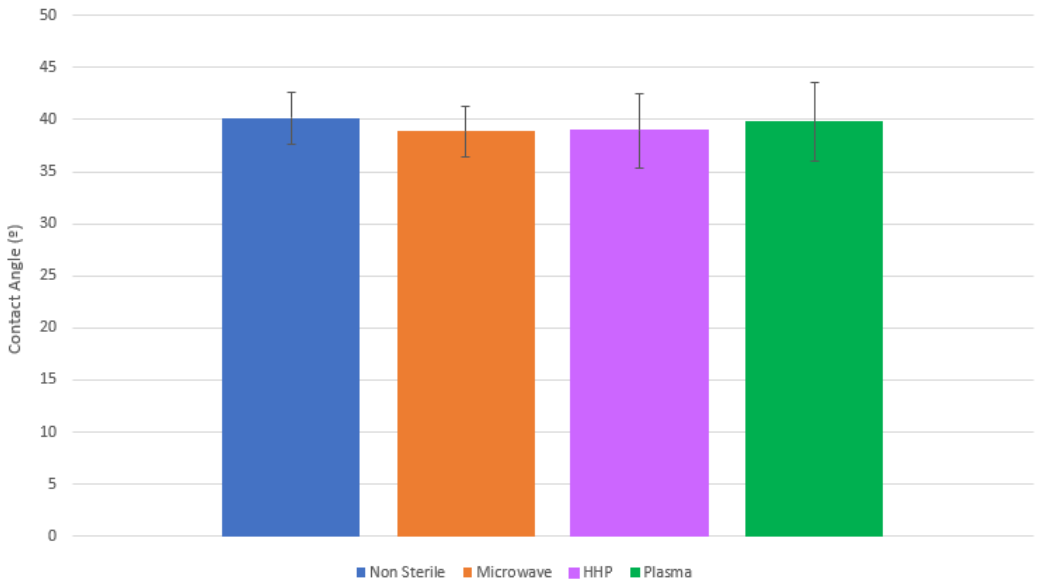

Figure 3.18: CA of the non-sterilized and sterilized PVA-Zylon hydrogels. The error represents the ± standard deviation (n=30).

3.6.2 Tribology

The CoF of the PVA-Zylon hydrogel was measured against porcine cartilage samples using a normal force load of 10, 20 and 30N, for $\approx$ 1 hour. DD water and SSF were tested as lubricants. The results for the maximum values measured during 2500 cycles are present in Figure 3.19. Higher loads led to a clear increase in the measured CoF in both types of lubricant. The CoF was lower for all tested normal forces with SSF as lubricant. SSF resulted in a CoF 53.3% lower at 10 N, 37.7% lower at 20 N, and 3.5% lower at 30 N than that obtained with DD water.

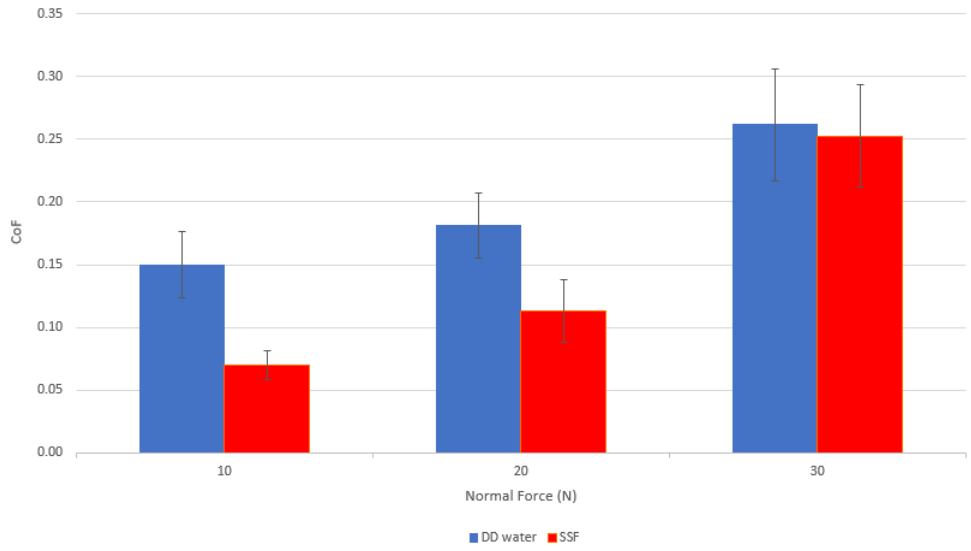

Figure 3.19: Maximum CoF of the non sterilized PVA-Zylon hydrogels against porcine cartilage at different loads, using DD water and SSF as lubricants. The error bars represent the ± standard deviations (n=3).

The effect of the sterilization procedures was studied, using the 30N load and SSF as lubricant. The maximum CoFs of the sterilized and non-sterilized hydrogels are shown in Figure 3.20. Microwave and HHP sterilization reduced the maximum CoF of the hydrogels by 31.26% and 32.94% respectively, while plasma sterilization increased the CoF by 8.11%. when compared to the non sterilized hydrogel. In all samples that underwent sliding at 30N load, markings were clearly visible in the hydrogel surface (Figure 3.21). The morphology of these markings was further observed by SEM (see section 3.6.3).

The evolution of the CoF in respect to time (with erroneous inertial effects - see section 2.4.7) can be seen in Appendix A.1.

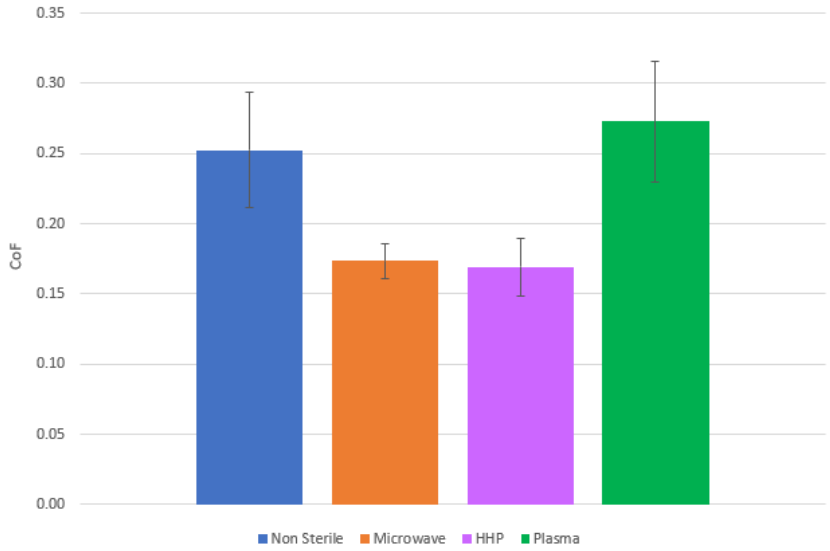

Figure 3.20: Maximum CoF of non sterilized and sterilized PVA-Zylon hydrogels against porcine cartilage, obtained by reciprocating analysis after 2500 cycles of linear friction, using SSF as lubricant. The error bars represent the ± standard deviations (n= 3).

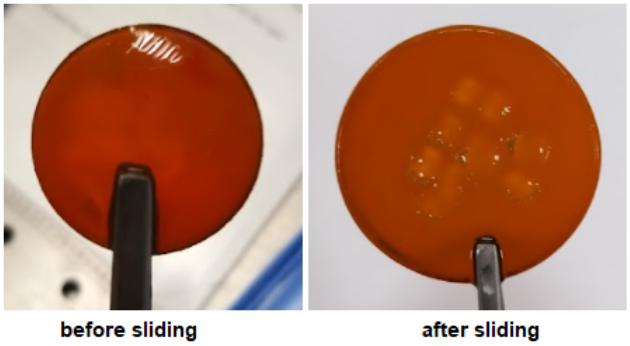

Figure 3.21: Exemplary image of PVA-Zylon hydrogels before and after the tribological tests at 30 N.

3.6.3 Surface Morphology

Surface analysis of the sterilized and non-sterilized hydrogels was performed by SEM (Figure 3.22). The micrographs did not show any micropores on the hydrogels. Due to low resolution, it is hard to observe the differences between the non sterilized samples and the ones subjected to microwave and HHP. However, the sterilized samples appear to show a slightly more homogenous and smooth surface. On the other hand, plasma sterilization seems to have increased roughness of the samples. Moreover, some samples showed the presence of etching-derived holes (Figure 3.23). It is possible to verify a large distribution of holes across the hydrogel's morphology, as well as the different stages of etching.

SEM images were taken from inside the wear tracks caused by the tribological testing (Figure 3.24). The non-sterile samples show a more delaminated surface compared to the sterilized ones. The sterilized samples show a wavy like pattern throughout the track, more striking for the hydrogel subjected to the plasma process, demonstrating a much rougher surface when compared to microwave and HHP samples, which is in agreement with the CoF results shown in Figure 3.20. This effect can also be seen

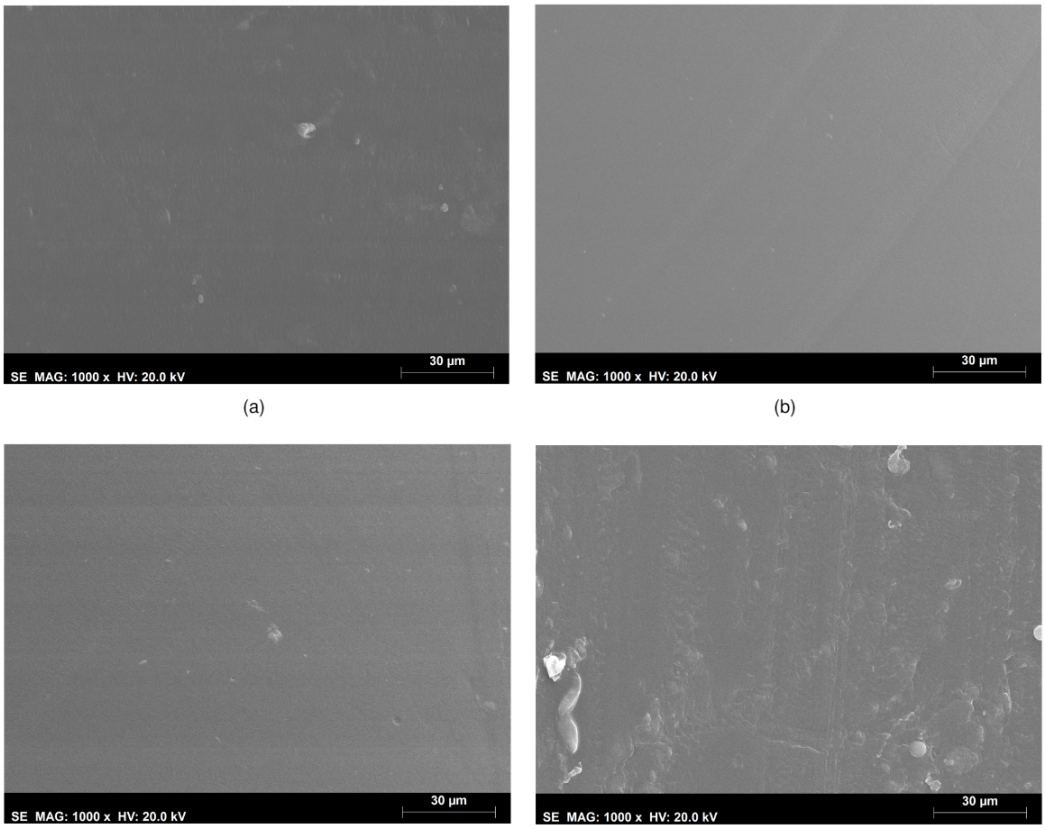

Figure 3.22: SEM micrographs of the PVA-Zylon hydrogels. (a) Non sterile; (b) Microwave; (c) HHP; (d) Plasma. All images were acquired with 1000x magnification.

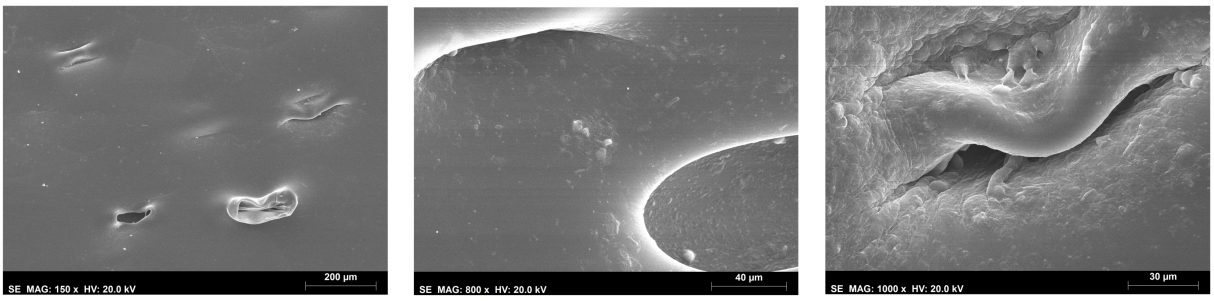

Figure 3.23: SEM micrographs of plasma sterilized PVA-Zylon hydrogels, at different magnifications, (a) 150x; (b) 800x; (c) 1000x

at the edge of the tracks, shown in Figure 3.25. The non-sterilized hydrogels show a delaminated edge while the hydrogels subjected to microwave irradiation present a much smoother transition, as focus is more continuous throughout the all image. The plasma samples show a much more pronounced effect. The track interface is clearly visible and rough, depicting in some areas extreme wear (Figure 3.25,c) .

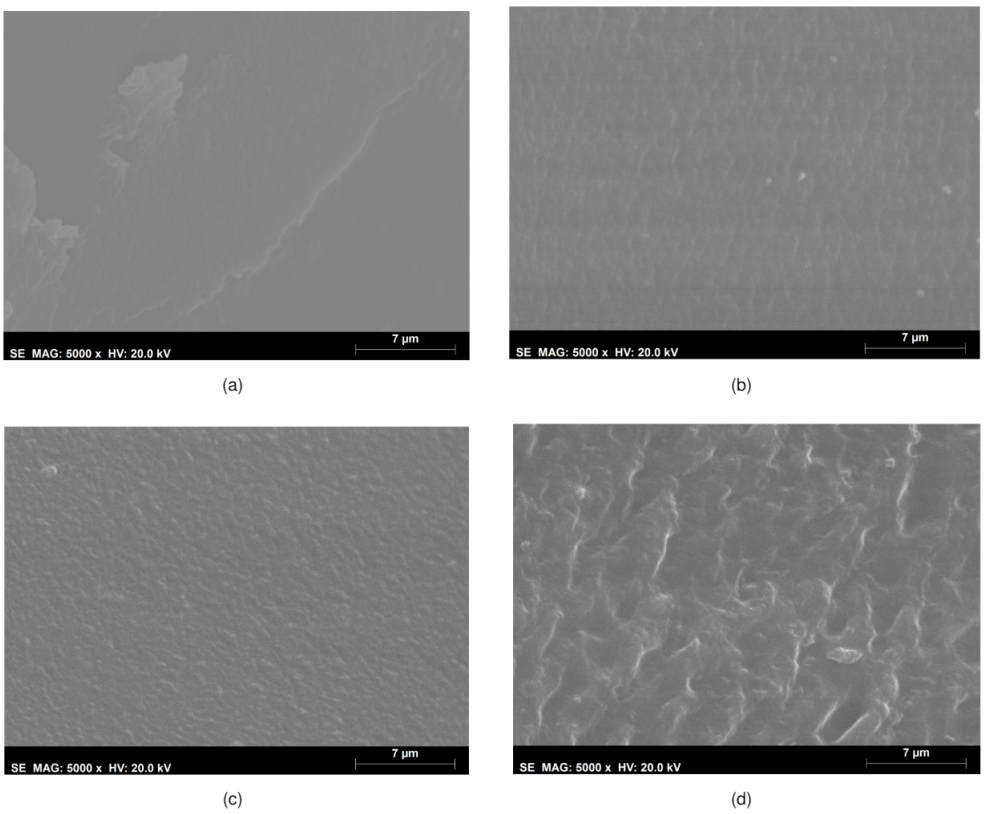

Figure 3.24: SEM micrographs of the PVA-Zylon hydrogels inside the tracks after the tribological tests. (a) Non sterile; (b) Microwave; (c) HHP; (d) Plasma. All images were acquired with 5000x magnification.

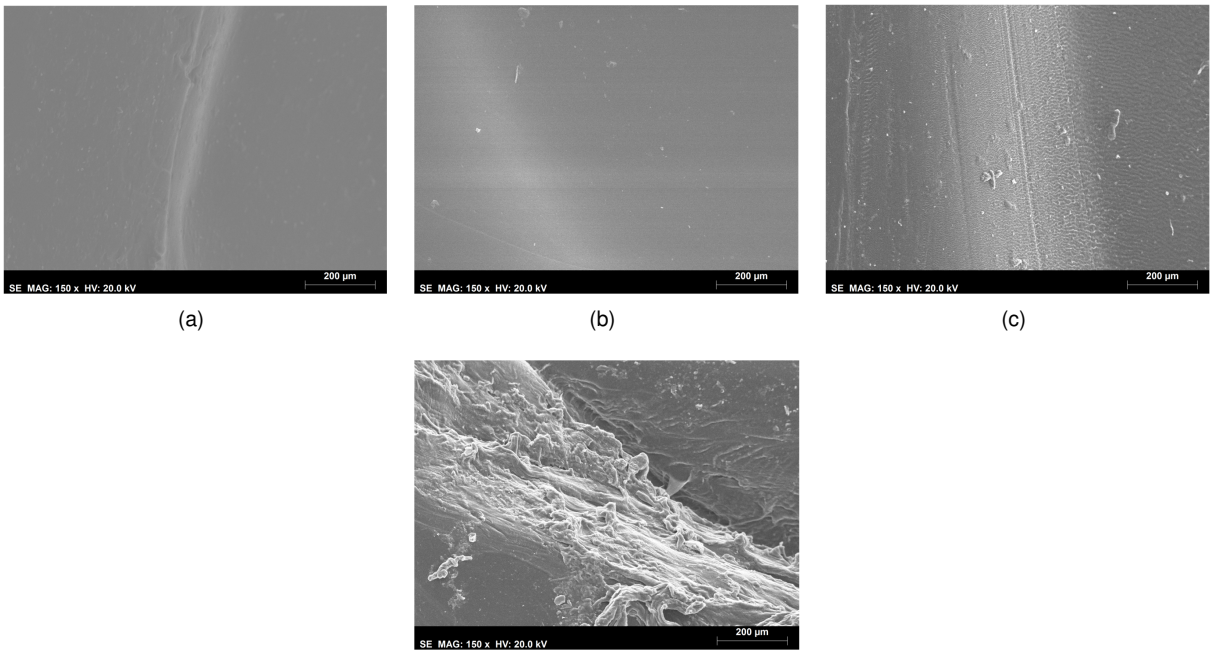

Figure 3.25: SEM micrographs of hydrogels surface at the interface of friction markings (a) Non sterile; (b) Microwave; (c,d) Plasma. All images were acquired with 150x magnification.

3.7 Biocompatibility

3.7.1 Irritability

Macroscopic photographs of the CAM after 5 minute of direct contact with the non-sterilized and sterilized PVA-Zylon hydrogels are presented in Figure 3.26. In the positive control, the addition of NaOH caused severe irritation, with an almost instant hemorrhage and coagulation (Figure 3.26,b). Contrarily, the effects of the hydrogel samples were similar to the negative control, with no visual signs of lysis, hemorrhage or coagulation, as such, the IS was equal to 0.

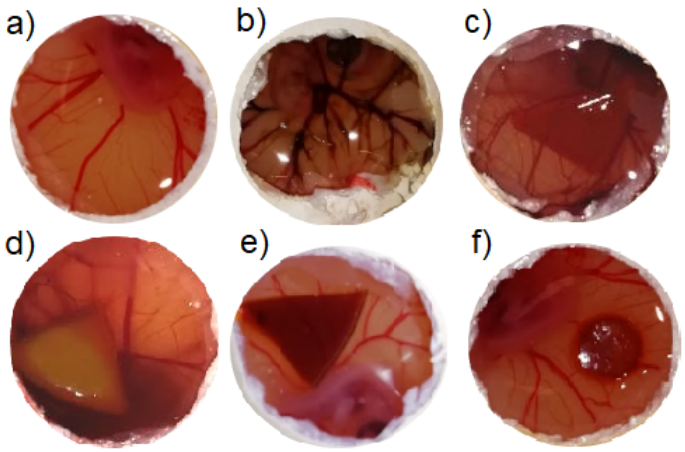

Figure 3.26: Chorioallantoic membrane images after 5 minute of exposure to the hydrogel samples. a) negative control (NaCl 0.9%); b) positive control (NaOH, 1 M); c) non-sterilized hydrogel; d) microwave; e) HHP; and f) plasma subjected hydrogels.

3.7.2 Citotoxicity and Cell Adhesion

Figure 3.27 presents the micrographs taken of the chondrocyte cells immediately before the MTT assay, with a magnification of 100x. Visual inspection of the cultured chondrocyte appear to show a greater number of cells on the wells containing extracts from the plasma treatment, than in the other methods. The MMT assay confirmed these results (Figure 3.28)), with the extracts from the hydrogels after microwave and HHP sterilization showing significantly lower percentage of viable cells (68.75% and 77.6%, respectively) when compared to the negative controls. Plasma, on the other hand, showed excellent results, with a cell viability of 98.57%.

Photographs of the chondrocytes at 1000x magnification images can be seen in Figure 3.29). All the cultured cells show a correct chondrocyte morphology, evidenced by their similarity with the negative control. A study of cell adhesion was also carried out (Appendix B.1). After 22 days cells were seen to adhere and thrive in all samples. Due to the color of the samples and low resolution of the pictures made it hard to correctly analyze the cell morphology. Unfortunately, due to time constraints, SEM micrographs of the cultured samples couldn´t be taken.

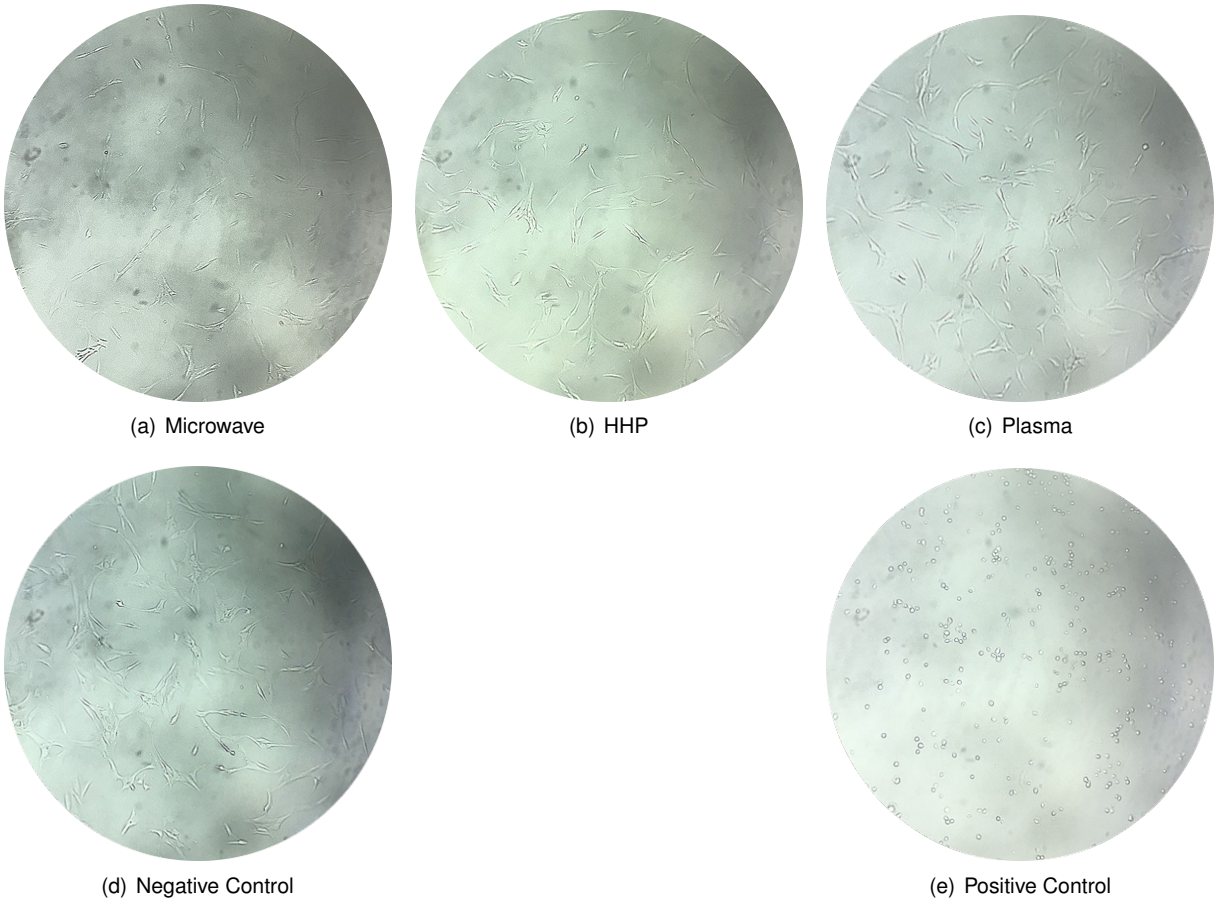

(a) Microwave (b) HHP (c) Plasma

(d) Negative Control (e) Positive Control

Figure 3.27: Micrographs of the chondrocytes cultured with sample extracts and controls at 100x magnification, immediately before the MTT assay.

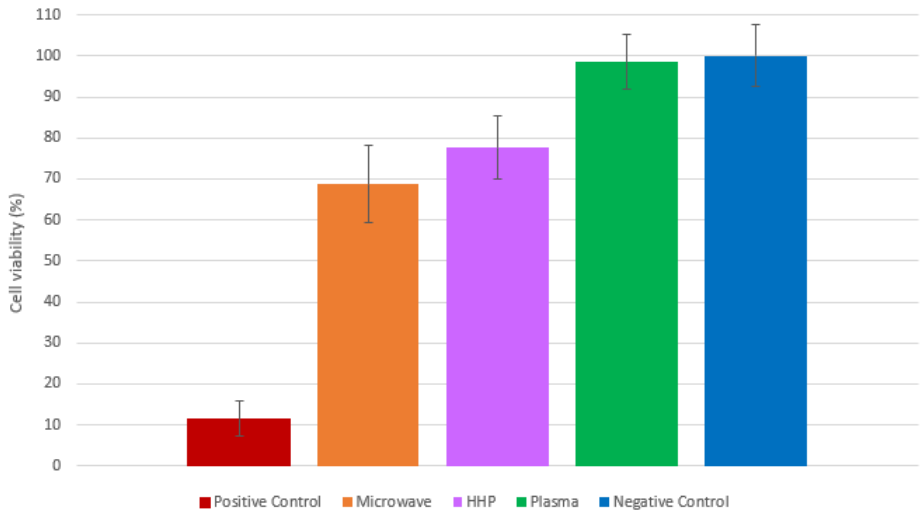

Figure 3.28: Chondrocyte cell viability (%) determined by the MTT assay, after 48 hours of exposure to the hydrogel sample extracts. The relative cell viability is presented as percentage of negative control cells. The error bars represent the ± standard deviations (n=4*2).

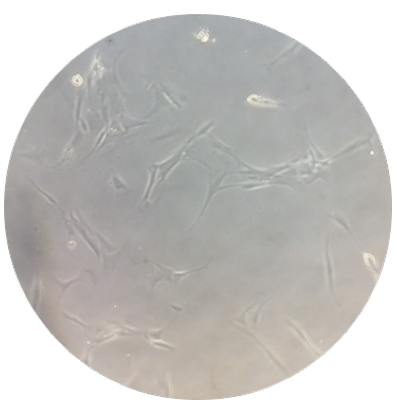

(a) Microwave

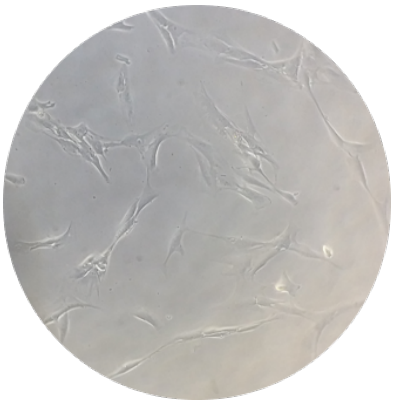

(b) HHP

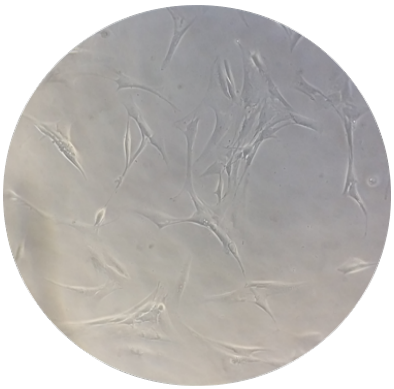

(c) Plasma

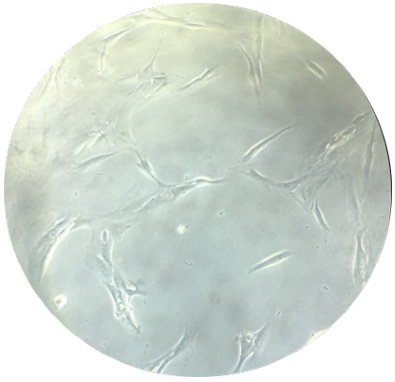

(d) Negative Control

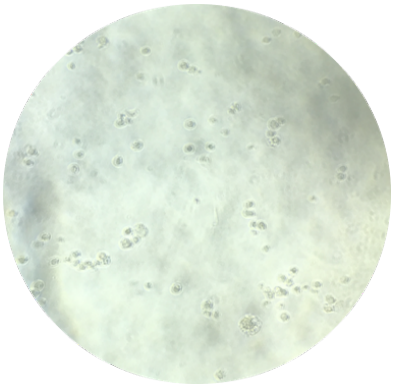

(e) Positive Control

Figure 3.29: Micrographs of the chondrocytes cultured with sample extracts and controls at 1000x magnification, immediately before the MTT assay.

Chapter 4

Discussion

PVA is to date the most employed synthetic hydrogel in research for cartilage replacement. All due to its unique properties that surpass those of other used hydrogels. However, PVA alone is not able to ensure all the required needs for the intended function, with mechanical and tribological properties below those of natural cartilage. Therefore, the reinforcement of PVA with fibers and/or co-polymerization with other complementary polymers has been applied for better solutions to repair damaged cartilage [45]. In this work PVA was reinforced with Zylon nanofibers, and to the best of the author' knowledge, there are no previous reports on such type of approach to get a cartilage replacement material. Additionally, the importance of sterilization of implantable biomaterials is undeniable, being a mandatory step for clinical use. It is known that sterilization processes can result in significant changes in the properties of hydrogels [67]. Also it can lead to damage of biologically active substances contained in the hydrogels. In this sense, the novelty of this work is not only based on the use of Zylon reinforced PVA hydrogels, but also in the characterization of its properties after non-conventional sterilization processes that involve lower temperatures than the common steam-heat sterilization.

Regarding these non-conventional methods, some remarks should be made. During the scope of this work, microwave irradiation and HHP sterilization proved to be highly reproducible procedures, and allowed for a terminal sterilization of the hydrogels. Unfortunately, such was not the case for the plasma treatment. The typically inert argon plasma is known to become unstable in the presence of water, dangerously increasing its temperature and amount of produced radicals [134]. Thus, the hydrogels had to be sterilized in their dry state, which meant terminal sterilization was not possible. This added an extra step of possible contamination, an effect which occurred during the scope of this work. Moreover, the equipment lacks a way to measure the gas flow rate, a crucial parameter which influences the efficacy and effects of the plasma sterilization procedure. While all possible measures were taken to try and maintain a consistent gas flow, small variations could have occurred between samples. Nevertheless, with added precaution, plasma sterilization still proved to be capable of sterilizing the PVA-Zylon hydrogel, and so its effects on the hydrogel's properties were measured.

PVA hydrogels reinforced with Zylon nanofibers were synthesized through the cast-drying method. Physical gelation of PVA has been assigned to the the formation of inter-chain hydrogen bonds between

the O–H groups of PVA [135]. The Zylon microfibres (i.e. PBO) were solubilized in a TFA/MSA mixture to carry out acid-catalyzed hydrolysis, tailoring the microfibers into nanofibres. The ratio of Zylon to TFA/MSA acid mixture is similar to other research, for the production of Zylon aerogels [129]. The high aspect ratio of the nanofibers can lead to multiple fiber interconnections, promoting the gelation process. Furthermore, this process creates functional sites in the nanofibres (i.e., carboxyl, amino and phenolic hydroxyl groups), which can combine with PVA molecules through hydrogen bonding [62].

Table 4.1 shows the measured properties of the hydrogels compared to those of natural articular cartilage. The PVA-Zylon hydrogel displayed adequate compressive, tensile and shear resistances, while maintaining a WC well within the range measured for articular cartilage. The reinforcement of the PVA matrix with Zylon nanofibers allowed for a superior compressive resistance compared to monopolymer, cast-dried PVA hydrogels [51]. Unfortunately, some properties still fell short of the natural tissue, particularly the Shore A hardness and CoF.

Table 4.1: Biomechanical properties of non-sterilized PVA-Zylon hydrogel and natural articular cartilage

Property	**PVA-Zylon**	**Articular Cartilage**	**Source**
E_c (MPa)	0.25	0.24–0.85	[25]
E_t (MPa)	5.74	5–25	[25]
G* (MPa)	0.3	0.2–2.5	[25]
Tensile strength (MPa)	7.8	0.8-25	[25]
Shore A Hardness	45	87.5	[26]
WC (%)	75	65-80	[3]
CoF	0.25	0.001-0.03	[6]

After undergoing sterilization, the PVA-Zylon properties were altered, with each sterilization method affecting the material in different ways. Microstructure analysis of the non-sterilized and sterilized samples was carried out to understand possible modifications from the chemical point of view of the materials.

FTIR analysis of the samples submitted to microwaves shows higher intensities in peaks attributed to carbonyl (C=O), C=N and vinyl (C=C) groups compared to non-sterilized samples. The microwave process seems to induce an increase in the amount of double bonds in the PVA-Zylon hydrogel network. Microwave samples also show a very slight increase in C–C and C–O–C peak intensity (i.e. 1141 cm^{-1}), which indicates intermolecular bonding. These results are congruent with other studies on the effect of microwave irradiation on PVA and PVA/graphene nanocomposites [125], which stated that after 5 minute irradiation exposure at 200 W, the intensities of peaks related to C=O and C=C groups increased. The researchers hypothesized that microwave irradiation led to side chain scission and formation of double bonds between the polymers. Contrary to gamma irradiation, microwave sterilization uses a non-ionizing radiation, and can be a cheaper, easier and safer alternative. However, similar results to those obtained in this thesis have been found in PVA samples after gamma irradiation [130, 132, 136]. El-Sawy *et al.* [130] found that moderate doses of gamma irradiation in crosslinked PVA films also led to this increase

in intensity for C=O and C=C groups. Bhat *et al.* [132] also evaluated the effect of gamma irradiation on the structure and morphology of PVA films, and observed an increase in the crosslinking density, when compared to non-irradiated samples, which was related to the improvement in the irradiated-PVA's mechanical resistance. The researchers hypothesized that, during irradiation, the PVA molecules underwent structure arrangement and main chain rupture, forming C=O and C=C groups. In the present work, it is plausible that the main chain of PVA was not ruptured, as for this to occur it would be expected a decrease in intensity in C–H and CH_2 bonds, which did not occur. In fact, in the peaks associated with these groups (2850-2950, 1430, 1132 and 705 cm^{-1}) the microwave and non-sterilized samples' spectra overlapped, indicating that no effects were caused in these bonds. Thus, chain rupture most likely occurs mainly in the side chains, further evidenced by the lower intensity in areas associated with -OH (3200-3400 cm^{-1}) and C-O (1088 cm^{-1}) groups in PVA. This could facilitate the segmental motion and chains become more free to realign [125], which ultimately can led to additional cross-linking.

In the case of HHP processing, the high applied pressure shall induce changes in the molecular structure. The results from FTIR analysis indicate that HHP sterilization increased the amount of hydrogen bonding across the PVA-Zylon hydrogel matrix as HHP samples showed increased intensity in peaks associated with -OH (3200-3400 cm^{-1}). Also, the intensity of peaks attributed to C-H (2850-2950 cm^{-1}), C-N-C (1500-1100 cm^{-1}), CH_2 (1430, 1132 and 916 cm^{-1}), C-O-C (1141 and 1016 cm^{-1}), C-O (1088 cm^{-1}) and C-C (850 cm^{-1}) groups increased, suggesting that deeper changes in the chemical structure of the polymeric matrix shall occur. Meanwhile, double bonding doesn´t seem to be very prevalent, as both spectra overlap in most regions associated to these bonds. Although, there does appear to be a small increase in C=C bonding (1495 cm^{-1}) when compared to the non-sterilize sample' spectrum (see Figure 3.7). To the best of the authors knowledge, no studies exist on the effect of HHP on the microstructure of crosslinked hydrogels. However, studies on HHP processing on pre-crosslinked hydrogels are in agreement with these results. Negishi *et al.* [137] found that HHP treatment on PVA-heparin solution could induce their crosslinking into hybrid gels, with an homogenous dispersion of heparin within the PVA matrix. The researchers postulated that HHP induced dehydration and subsequent inter/intra-molecular hydrogen bonding between molecules. Additionally, Lian *et al* [126] found that HHP treatment at 600 MPa on pre-processed PVA-chitosan-TiO_2 solution led an increase in -OH stretching peak (3200-3400 cm^{-1}). The treated samples produced composite films with improved homogeneity and tensile properties , which was related to the breaking of H-bonds between chitosan and PVA molecules, and new H-bonds forming between the amino groups of the polymer chains. Overall, HHP sterilization seems to induce the formation of hydrogen and single bonds across the PVA-Zylon hydrogel matrix. The extreme pressures during the HHP process may cause breakage of H-bonds and the creation of new intra/inter-molecular bridges between the polymer molecules.

Plasma sterilized samples show a reduced peak intensity across the whole FTIR spectrum, with the bulk sample showing overall lower intensity than the surface. These results could indicate the general rupture of bonds in the hydrogel structure due to plasma sterilization. The only peaks where plasma samples show slightly higher intensities than the non-sterile are those associated to C-O stretch (1088 cm^{-1}). Samples from the surface of plasma samples also showed higher intensity at peaks attributed

to C-C and C-O-C stretching (1141 cm^{-1}). Accordingly, Paneru *et al.* [138] found that a 5 min argon plasma treatment in PVA-Chitosan films, led to the appearance of new oxygen containing functionalities (O-C=O) and an increase in O/C ratio of the films. Other researchers found that Ar plasma treatment caused a very small increase in the amount of oxygen atoms in Zylon fibers [139]. During plasma treatment, the inert argon plasma is thought to break the chemical bonds of the hydrogel's surface and create radicals. When the material is exposed to air, these radicals can then form polar bonds with oxygen atoms in the atmosphere [140]. Furthermore, if small amounts of air are left in the chamber when the plasma treatment is initiated, it could also be ionized and react with the polymers [141]. As sources of oxygen atoms are limited in argon plasma, the increase in C-O bonds should be low, which is in agreement with the small peak increase we observed. A lower intensity of the C=O peak was verified for plasma samples when compared to non-sterilized ones. This could be related to the plasma treatment mainly inducing the formation of C-O bonds between oxygen atoms in the atmosphere and carbon atoms which were free due to the breakage of bonds in the main polymer chains. Some of these C–O groups could then form bonds between other free carbon atoms, inducing C–O–C intermolecular bonding. This is more clear for the surface plasma sample than for the bulk sample, as expected, being plasma sterilization process a more superficial method.

Concerning the swelling capacity of the non-sterile and sterile PVA-Zylon samples, none of the sterilization procedures seems to have affected the capacity of the hydrogels to retain water. These results are somewhat surprising, compared with the microstructural effects seen in the FTIR spectrum. The microwave samples displayed a significant variation in WC. This may be due to the uneven heating of the samples during the microwave sterilization process [83]. Thus, possible modifications in the hydrogels' matrix and in the chemical interactions are irregular, an effect which is more evident in high-moisture materials, such as hydrogels [84]. A study on crosslinked cast dried PVA hydrogels showed that HHP processing lead to a significant increase in their swelling capacity, and decrease their mechanical resistance [54]. This effect is suggested to be due to the destruction of H-bonds between PVA molecules. Contrary, in this study, HHP sterilization almost did not affect the PVA-Zylon hydrogel's WC. This divergence could suggest that the addition of Zylon fibers into the PVA hydrogel network allow it to better withstand the HHP processing compared to mono-polymer PVA hydrogels. Regardless, non-sterile and sterile samples display a WC well within the range measured for articular cartilage (65-80%) [3].

Mechanical properties of implantable biomaterials should be as similar as possible to the natural tissue, in order to minimize interfacial strain mismatch at the implant/tissue interface. Overall, research suggests that the compressive stiffness of native cartilage is more dependant on the viscous phase (i.e. interstitial fluid) [21, 24, 25], while tensile and shear stiffness is more dependant on the elastic phase (i.e. collagenous matrix) [142, 143].

Microwave irradiation appears to have had a very positive effect on the mechanical properties of the PVA-Zylon hydrogel. The compressive, tensile and shear resistances, as well as the Shore A hardness of the material significantly increased. After irradiation, samples show a compressive Young modulus, E_c (1% strain) more than double that of the non sterilized samples, which indicates a stiffer material as expected considering the hardness of the hydrogel. The compressive tangent modulus also increase

across the whole tested range (5–35%), however these increases were smaller than those observed at 1% strain. In this initial portion of the compressive strain, fluid flow plays the most significant role in resisting the applied load [21]. Besides increasing the stiffness of the crosslinking matrix, microwave irradiation could also have an effect on the interaction between interstitial water and the polymer chains, increasing the frictional drag between liquid and solid phases and subsequently increasing E_c. This is corroborated with the increase in phase angle (δ) observed in the rheological isothermal time test, which indicates a higher viscous dissipation of energy. Besides increasing the tensile modulus until 35% strain, microwaves also improved the maximum stress but decreased the maximum strain, thus further indicating a higher stiffness of the hydrogel.

For its part, HHP processing resulted in the increase in shear and tensile moduli, as well as in the Shore A hardness of the samples, which is in agreement with the higher amount of single bonds in the hydrogels' matrix. It was expected that the HHP hydrogels would also show increased compressive modulus, however this was only true at lower strains (between 5–15%). In this range, the HHP hydrogels actually showed the best compressive stiffness out of all the tested methods. However, at higher compressive strains, the modulus became lower than that shown by the non-sterilized samples. Weaker bonds could be the cause for this behavior, hindering the hydrogels' capacity to resist stronger stresses. Concerning E_c (1% strain), the HHP process had no effect. Nevertheless, the HHP samples showed the lowest δ in the rheological isothermal time test, indicating a lower amount of viscous dissipated energy. These results could be correlated with the possibility that HHP may decrease the interaction of the polymeric chain with water.

Plasma sterilized hydrogels showed contradicting results in the mechanical testing. After plasma treatment, the E_c (1% strain) of the hydrogels was unaffected and while a small increase was found at lower strains (5-15%) the compressive modulus significantly decreased at higher strains. The Shore A hardness of the plasma sterilized hydrogels was also slightly lower (6.11%) than that of the non-sterilized material. The results from FTIR analysis indicated an overall bond degradation in the PVA-Zylon hydrogel. This factor could explain the reduced compressive stiffness observed at higher strains and lower hardness. Meanwhile, the results from the tensile testing indicate that plasma treatment actually improved the hydrogel's tensile resistance across the whole tested strain. Contrary to the microwave and HHP methods, the plasma samples actually maintained a maximum strain close to the non-sterilized samples. Regarding shear resistance, the plasma samples showed slightly higher G' than the non-sterilized, while the δ remained unaltered. This indicates that while the viscous dissipation of energy remains constant, the plasma sterilized material has a higher shear stiffness. In the literature, Ar plasma treatment of PVA-Chitosan films was found to increased their tensile resistance after 5 min exposure [138]. Liu *et al.* found that Zylon fibers treated with Ar plasma treatment at low power (<100 W) kept their excellent tensile resistance, indicating that the procedure did not degrade the fibers [139]. Argon plasma treatment on Zylon fibers was also found to increase their interfacial adhesions with resin matrices while preserving their tensile properties [122, 140]. In tensile resistance, the Zylon nanofibers are thought to play a bigger role than the PVA polymer, due to the extremely high tensile modulus of this material (180 GPa). Thus, if the plasma treatment did improve the fibre–matrix interface adhesion, it

could lead to the improved tensile properties compared to the non-sterilized hydrogels. This effect could also explain the contradicting results from the compressive testing, as in this case, the Zylon fibers contribution to the hydrogels' stiffness is lower and the degradation of the PVA matrix should be more significant. This also leads to the assumption that the plasma treatment affects mainly the PVA chains rather than the Zylon fibers.

Predominantly, in all samples, the compressive tangent modulus increased with the strain, while the tensile modulus decreased with increased strain, until an almost constant value was reached. This behavior has already been reported in other publications on cast-dried PVA hydrogels for cartilage repair [54]. In compression, the increasing loads enhance the interpenetration of the polymer chains, which in turn caused the release of water molecules from within the matrix, hardening the material. This mechanism also occurs in articular cartilage (see section 1.2.3), protecting the tissue from strong compressive forces [21].

Regarding the rheological properties, both non-sterilized and sterilized PVA-Zylon hydrogels show a G* within the reported range for articular cartilage, particularly the microwave irradiated samples. While the reported values for the G* of articular cartilage vary between studies, they are typically in a range of 0.2-2.5 MPa [25]. Studies of lamb cartilage plugs on a similar device as the one used in this study (1 Hz frequency and effective shear strain amplitude of 0.023%) reported storage moduli in the range of 0.4–0.6 MPa [144]. Yet, the δ of the hydrogels was significantly lower than the one reported for native cartilage (15%) [142], indicative of a higher elastic contribution in the PVA-Zylon hydrogel. Moreover, testing on bovine cartilage found that natural tissue is more susceptible to frequency changes, with G' increasing with frequency [101, 111].

In respect to hardness, the samples subjected to microwave irradiation showed a particularly significant increase (19.72%), which is in agreement with the microstructural changes and highest increase in mechanical resistance previously observed. The increase in strong C=O bonds produces a stiffer and more resistant hydrogel matrix. The increase in hydrogel hardness after HHP processing is not as significant (4.44%), which is expected considering the reduced mechanical properties compared to microwave irradiated samples. Meanwhile the plasma treatment reduced the hydrogel's hardness by 6.11%, which is in line with the overall decrease in FTIR peak intensity and reduced compressive stiffness.

Wettability of polymers is often defined as a crucial parameter for cell attachment [145]. The optimal CA value seems to depend on cell types, but research suggests that moderate CA values are more adequate than having hydrogels with a very high or low wettability [146]. Gupta *et al.* studied freeze-thawed PVA hydrogels with different concentration of PVA, and verified an increase in fibroblast and epithelial cell attachment for hydrogels with the lowest CA (50º) and highest crosslinking density [147]. The PVA-Zylon hydrogels showed even lower CA values, close to 40º, indicating a hydrophilic behaviour. These results are in agreement with previous research on cast dried PVA hydrogels, which showed CAs between 33 and 37º [54]. The slightly higher obtained CA values in this study, can be due to differences in surface roughness of the hydrogels and/or the addition of the Zylon nanofibers. In fact, Zylon fibers have a reported CA >90º [139].

None of the sterilization methods induced changes in the wettability of the hydrogels. The lack of

significant changes in CA is somewhat surprising, when compared to the results seen in tribological testing and SEM analysis. It is reported that plasma treatment can induce two main processes that affect wettability in PVA, the addition of new polar groups on the surface and the etching process, which lead to lower and higher CA values respectively [133]. The FTIR analysis does show a slight increase in C-O bonds in plasma treated samples, which could indicate the formation of polar groups in the hydrogel surface. The measured CoF values and SEM analysis indicate that plasma treatment induced significant changes in the hydrogel surface, which should lead to variations in the CA values. Moreover, argon plasma was actually shown to significantly decrease the CA of treated Zylon fibers [139]. Unfortunately, other methods of surface analysis such as AFM and optical profilometer showed inadequate imaging when trying to test the PVA-Zylon hydrogel, and thus, the changes in surface roughness could not be quantified. The two effects can compensate and therefore not lead to significant changes in hydrophilicity. Also CoF value was not significantly affected due to plasma treatment, but here other factors besides the surface changes must be taken into consideration to explain the observed behaviour. However, the effects of plasma treatment on the CA of some hydrogels can be reversible. Researchers treated hydrogel contact lenses with nitrogen plasma and found higher CA values right after the treatment, but after 1 week the CA values reversed to become similar to non-treated samples [148]. While in this work, argon plasma was used, rather than nitrogen plasma, these effects could also possibly occur. Unfortunately, the specific time between the wettability measurements and the plasma treatment wasn´t quantified. Thus, further testing on the surface energy and roughness of the hydrogel as well as the effects of post treatment times should be performed.

Moving on the tribological behaviour, *in vivo* whole joint CoF is reported to be in the range of 0.001-0.03 [6]. Still, it is important to note that friction measurements on intact, undisturbed and *in vivo* articular cartilage are extremely challenging to perform, and the actual CoF of articular cartilage may deviate from these values. Size of samples, different harvest locations and animal from which they were removed can all result in cartilage samples with different properties. Swine articular cartilage typically measures $\approx$ 1.5 mm, which is slightly thinner than human cartilage ($\approx$ 2.35 mm) [149]. However, it shows a similar composition and is readily available, making it a suitable candidate to be used as a model to study the effects of friction between cartilage surfaces and other materials. Similarly, viscosity measurements of SF also vary, depending on the type of equipment used to make the measurements, the shear rate, the freshness of the samples, the temperature of the SF, and also the health condition of the individual from which it was removed. Joints affected with OA usually have SF with a viscosity between 0.05-14.05 Pa.s, while healthy SF typically shows much higher values, between 1–175 Pa.s [15]. In this work, the viscosity of the SSF solution used was measured through oscillatory tests in a rheometer. SSF viscosity had a value of 17.52 ± 0.65 mPa.s at room temperature (22.7ºC) and slightly decreased to 14.07±1.18 at 37ºC. As expected, the SSF was not as viscous as natural SF, due to the lack of some of the SF lubricant molecules. Still, the used fluid shows a significantly higher viscosity than water (0.9321 mPa.s at 23ºC, according to IAPWS 2008). Consequently, SSF used as lubricant resulted in lower CoF values than when using DD water (see Figure 3.19). The results also indicate that the lubrication mechanism of fluid is more significant at lower loads. At higher loads the boundary lubrication regime becomes more

significant than the fluid film regime (see section 1.2.3), and lubrication is more dependent on surface characteristics. Considering this factor, to better test the tribological behavior of the sterilized materials, they were tested with the highest load (i.e., 30 N).

All of the tested PVA-Zylon hydrogels presented CoFs significantly higher than the ones reported for natural cartilage. A probable cause, could be the lower value of Shore A hardness found in these hydrogels. A difference in the hardness of contacting surfaces can cause an effect known as ploughing, in which the softer hydrogel surfaces suffer a viscoelastic deformation after contact with the stiffer cartilage surfaces, and permanent physical markings appear in their surface (see Figure 3.21). Indeed the harder hydrogels (microwave and HHP) presented the lowest CoF values. However, the difference in CoF values between the microwave and HHP samples was not as significant as expected considering their hardness values.

Both microwave irradiation and HHP sterilization led to similar results in both the average CoF and the observed SEM micrographs (see sections 3.6.2 and 3.6.3, respectively). These procedures lead to a significant reduction in the CoF and their wear tracks showed an homogenous wavy pattern, as opposed to the delaminated effect seen in the non-sterilized samples. This wavy-like pattern is similar to the one observed in other tribological studies of PVA hydrogels against bovine cartilage [150]. The surfaces of the sterilized hydrogels also appeared smoother. Unfortunately, the roughness of the hydrogels could not be adequately measured and as SEM evaluates morphology and not topography, this analysis was not carried out. The increased crosslinking and polymer interaction within the hydrogel network is known to affect roughness. This smoothing effect was also been observed in PVA-graphene nanocomposites, after 5 minutes of exposure to microwave irradiation [125]. The irradiation caused an increased polymer interaction, evidenced by FTIR analysis, which resulted in a more homogenous surface. However, CoF measurements were not performed in such work. Moreover, Sasaki *et al.* found that a low dose of gamma irradiation (10 kGy) on hybrid cast-dried and freeze-thawed PVA hydrogels improved their CoF while reducing the WC by only 7% [136]. Regarding HHP, the effects of pressure could also explain the decrease in CoF. The extreme pressure (600 MPa) could smooth micro-asperities in the hydrogel surface, thus reducing roughness.

The effects of the plasma treatment were contrary to the other two sterilization methods. The CoF of the hydrogels actually increased and SEM analysis found a rougher surface after plasma treatment, and the presence of etching-derived holes. Etching is a very common side effect of the plasma procedure, and already reported in literature [75]. The highly energetic particles in the plasma gas are responsible for the opening of holes in the hydrogel's surface. Moreover, the position of the sample inside the plasma sterilizer is crucial in preventing this effect, as the sections of the hydrogels closest to the electromagnetic coil show larger holes, and in greater number. Some even visible to the naked-eye. Additional research on the effect of Ar plasma treatment in PVA-chitosan films also found that after 5 minute exposure, the surface roughness of the films was increased by 85% [138]. This analysis concludes that, for enhanced tribological behaviour, microwave and HHP procedures are very adequate, while plasma sterilization, at these conditions, should be avoided.

Regarding biocompatibility, the HET-CAM test is a well-established prediction model for eye irritation

due to chemicals, but it can also be used as a model for implant irritation [151, 152]. Although cartilage presents an avascular structure, the surrounding tissues of the joints and bone are vascularized, thereby making the HET-CAM test relevant. All of the tested samples presented an IS score of 0, which means that the hydrogel can be classified as non-irritant and that none of the sterilization methods induced irritative effects. The citotoxicity results, however, varied between the sterilization methods. ISO 10993-5:2009 states that for a material to be considered non-citotoxic, it must allow for a cellular viability $\geq$70%. While HHP and plasma sterilized hydrogels fall within the necessary range, microwave sterilized samples are right at the threshold of this parameter. However, the variability of the results was significant. Interestingly, at higher magnification, it was possible to observe that the chondrocytes cultured in microwave sample extracts possessed the correct morphology after 48 hours of culture (Figure 3.29). Furthermore, while their morphology couldn't be ascertained, cells were seen to adhere and thrive, after 22 days of culture on top of hydrogel samples that underwent microwave sterilization (Appendix B.1). This leads to think that microwave irradiation, while not showing the best results, can still be considered non-citotoxic.

Chapter 5

Conclusions and Future Work

5.1 Conclusion

The novel PVA-Zylon hydrogels have shown to be promising materials for cartilage substitution. All the tested mechanical properties are within the range measured for articular cartilage. However, its tribological behaviour still falls slightly short, and further effort should be made to optimize it. The unconventional sterilization methods tested in this work proved to be able to sterilize the PVA-Zylon hydrogels. These methods present advantages over conventional sterilization procedures such as autoclaving and gamma-ray irradiation which require lengthy processing times and specialized equipment and staff.

Of the three methods, microwave irradiation proved to be the most adequate to sterilize the PVA-Zylon hydrogels. This method is, by far, the easiest to perform, as it can be done in a common household microwave and doesn´t require a very specific *modus of operandi*. The microwave radiation shows a highly penetrative effect and while it can achieve high temperatures, it does so with great efficiency and speed, which allows for a terminal sterilization at reduced exposure times. This is coupled with an overall improvement of the properties of the hydrogel after 3 min of exposure. Microwave irradiation was shown to increase the interactions of PVA and Zylon molecules, leading to a stiffer, and more mechanically resistant material, with increased tribological behaviour. This makes the sterilized PVA-Zylon hydrogels even more promising as a cartilage substitute material.

The HHP sterilization of PVA-Zylon hydrogels also showed some promising results. The procedure increased hydrogen bonding throughout the PVA-Zylon hydrogel matrix, producing a slightly stiffer material, with tribological behaviour similar to the microwave irradiated hydrogels and superior to the non-sterilized material. Both its tensile and shear resistance improved over the non-sterilized hydrogels, but not as much as the microwave procedure. While the mechanical resistance of the hydrogels at higher loads decreased after HHP treatment, it is still within the range of articular cartilage. Moreover, HHP samples showed the best compressive stiffness at lower loads. However, of the three methods, HHP has the need of the most specialized and expensive equipment, and is not readily available, which hinder its worldwide application.

Regarding plasma sterilization, while it showed the best biocompatibility of all the methods, its effects

on the mechanical and tribological properties of the hydrogel were less than adequate. At 5 min exposure, etching of the surface was clearly evidenced, which led to higher CoF and wear. While the shear and tensile moduli actually increased, the compressive stiffness as well as hardness of the hydrogel significantly decreased. Besides the unwanted effects on the hydrogel properties, the used equipment also shows some drawbacks, particularly the lack of a measuring device for gas flow. Moreover, with the use of argon gas, terminal sterilization of hydrogels is impossible. Thus, while the method could be interesting for certain applications, more optimization is still required.

5.1.1 Future Work

While the optimization of the HHP procedure has already been studied in a wide range of hydrogels [93], microwave irradiation and plasma treatment still lack this research. The sterilization capabilities of these methods could be studied in other hydrogel materials, to find the optimum exposure times for an efficient sterilization. The efficacy of these methods should also be tested on materials with an elevated bioburden.

Microwave irradiation of PVA-Zylon hydrogels may be performed at different exposure times and powers, to discover the optimal point at where the properties are most enhanced. Additional studies ought to be done on the citotoxicity of this procedure, possibly by analysing the chemical formulation and pH of the extracts used for citotoxicity assays. Plasma sterilization should also be tested at lower exposure times, to see if the unwanted etching and degradation of the hydrogels could be diminished. Also, thorough cell-adhesion tests could be performed to understand if the etched surface of the hydrogels would improve the cellular adhesion of chondrocytes to the material.

The topographical analysis of the surface of the hydrogels is important to better understand the results. Further efforts should be made to try and find ways for an appropriate roughness characterization. The tribological behaviour of the PVA-Zylon hydrogels also needs to be improved. For this, effort should be made to improve the hardness of the hydrogels, or possibly the addition of a zwiterrionic polymer to the surface of the hydrogel, to diminish the CoF at boundary lubrification. To finalize, regarding future *in vivo* application, the addition of hydroxyapatite nanoparticles to the matrix could possibly favour the integration of the hydrogel grafts to the subchondral bone.

Bibliography

[1] A. J. S. Fox, A. Bedi, and S. A. Rodeo. The basic science of articular cartilage: Structure, composition, and function. *Sports Health*, 1(6):461–468, 2009. doi: 10.1177/1941738109350438.

[2] C. Gentili and R. Cancedda. Cartilage and bone extracellular matrix. *Current pharmaceutical design*, 15:1334–48, 02 2009. doi: 10.2174/138161209787846739.

[3] A. Armiento, M. Stoddart, M. Alini, and D. Eglin. Biomaterials for articular cartilage tissue engineering: Learning from biology. *Acta Biomaterialia*, 65:1–20, 2018. doi: https://doi.org/10.1016/j.actbio.2017.11.021.

[4] L. Han, A. J. Grodzinsky, and C. Ortiz. Nanomechanics of the cartilage extracellular matrix. *Annual Review of Materials Research*, 41(1):133–168, 2011. doi: 10.1146/annurev-matsci-062910-100431.

[5] D. Duarte Campos, W. Drescher, B. Rath, M. Tingart, and H. Fischer. Supporting biomaterials for articular cartilage repair. *Cartilage*, 3:205–221, 07 2012. doi: 10.1177/1947603512444722.

[6] S. Jahn, J. Seror, and J. Klein. Lubrication of articular cartilage. *Annual Review of Biomedical Engineering*, 18(1):235–258, 2016. doi: 10.1146/annurev-bioeng-081514-123305. PMID: 27420572.

[7] V. C. Mow, A. Ratcliffe, and A. Robin Poole. Cartilage and diarthrodial joints as paradigms for hierarchical materials and structures. *Biomaterials*, 13(2):67–97, 1992. ISSN 0142-9612. doi: https://doi.org/10.1016/0142-9612(92)90001-5.

[8] F. Guilak, L. G. Alexopoulos, M. L. Upton, I. Youn, J. B. Choi, L. Cao, L. A. Setton, and M. A. Haider. The pericellular matrix as a transducer of biomechanical and biochemical signals in articular cartilage. *Annals of the New York Academy of Sciences*, 1068(1):498–512. doi: https://doi.org/10.1196/annals.1346.011.

[9] S. Grässel and A. Aszódi. *Cartilage, Volume 2: Pathophysiology*. Springer, 2017. doi: 10.1007/978-3-319-45803-8.

[10] T. Lyons, R. Stoddart, S. McClure, and J. McClure. The tidemark of the chondro-osseous junction of the normal human knee joint. *Journal of molecular histology*, 36(3):207—215, March 2005. ISSN 1567-2379. doi: 10.1007/s10735-005-3283-x.

[11] K. A. Athanasiou, E. M. Darling, G. D. DuRaine, , J. C. Hu, and A. H. Reddi. *Articular Cartilage (2nd ed.)*, chapter 1, pages 1–77. CRC Press, 2016. doi: 10.1201/9781315194158.

[12] S. Park, R. Krishnan, S. Nicoll, and G. Ateshian. Cartilage interstitial fluid load support in unconfined compression. *Journal of biomechanics*, 36:1785–96, 01 2004. doi: 10.1016/S0021-9290(03)00231-8.

[13] M. E. Blewis, G. E. Nugent-Derfus, T. A. Schmidt, B. L. Schumacher, and R. L. Sah. A model of synovial fluid lubricant composition in normal and injured joints. *European cells & materials*, 13: 26–39, 2007.

[14] V. Adibnia, M. Mirbagheri, J. Faivre, J. Lee, K. Matyjaszewski, D. Lee, and X. Banquy. Bioinspired polymers for lubrication and wear resistance. *Progress in Polymer Science*, 110:101298, 11 2020. doi: 10.1016/j.progpolymsci.2020.101298.

[15] S. More, A. Kotiya, A. Kotia, S. Ghosh, L. Spyrou, and I. Sarris. Rheological properties of synovial fluid due to viscosupplements: A review for osteoarthritis remedy. *Computer Methods and Programs in Biomedicine*, 196:105644, 2020. ISSN 0169-2607. doi: https://doi.org/10.1016/j.cmpb.2020.105644.

[16] J. Link, E. Salinas, J. Hu, and K. Athanasiou. The tribology of cartilage: Mechanisms, experimental techniques, and relevance to translational tissue engineering. *Clinical Biomechanics*, 79, 10 2019. doi: 10.1016/j.clinbiomech.2019.10.016.

[17] C. McCutchen. Mechanism of animal joints: Sponge-hydrostatic and weeping bearings. *Nature*, 184:1284–1285, 1959. doi: 10.1038/1841284a0.

[18] P. S. Walker, D. Dowson, M. D. Longfield, and V. Wright. "boosted lubrication" in synovial joints by fluid entrapment and enrichment. *Annals of the Rheumatic Diseases*, 27(6):512–520, 1968. ISSN 0003-4967. doi: 10.1136/ard.27.6.512.

[19] E. Bonnevie, V. Baro, L. Wang, and D. Burris. Fluid load support during localized indentation of cartilage with a spherical probe. *Journal of biomechanics*, 45:1036–41, 01 2012. doi: 10.1016/j.jbiomech.2011.12.019.

[20] S. Camarero-Espinosa, B. Rothen-Rutishauser, E. J. Foster, and C. Weder. Articular cartilage: from formation to tissue engineering. *Biomater. Sci.*, 4:734–767, 2016. doi: 10.1039/C6BM00068A.

[21] J. Eschweiler, N. Horn, B. Rath, M. Betsch, A. Baroncini, M. Tingart, and F. Migliorini. The biomechanics of cartilage—an overview. *Life*, 11:302, 04 2021. doi: 10.3390/life11040302.

[22] V. Mow, S. Kuei, W. M. Lai, and C. Armstrong. Mow vc, kuei sc, lai wm, armstrong cg. biphasic creep and stress relaxation of articular cartilage in compression: Theory and experiments. j biomech eng 102: 73-84. *Journal of biomechanical engineering*, 102:73–84, 03 1980. doi: 10.1115/1.3138202.

[23] M. H. Holmes, W. M. Lai, and V. C. Mow. Singular Perturbation Analysis of the Nonlinear, Flow-Dependent Compressive Stress Relaxation Behavior of Articular Cartilage. *Journal of Biomechanical Engineering*, 107(3):206–218, 08 1985. doi: 10.1115/1.3138545.

[24] S. Park, R. Krishnan, S. Nicoll, and G. Ateshian. Cartilage interstitial fluid load support in unconfined compression. *Journal of biomechanics*, 36:1785–96, 01 2004. doi: 10.1016/S0021-9290(03)00231-8.

[25] C. Little, N. Bawolin, and X. Chen. Mechanical properties of natural cartilage and tissue-engineered constructs. *Tissue engineering. Part B, Reviews*, 17:213–27, 03 2011. doi: 10.1089/ten.TEB.2010.0572.

[26] G. Spahn, H. Plettenberg, H. Nagel, E. Kahl, H. M. Klinger, T. Mückley, M. Günther, G. O. Hofmann, and J. A. Mollenhauer. Evaluation of cartilage defects with near-infrared spectroscopy (nir): An ex vivo study. *Medical Engineering Physics*, 30(3):285–292, 2008. ISSN 1350-4533. doi: https://doi.org/10.1016/j.medengphy.2007.04.009.

[27] P. Abdel-Sayed and D. Pioletti. Strategies for improving the repair of focal cartilage defects. *Nanomedicine (London, England)*, 10:2893–905, 09 2015. doi: 10.2217/nnm.15.119.

[28] J. Browne and T. Branch. Surgical alternatives for treatment of articular cartilage lesions. *The Journal of the American Academy of Orthopaedic Surgeons*, 8:180–9, 05 2000. doi: 10.5435/00124635-200005000-00005.

[29] M. Brittberg and C. S. Winalski. Evaluation of cartilage injuries and repair. *The Journal of bone and joint surgery. American volume*, 85-A Suppl 2:58—69, 2003. ISSN 0021-9355. doi: 10.2106/00004623-200300002-00008.

[30] W. Curl, J. Krome, E. Gordon, J. Rushing, B. Smith, and G. Poehling. Cartilage injuries: a review of 31,516 knee arthroscopies. *Arthroscopy : the journal of arthroscopic amp; related surgery : official publication of the Arthroscopy Association of North America and the International Arthroscopy Association*, 13(4):456—460, August 1997. ISSN 0749-8063. doi: 10.1016/s0749-8063(97)90124-9.

[31] J. T. Kerker, A. J. Leo, and N. A. Sgaglione. Cartilage repair: synthetics and scaffolds: basic science, surgical techniques, and clinical outcomes. *Sports medicine and arthroscopy review*, 16(4):208—216, December 2008. ISSN 1062-8592. doi: 10.1097/jsa.0b013e31818cdbaa.

[32] J. T. Kerker, A. J. Leo, and N. A. Sgaglione. Cartilage repair: Synthetics and scaffolds: Basic science, surgical techniques, and clinical outcomes. *Sports Medicine and Arthroscopy Review*, 16:208–216, 2008.

[33] L. Hangody and P. Füles. Autologous osteochondral mosaicplasty for the treatment of full-thickness defects of weight-bearing joints: Ten years of experimental and clinical experience. *The Journal of bone and joint surgery. American volume*, 85-A Suppl 2:25–32, 02 2003. doi: 10.2106/00004623-200300002-00004.

[34] C. DeJulius, S. Gulati, K. Hasty, L. Crofford, and C. Duvall. Recent advances in clinical translation of intra-articular osteoarthritis drug delivery systems. *Advanced Therapeutics*, 4:2000088, 09 2020. doi: 10.1002/adtp.202000088.

[35] H. Bodugoz Senturk, C. Macias, J. Kung, and O. Muratoglu. Poly(vinyl alcohol)-acrylamide hydrogels as load-bearing cartilage substitute. *Biomaterials*, 30:589–96, 12 2008. doi: 10.1016/j.biomaterials.2008.10.010.

[36] E. Ingham and J. Fisher. Biological reaction to wear debris in total joint replacement. *Proceedings of the Institution of Mechanical Engineers. Part H, Journal of engineering in medicine*, 214:21–37, 02 2000. doi: 10.1243/0954411001535219.

[37] K. D. Ngadimin, A. Stokes, P. Gentile, and A. M. Ferreira. Biomimetic hydrogels designed for cartilage tissue engineering. *Biomater. Sci.*, 9:4246–4259, 2021. doi: 10.1039/D0BM01852J.

[38] D. Jackson, M. Scheer, and T. Simon. Cartilage substitutes: Overview of basic science and treatment options. *The Journal of the American Academy of Orthopaedic Surgeons*, 9:37–52, 01 2001. doi: 10.5435/00124635-200101000-00005.

[39] S. J. Buwalda, K. W. Boere, P. J. Dijkstra, J. Feijen, T. Vermonden, and W. E. Hennink. Hydrogels in a historical perspective: From simple networks to smart materials. *Journal of Controlled Release*, 190:254–273, 2014. ISSN 0168-3659. doi: https://doi.org/10.1016/j.jconrel.2014.03.052. 30th Anniversary Special Issue.

[40] M. C. Koetting, J. T. Peters, S. D. Steichen, and N. A. Peppas. Stimulus-responsive hydrogels: Theory, modern advances, and applications. *Materials Science and Engineering: R: Reports*, 93:1–49, 2015. ISSN 0927-796X. doi: https://doi.org/10.1016/j.mser.2015.04.001.

[41] C. Magin and K. Anseth. Hydrogels in healthcare: From static to dynamic material microenvironments. *Acta materialia*, 61:931–944, 02 2013. doi: 10.1016/j.actamat.2012.10.037.

[42] W. Hu, Z. Wang, Y. Xiao, S.-m. Zhang, and J. Wang. Advances in crosslinking strategies of biomedical hydrogels. *Biomaterials Science*, 7, 12 2018. doi: 10.1039/C8BM01246F.

[43] A. Kumar and S. S. Han. Pva-based hydrogels for tissue engineering: A review. *International Journal of Polymeric Materials and Polymeric Biomaterials*, 66:159–182, 06 2016. doi: 10.1080/00914037.2016.1190930.

[44] M. Baker, S. Walsh, Z. Schwartz, and B. Boyan. A review of polyvinyl alcohol and its uses in cartilage and orthopedic applications. *Journal of biomedical materials research. Part B, Applied biomaterials*, 100:1451–7, 07 2012. doi: 10.1002/jbm.b.32694.

[45] Y. Chen, J. Song, S. Wang, and W. Liu. Pva-based hydrogels: Promising candidates for articular cartilage repair. *Macromolecular Bioscience*, 21(10):2100147, 2021. doi: https://doi.org/10.1002/mabi.202100147.

[46] S. Farris and L. Piergiovanni. 14 - emerging coating technologies for food and beverage packaging materials. In K. L. Yam and D. S. Lee, editors, *Emerging Food Packaging Technologies*, Woodhead Publishing Series in Food Science, Technology and Nutrition, pages 274–302. Woodhead Publishing, 2012. ISBN 978-1-84569-809-6. doi: https://doi.org/10.1533/9780857095664.3.274.

[47] D. Moreau. *Design and Characterization of Hydrogel Films and Hydrogel-Ceramic Composites for Biomedical Applications.* PhD thesis, Research University, Paris, France, 2016.

[48] J. Katta, M. Marcolongo, A. Lowman, and K. Mansmann. Friction and wear behavior of poly(vinyl alcohol)/poly(vinyl pyrrolidone) hydrogels for articular cartilage replacement. *Journal of biomedical materials research. Part A*, 83:471–9, 11 2007. doi: 10.1002/jbm.a.31238.

[49] H. Bodugoz Senturk, J. Choi, E. Oral, J. Kung, C. Macias, G. Braithwaite, and O. Muratoglu. The effect of polyethylene glycol on the stability of pores in polyvinyl alcohol hydrogels during annealing. *Biomaterials*, 29:141–9, 02 2008. doi: 10.1016/j.biomaterials.2007.09.015.

[50] A. Kumar, R. Mishra, Y. Reinwald, and S. Bhat. Cryogels: Freezing unveiled by thawing. *Materials Today - MATER TODAY*, 13:42–44, 11 2010. doi: 10.1016/S1369-7021(10)70202-9.

[51] A. Oliveira, O. Seidi, N. Ribeiro, R. Colaço, and A. Serro. Tribomechanical comparison between pva hydrogels obtained using different processing conditions and human cartilage. *Materials*, 12: 3413, 10 2019. doi: 10.3390/ma12203413.

[52] M. Kobayashi and H. S. Hyu. Development and evaluation of polyvinyl alcohol-hydrogels as an artificial articular cartilage for orthopedic implants. *Materials*, 3(4):2753–2771, 2010.

[53] W. ill Cha, S. hyu Hyon, M. Oka, and Y. Ikada. Mechanical and wear properties of poly(vinyl alcohol) hydrogels. *Macromolecular Symposia*, 109:115–126, 1996.

[54] A. Oliveira, S. Schweizer, P. Nolasco, I. Barahona, J. Saraiva, R. Colaço, and A. Serro. Tough and low friction polyvinyl alcohol hydrogels loaded with anti-inflammatories for cartilage replacement. *Lubricants*, 8:36, 03 2020. doi: 10.3390/lubricants8030036.

[55] R. Li, J. Lin, Y. Fang, C. Yu, J. Zhang, Y. Xue, Z. Liu, J. Zhang, and C. Tang. Porous boron nitride nanofibers/pva hydrogels with improved mechanical property and thermal stability. *Ceramics International*, 44, 09 2018. doi: 10.1016/j.ceramint.2018.09.011.

[56] Z. Xu, J. Li, H. Zhou, X. Jiang, C. Yang, F. Wang, Y. Pan, N. Li, X. Li, L. Shi, and X. Shi. Morphological and swelling behavior of cellulose nanofiber (cnf)/poly(vinyl alcohol) (pva) hydrogels: Poly(ethylene glycol) (peg) as porogen. *RSC Adv.*, 6:43626–43633, 04 2016. doi: 10.1039/C6RA03620A.

[57] J. Zhang, T. Liu, Z. Liu, and Q. Wang. Facile fabrication of tough photocrosslinked polyvinyl alcohol hydrogels with cellulose nanofibrils reinforcement. *Polymer*, 173, 04 2019. doi: 10.1016/j.polymer.2019.04.028.

[58] A. Rodrigues, N. Batista, V. Bavaresco, V. Baranauskas, H. Ceragioli, A. Peterlevitz, J. Mariolani, and M. H. Santana. In vivo evaluation of hydrogels of polyvinyl alcohol with and without carbon nanoparticles for osteochondral repair. *Carbon*, 50:2091–2099, 05 2012. doi: 10.1016/j.carbon.2011.12.060.

[59] Y. Teramoto and F. Kubota. *Zylon®: Super Fiber from Lyotropic Liquid Crystal of the Most Rigid Polymer*, pages 191–216. 08 2016. ISBN 978-4-431-55202-4. doi: 10.1007/978-4-431-55203-1_11.

[60] *PBO fiber Zylon: Technical Information*. Toyobo.Co.Ltd, Revised 2005.6. URL `https://www.toyobo-global.com/seihin/kc/pbo/zylon-p/bussei-p/technical.pdf`.

[61] M. Chen, Y. Mo, Z. Li, X. Lin, and Q. He. Poly(p-phenylenebenzobisoxazole) nanofiber layered composite films with high thermomechanical performance. *European Polymer Journal*, 84:622–630, 2016. ISSN 0014-3057. doi: https://doi.org/10.1016/j.eurpolymj.2016.10.005.

[62] S. Ifuku, H. Maeta, H. Izawa, M. Morimoto, and H. Saimoto. Preparation of polybenzoxazole nanofibers by a downsizing process. *RSC Adv.*, 5, 04 2015. doi: 10.1039/C5RA04679C.

[63] ISO 11607-1:2019. Packaging for terminally sterilized medical devices - part 1: Requirements for materials, sterile barrier systems and packaging systems. Standard, International Organization for Standardization, Geneva, CH, 2019. URL `www.iso.org/standard/70799.html`.

[64] S. Lerouge and A. Simmons. *Sterilisation of Biomaterials and Medical Devices*, chapter 1-Introduction to sterilization: definitions and challenges, pages 1–19. Woodhead Publishing Series, 2012. doi: eBookISBN:9780857096265.

[65] S. S. Karajanagi, R. Yoganathan, R. Mammucari, H. Park, J. Cox, S. M. Zeitels, R. Langer, and N. R. Foster. Application of a dense gas technique for sterilizing soft biomaterials. *Biotechnology and Bioengineering*, 108(7):1716–1725, 2011. doi: https://doi.org/10.1002/bit.23105.

[66] Q.-Q. Qiu, W. Sun, and J. Connor. Sterilization of biomaterials of synthetic and biological origin. *Comprehensive Biomaterials*, 4:127–144, 10 2011. doi: 10.1016/B978-0-08-055294-1.00248-8.

[67] R. Galante, T. Pinto, R. Colaço, and A. Serro. Sterilization of hydrogels for biomedical applications: A review: Sterilization of hydrogels. *Journal of Biomedical Materials Research Part B: Applied Biomaterials*, 106, 12 2017. doi: 10.1002/jbm.b.34048.

[68] P. Chansoria, L. Narayanan, M. Wood, C. Alvarado, A. Lin, and R. Shirwaiker. Effects of autoclaving, etoh, and uv sterilization on the chemical, mechanical, printability, and biocompatibility characteristics of alginate. *ACS Biomaterials Science Engineering*, XXXX, 07 2020. doi: 10.1021/acsbiomaterials.0c00806.

[69] B. Parsons. *Sterilisation of healthcare products by ionising radiation: Principles and standards*, pages 56–70. 12 2012. ISBN 9781845699321. doi: 10.1533/9780857096265.56.

[70] Z. Dai, J. Ronholm, Y. Tian, B. Sethi, and X. Cao. Sterilization techniques for biodegradable scaffolds in tissue engineering applications. *Journal of Tissue Engineering*, 7:2041731416648810, 2016. doi: 10.1177/2041731416648810.

[71] G. Mendes, T. Brandão, and C. Silva. Ethylene oxide sterilization of medical devices: A review. *American journal of infection control*, 35:574–81, 12 2007. doi: 10.1016/j.ajic.2006.10.014.

[72] M. Noh, S. Jung, O. Kwon, S.-I. Lee, S.-J. Yang, H. Eunil, and B.-H. Jun. Evaluation of sterilization performance for vaporized-hydrogen-peroxide-based sterilizer with diverse controlled parameters. *ACS Omega*, 5:29382–29387, 11 2020. doi: 10.1021/acsomega.0c04208.

[73] G. E. Mcdonnell and A. D. Russell. Antiseptics and disinfectants: Activity, action, and resistance. *Clinical Microbiology Reviews*, 12:147 – 179, 1999.

[74] S. Sasaki, T. Murakami, and A. Suzuki. Frictional properties of physically cross-linked pva hydrogels as artificial cartilage. *Biosurface and Biotribology*, 2, 02 2016. doi: 10.1016/j.bsbt.2016.02.002.

[75] Low-temperature sterilization using gas plasmas: a review of the experiments and an analysis of the inactivation mechanisms. *International Journal of Pharmaceutics*, 226(1):1–21, 2001. ISSN 0378-5173. doi: https://doi.org/10.1016/S0378-5173(01)00752-9.

[76] A. Bernhardt, M. Wehrl, B. Paul, T. Hochmuth, M. Schumacher, K. Schütz, and M. Gelinsky. Improved sterilization of sensitive biomaterials with supercritical carbon dioxide at low temperature. *PLoS ONE*, 10, 06 2015. doi: 10.1371/journal.pone.0129205.

[77] M. D. Rohrer, M. A. Terry, R. A. Bulard, D. C. Graves, and E. M. Taylor. Microwave sterilization of hydrophilic contact lenses. *American Journal of Ophthalmology*, 101(1):49–57, 1986. ISSN 0002-9394. doi: https://doi.org/10.1016/0002-9394(86)90464-2.

[78] A. Machado, L. Breeding, C. Vergani, and L. Perez. Hardness and surface roughness of reline and denture base acrylic resins after repeated disinfection procedures. *The Journal of prosthetic dentistry*, 102:115–22, 09 2009. doi: 10.1016/S0022-3913(09)60120-7.

[79] K. Neppelenbroek, A. Pavarina, D. Spolidorio, C. Vergani, E. Mima, and A. Machado. Effectiveness of microwave sterilization on three hard chairside reline resins. *The International journal of prosthodontics*, 16:616–20, 11 2003.

[80] R. A. Dunsmuir and G. Gallacher. Microwave sterilization of femoral head allograft. *Journal of Clinical Microbiology*, 41(10):4755–4757, 2003. doi: 10.1128/JCM.41.10.4755-4757.2003.

[81] H. S. R. Jasim Ahmed. Microwave pasteurization and sterilization of foods. In *Handbook of Food Preservation*, chapter 28. CRC Press, 3rd edition edition, 2014.

[82] A. Crabbe and P. Thompson. Effects of microwave irradiation on the parameters of hydrogel contact lenses. *Optometry and vision science : official publication of the American Academy of Optometry*, 78:610–5, 09 2001. doi: 10.1097/00006324-200108000-00014.

[83] R. Vadivambal and D. Jayas. Non-uniform temperature distribution during microwave heating of food materials—a review. *Food and Bioprocess Technology*, 3:161–171, 04 2008. doi: 10.1007/s11947-008-0136-0.

[84] M. Yaldagard, S. Mortazavi, and F. Tabatabaie. The principles of ultra high pressure technology and its application in food processing/preservation: A review of microbiological and quality aspects. *African Journal of Biotechnology*, 7:2739–2767, 09 2008.

[85] Y. Shamis, S. Patel, A. Taube, Y. Morsi, I. Sbarski, Y. Shramkov, R. J. Croft, R. J. Crawford, and E. P. Ivanova. A new sterilization technique of bovine pericardial biomaterial using microwave radiation. *Tissue Engineering Part C: Methods*, 15(3):445–454, 2009. doi: 10.1089/ten.tec.2008.0350.

[86] H. Fleming. Effect of high frequency on microorganisms. Electrical Eng., 1944.

[87] D. Knorr, M. Geulen, T. Grahl, and W. Sitzmann. Food application of high electric field pulses. *Trends in Food Science Technology*, 5(3):71–75, 1994. ISSN 0924-2244. doi: https://doi.org/10.1016/0924-2244(94)90240-2.

[88] D. Stuerga and P. Gaillard. Microwave athermal effects in chemistry: A myth's autopsy: Part i: Historical background and fundamentals of wave-matter interaction. *Journal of Microwave Power and Electromagnetic Energy*, 31(2):87–100, 1996. doi: 10.1080/08327823.1996.11688299.

[89] Y. Rigaldie, A. Largeteau, G. Lemagnen, I. Fabienne, P. Pardon, G. Demazeau, and L. Grislain. Effects of high hydrostatic pressure on several sensitive therapeutic molecules and a soft nanodispersed drug delivery system. *Pharmaceutical research*, 20:2036–40, 01 2004. doi: 10.1023/B:PHAM.0000008054.80136.5a.

[90] V. Balasubramaniam, S. Martinez-Monteagudo, and R. Gupta. Principles and application of high pressure–based technologies in the food industry. *Annual Review of Food Science and Technology*, 6, 02 2015. doi: 10.1146/annurev-food-022814-015539.

[91] E. Y. Wuytack, J. Soons, F. Poschet, and C. W. Michiels. Comparative study of pressure- and nutrient-induced germination of bacillus subtilis spores. *Applied and Environmental Microbiology*, 66(1):257–261, 2000. doi: 10.1128/AEM.66.1.257-261.2000.

[92] V. Heinz and D. Knorr. Effects of high pressure on spores. In *Food Engineering Series*, pages 77–113. Springer US, 2001. doi: 10.1007/978-1-4615-0723-9_4. URL `https://doi.org/10.10072F978-1-4615-0723-9_4`.

[93] A. Topete, C. Pinto, M. Barroso, J. Saraiva, I. Barahona, B. Saramago, and A. Serro. High hydrostatic pressure (hhp) as sterilization method for drug-loaded intraocular lenses. *ACS Biomaterials Science Engineering*, XXXX, 06 2020. doi: 10.1021/acsbiomaterials.0c00412.

[94] E. Nydrioti. Drug loaded chitosan wound dressings: choosing the best sterilization method. Master's thesis, Instituto Superior Técnico, 2019.

[95] L. Yang, J. Chen, and J. Gao. Low temperature argon plasma sterilization effect on pseudomonas aeruginosa and its mechanisms. *Journal of Electrostatics*, 67:646–651, 07 2009. doi: 10.1016/j.elstat.2009.01.060.

[96] B. J. Park, K. Takatori, M. H. Lee, D.-W. Han, Y. I. Woo, H. J. Son, J. K. Kim, K.-H. Chung, S. O. Hyun, and J.-C. Park. Escherichia coli sterilization and lipopolysaccharide inactivation using microwave-induced argon plasma at atmospheric pressure. *Surface and Coatings Technology*, 201(9):5738–5741, 2007. ISSN 0257-8972. doi: https://doi.org/10.1016/j.surfcoat.2006.07.039. Proceedings of the Fifth Asian-European International Conference on Plasma Surface Engineering.

[97] C. Holy, C. Cheng, J. Davies, and M. Shoichet. Optimizing the sterilization of plga scaffolds for use in tissue engineering. *Biomaterials*, 22:25–31, 02 2001. doi: 10.1016/S0142-9612(00)00136-8.

[98] G. Dalei, S. Das, and S. Das. Non-thermal plasma assisted surface nano-textured carboxymethyl guar gum/chitosan hydrogels for biomedical applications. *RSC Advances*, 9:1705–1716, 01 2019. doi: 10.1039/C8RA09161G.

[99] G. Verberne, Y. Merkher, G. Halperin, A. Maroudas, and I. Etsion. Techniques for assessment of wear between human cartilage surfaces. *Wear*, 266:1216–1223, 05 2009. doi: 10.1016/j.wear.2009.03.042.

[100] L. Shi, V. Sikavitsas, and A. Striolo. Experimental friction coefficients for bovine cartilage measured with a pin-on-disk tribometer: Testing configuration and lubricant effects. *Annals of biomedical engineering*, 39:132–46, 01 2011. doi: 10.1007/s10439-010-0167-3.

[101] C. Schwartz and S. Bahadur. Investigation of articular cartilage and counterface compliance in multi-directional sliding as in orthopedic implants. *Wear*, 262:1315–1320, 05 2007. doi: 10.1016/j.wear.2007.01.007.

[102] *Council of Europe, European Pharmacopoeia (Ph. Eur.) 10th Edition, (2019).*

[103] Y. Shi, J. Li, D. Xiong, L. Li, and Q. Liu. Mechanical and tribological behaviors of pva / paam double network hydrogels under varied strains as cartilage replacement. *Journal of Applied Polymer Science*, 138:50226, 11 2020. doi: 10.1002/app.50226.

[104] Storage and Loss Modulus, sep 12 2021. [Online; accessed 2021-11-06].

[105] T. G. Mezger. *Applied Rheology*. Anton Paar GmbH, Austria, 2019.

[106] A. de Souza Gomes. *Polymerization*, pages 395–443. 2012.

[107] H. Murata. *Rheology – Theory and Application to Biomaterials*, chapter 17, pages 403–426.

[108] P. Moitra, H. M. Gonnermann, B. F. Houghton, and C. S. Tiwary. *Fragmentation and Plinian eruption of crystallizing basaltic magma*. Earth and Planetary Sciences Letters 500, 2018. doi: 10.1016/j.epsl.2018.08.003.

[109] A. Franck. Viscoelasticity and dynamic mechanical testing. TA Instruments Germany.

[110] H. Nia, I. Soltani, Y. Li, L. Han, H.-H. Hung, E. Frank, K. Youcef-Toumi, C. Ortiz, and A. Grodzinsky. High-bandwidth afm-based rheology reveals that cartilage is most sensitive to high loading rates at early stages of impairment. *Biophysical journal*, 104:1529–37, 04 2013. doi: 10.1016/j.bpj.2013.02.048.

[111] S. Perni and P. Prokopovich. Rheometer enabled study of cartilage frequency-dependent properties. *Scientific Reports*, 10, 11 2020. doi: 10.1038/s41598-020-77758-9.

[112] G. Spahn, E. Kahl, H. Klinger, T. Mückley, M. Günther, and G. Hofmann. Mechanical behavior of intact and low-grade degenerated cartilage. *Biomedizinische Technik. Biomedical engineering*, 52:216–22, 02 2007. doi: 10.1515/BMT.2007.039.

[113] A. S. G. de Oliveira. Effects of sterilization on drug loaded ophthalmic lenses materials. Master's thesis, Instituto Superior Técnico, 2016.

[114] M. I. F. da Cunha Monteiro. Drug loaded cartilage-like materials for hip prosthesis. Master's thesis, Instituto Superior Técnico, 2019.

[115] S. Oungoulian, K. Durney, B. Jones, C. Ahmad, C. Hung, and G. Ateshian. Wear and damage of articular cartilage with friction against orthopaedic implant materials. *Journal of biomechanics*, 48, 04 2015. doi: 10.1016/j.jbiomech.2015.04.008.

[116] G. Stachowiak. *Engineering Tribology*. Butterworth Heinemann, 2001.

[117] A. Khalladi and K. Elleuch. Effect of surface topography with different groove angles on tribological behavior of the wheel/rail contact using alternative machine. *Friction*, 4, 08 2016. doi: 10.1007/s40544-016-0121-y.

[118] M. Blum and T. Ovaert. A novel polyvinyl alcohol hydrogel functionalized with organic boundary lubricant for use as low-friction cartilage substitute: Synthesis, physical/chemical, mechanical, and friction characterization. *Journal of biomedical materials research. Part B, Applied biomaterials*, 100B:1755–63, 10 2012. doi: 10.1002/jbm.b.32742.

[119] W. Zhou, Z. Wang, and D. Joy. *Scanning Microscopy for Nanotechnology*, chapter 1, Fundamentals of scanning electron microscopy, pages 1–40. 2007. doi: 10.1007/978-0-387-39620-0_1.

[120] L. Zhong, J. Wang, and L.Lee. *Developments in Surface Contamination and Cleaning (Second Edition), Volume 1: Fundamentals and Applied Aspects*, chapter 9, Electron Microscopy Techniques for Imaging and Analysis of Nanoparticles, pages 395–443. 2008. doi: 10.1016/B978-0-323-29960-2.00009-5.

[121] T. Noguchi, T. Yamamuro, M. Oka, P. Kumar, Y. Kotoura, S.-H. Hyonyt, and Y. Ikadat. Poly(vinyl alcohol) hydrogel as an artificial articular cartilage: Evaluation of biocompatibility. *Journal of Applied Biomaterials*, 2(2):101–107, 1991. doi: https://doi.org/10.1002/jab.770020205.

[122] C. Hu, F. Wang, H. Yang, J. Ai, L. Wang, D. Jing, L. Shao, and X. Zhou. Preparation and characterisation of poly p-phenylene-2,6-benzobisoxazole fibre-reinforced resin matrix composite for endodontic post material: A preliminary study. *Journal of Dentistry*, 42(12):1560–1568, 2014. ISSN 0300-5712. doi: https://doi.org/10.1016/j.jdent.2014.10.007.

[123] *Current Status of In Vitro Test Methods for Identifying Mild/Moderate Ocular Irritants: The Hen's Egg Test–Chorioallantoic Membrane (HET-CAM) Test Method*. 2010.

[124] H. Spielmann, S. Kalweit, M. Liebsch, T. Wirnsberger, I. Gerner, E. Bertram-Neis, K. Krauser, R. Kreiling, H. Miltenburger, W. Pape, and W. Steiling. Validation study of alternatives to the draize eye irritation test in germany: Cytotoxicity testing and het-cam test with 136 industrial chemicals. *Toxicology in Vitro*, 7(4):505–510, 1993. ISSN 0887-2333. doi: https://doi.org/10.1016/0887-2333(93)90055-A.

[125] H. Afzal, F. Shehzad, M. Zubair, O. Bakather, and M. Al-Harthi. Influence of microwave irradiation on thermal properties of pva and pva/graphene nanocomposites. *Journal of Thermal Analysis and Calorimetry*, 139, 06 2019. doi: 10.1007/s10973-019-08419-x.

[126] Z. Lian, Y. Zhang, and Y. Zhao. Nano-tio2 particles and high hydrostatic pressure treatment for improving functionality of polyvinyl alcohol and chitosan composite films and nano-tio2 migration from film matrix in food simulants. *Innovative Food Science Emerging Technologies*, 33, 11 2015. doi: 10.1016/j.ifset.2015.10.008.

[127] L. Yu, Y. Zhang, J. Tang, and J. Gao. Friction and wear behavior of polyimide composites reinforced by surface-modified poly-p-phenylenebenzobisoxazole (pbo) fibers in high ambient temperatures. *Polymers*, 11, 11 2019. doi: 10.3390/polym11111805.

[128] Y. Cheng, J. Dong, C. Yang, T. Wu, and Q. Zhang. Synthesis of poly(benzobisoxazole- co -imide) and fabrication of high-performance fibers. *Polymer*, 133, 11 2017. doi: 10.1016/j.polymer.2017.11.015.

[129] M. Chen, D. Wang, M. Yue, X. Lin, M. Yang, and Q. He. "zylon" aerogels. *Macromolecular Materials and Engineering*, 303(10):1800229, 2018. doi: https://doi.org/10.1002/mame.201800229.

[130] N. El-Sawy, M. El-Arnaouty, and A. Abdel Ghaffar. γ-irradiation effect on the non-cross-linked and cross-linked polyvinyl alcohol films. *Polymer-plastics Technology and Engineering - POLYM-PLAST TECHNOL ENG*, 49:169–177, 01 2010. doi: 10.1080/03602550903284248.

[131] Z. Xu, J. Li, H. Zhou, X. Jiang, C. Yang, F. Wang, Y. Pan, N. Li, X. Li, L. Shi, and X. Shi. Morphological and swelling behavior of cellulose nanofiber (cnf)/poly(vinyl alcohol) (pva) hydrogels: Poly(ethylene glycol) (peg) as porogen. *RSC Adv.*, 6:43626–43633, 04 2016. doi: 10.1039/C6RA03620A.

[132] N. Bhat, M. Nate, M. Kurup, V. Bambole, and S. Sabharwal. Effect of γ-radiation on the structure and morphology of polyvinyl alcohol films. *Nuclear Instruments Methods in Physics Research*

Section B-beam Interactions With Materials and Atoms - NUCL INSTRUM METH PHYS RES B, 237:585–592, 08 2005. doi: 10.1016/j.nimb.2005.04.058.

[133] J. Ino, P. Chevallier, D. Letourneur, D. Mantovani, and C. Le Visage. Plasma functionalization of poly(vinyl alcohol) hydrogel for cell adhesion enhancement. *Biomatter*, 3, 07 2013. doi: 10.4161/biom.25414.

[134] N. Srivastava and C. Wang. Effects of water addition on oh radical generation and plasma properties in an atmospheric argon microwave plasma jet. *Journal of Applied Physics*, 110:053304, 09 2011. doi: 10.1063/1.3632970.

[135] E. Otsuka and A. Suzuki. A simple method to obtain a swollen pva gel crosslinked by hydrogen bonds. *Journal of Applied Polymer Science*, 114:10 – 16, 10 2009. doi: 10.1002/app.30546.

[136] S. Sasaki, S. Omata, T. Murakami, N. Nagasawa, M. Taguchi, and A. Suzuki. Effect of gamma ray irradiation on friction property of poly(vinyl alcohol) cast-drying on freeze-thawed hybrid gel. *Gels*, 4:30, 03 2018. doi: 10.3390/gels4020030.

[137] J. Negishi, K. Nam, T. Kimura, T. Fujisato, and A. Kishida. Ultra high pressure technique is an effective method for the preparation of pva-heparin hybrid gel. *European journal of pharmaceutical sciences : official journal of the European Federation for Pharmaceutical Sciences*, 41:617–22, 12 2010. doi: 10.1016/j.ejps.2010.09.001.

[138] R. Paneru, s. h. Ki, P. Lamichhane, L. Nguyen, B. Adhikari, I. Jeong, S. Mumtaz, J. Choi, J.-S. Kwon, and E. Choi. Enhancement of antibacterial and wettability performances of polyvinyl alcohol/chitosan film using non-thermal atmospheric pressure plasma. *Applied Surface Science*, 532:147339, 08 2020. doi: 10.1016/j.apsusc.2020.147339.

[139] D. Liu, J. Hu, Y. Zhao, X. Zhou, P. Ning, and Y. Wang. Surface modification of pbo fibers by argon plasma and argon plasma combined with coupling agents. *Journal of Applied Polymer Science*, 102(2):1428–1435, 2006. doi: https://doi.org/10.1002/app.24287.

[140] D. Liu, P. Chen, M. Chen, and Z. Liu. Surface modification of high performance pbo fibers using radio frequency argon plasma. *Surface and Coatings Technology*, 206:3534–3541, 04 2012. doi: 10.1016/j.surfcoat.2012.02.033.

[141] X. Lu and S. Wu. On the active species concentrations of atmospheric pressure nonequilibrium plasma jets. *Plasma Science, IEEE Transactions on*, 41:2313–2326, 08 2013. doi: 10.1109/TPS.2013.2268579.

[142] V. Mow and X. E. Guo. Mechano-electrochemical properties of articular cartilage: Their inhomogeneities and anisotropies. *Annual review of biomedical engineering*, 4:175–209, 02 2002. doi: 10.1146/annurev.bioeng.4.110701.120309.

[143] S. Akizuki, V. C. Mow, F. Müller, J. C. Pita, D. S. Howell, and D. H. Manicourt. Tensile properties of human knee joint cartilage: I. influence of ionic conditions, weight bearing, and fibrillation on the

tensile modulus. *Journal of Orthopaedic Research*, 4(4):379–392, 1986. doi: https://doi.org/10.1002/jor.1100040401.

[144] K. Boettcher, S. Grumbein, U. Winkler, J. Nachtsheim, and O. Lieleg. Adapting a commercial shear rheometer for applications in cartilage research. *Review of Scientific Instruments*, 85(9): 093903, 2014. doi: 10.1063/1.4894820.

[145] T. Groth, B. Seifert, G. Malsch, W. Albrecht, D. Paul, A. Kostadinova, N. Krasteva, and G. Altankov. Interaction of human fibroblasts with moderate wettable polyacrylonitrile-copolymer membranes. *Journal of biomedical materials research*, 61:290–300, 09 2002. doi: 10.1002/jbm.10191.

[146] Y. Mei, K. Saha, S. Bogatyrev, J. Yang, A. Hook, Z. Kalcioglu, S.-W. Cho, M. Mitalipova, N. Pyzocha, F. Rojas, K. Van Vliet, M. Davies, M. Alexander, R. Langer, R. Jaenisch, and D. Anderson. Combinatorial development of biomaterials for clonal growth of human pluripotent stem cells. *Nature materials*, 9:768–78, 09 2010. doi: 10.1038/nmat2812.

[147] S. Gupta, T. Webster, and A. Sinha. Evolution of pva gels prepared without crosslinking agents as a cell adhesive surface. *Journal of materials science. Materials in medicine*, 22:1763–72, 06 2011. doi: 10.1007/s10856-011-4343-2.

[148] P. Paradiso, V. Chu, L. Santos, A. Serro, R. Colaço, and B. Saramago. Effect of plasma treatment on the performance of two drug-loaded hydrogel formulations for therapeutic contact lenses. *Journal of Biomedical Materials Research Part B: Applied Biomaterials*, 103, 09 2014. doi: 10.1002/jbm.b.33287.

[149] C. Chu, M. Szczodry, and S. Bruno. Animal models for cartilage regeneration and repair. *Tissue engineering. Part B, Reviews*, 16:105–15, 10 2009. doi: 10.1089/ten.TEB.2009.0452.

[150] V. Sardinha, L. Lima, W. Belangero, C. Zavaglia, V. Bavaresco, and J. Gomes. Tribological characterization of polyvinyl alcohol hydrogel as substitute of articular cartilage. *Wear*, 301(1):218–225, 2013. ISSN 0043-1648. doi: https://doi.org/10.1016/j.wear.2012.11.054. Wear of Materials 2013.

[151] P. Adelina, C. Dehelean, H. Calniceanu, C. Watz, S. Brad, C. Sinescu, O. Marcu, S. Casiana, Popa, S. Avram Feflea, M. Nicolov, and C. Szuhanek. A custom-made orthodontic mini-implant-effect of insertion angle and cortical bone thickness on stress distribution with a complex in vitro and in vivo biosafety profile. *Materials*, 13:4789, 10 2020. doi: 10.3390/ma13214789.

[152] I. Moreno-Jiménez, J. M. Kanczler, G. Hulsart-Billstrom, S. Inglis, and R. O. Oreffo. The chorioallantoic membrane assay for biomaterial testing in tissue engineering: A short-term in vivo preclinical model. *Tissue Engineering Part C: Methods*, 23(12):938–952, 2017. doi: 10.1089/ten.tec.2017.0186.

Appendix A

Tribology - Evolution of CoF with respect to time

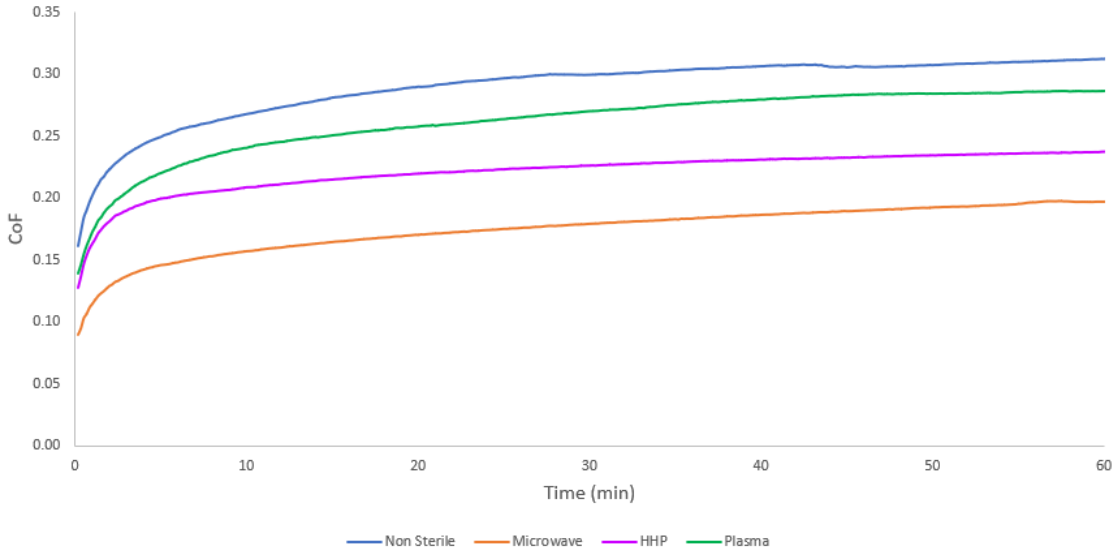

Figure A.1: Measured CoF values of hydrogel samples against swine cartilage pins, normal analysis with inertial effects leads to higher CoF values than in the recyprocating analysis mode, especially in the case of HHP and non sterilized samples.

Appendix B

Adhesion of chondrocyte cells to hydrogel samples

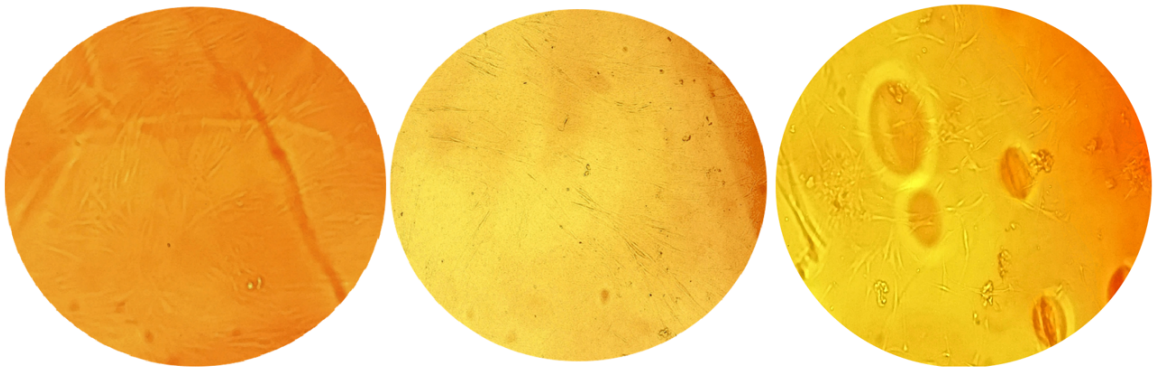

Figure B.1: Micrographs of the chondrocytes cultured on top of the sterilized samples, for 22 days (left-Microwave, center-HHP, right-Plasma), at a 100x magnification.